



HAL
open science

Solution and solid-state light-induced transformations in heterometallic vanadium-ruthenium nitrosyl complex

Iakov S Fomenko, Artem A Mikhailov, Vasily Vorobyev, Natalia V Kuratieva, Gennadiy A Kostin, Dominik Schaniel, Vladimir A Nadolinny, Artem L Gushchin

► **To cite this version:**

Iakov S Fomenko, Artem A Mikhailov, Vasily Vorobyev, Natalia V Kuratieva, Gennadiy A Kostin, et al.. Solution and solid-state light-induced transformations in heterometallic vanadium-ruthenium nitrosyl complex. *Journal of Photochemistry and Photobiology A: Chemistry*, 2021, 407, pp.113044. 10.1016/j.jphotochem.2020.113044 . hal-03081246

HAL Id: hal-03081246

<https://hal.univ-lorraine.fr/hal-03081246v1>

Submitted on 18 Dec 2020

HAL is a multi-disciplinary open access archive for the deposit and dissemination of scientific research documents, whether they are published or not. The documents may come from teaching and research institutions in France or abroad, or from public or private research centers.

L'archive ouverte pluridisciplinaire **HAL**, est destinée au dépôt et à la diffusion de documents scientifiques de niveau recherche, publiés ou non, émanant des établissements d'enseignement et de recherche français ou étrangers, des laboratoires publics ou privés.

Solution and solid-state light-induced transformations in heterometallic vanadium-ruthenium nitrosyl complex

Iakov S. Fomenko^{a,*}, Artem A. Mikhailov^{a,*}, Vasily Vorobyev^a, Natalia V. Kuratieva^a, Gennadiy A. Kostin^a, Dominik Schaniel^b, Vladimir A. Nadolnyy^a, Artem L. Gushchin^{a,*}

^a Nikolaev Institute of Inorganic Chemistry SB RAS, 3 Acad. Lavrentiev Ave., Novosibirsk, 630090, Russia

^b Université de Lorraine, CNRS, CRM2, UMR 7036, Nancy 54000, France

Abstract

The work is devoted to the preparation and photochemical investigations of the novel binuclear heterometallic complex $[\text{Ru}(\text{NO})(\text{NO}_2)_2(\mu\text{-NO}_2)(\mu\text{-CH}_3\text{COO})(\mu\text{-O})\text{VO}(\text{dbbpy})]\cdot\text{CH}_3\text{CN}$ (dbbpy - 4,4'-di-tert-butyl-2,2'-bipyridyl), which is obtained with quantitative yield. The structure of the complex is determined by single crystal X-ray diffraction and by DFT calculations. On the one hand, irradiation at 445 nm of an acetonitrile solution of the complex leads to a NO photo-release reaction. The light excitation induces the charge transfer from NO_2 and dbbpy ligands to the antibonding orbitals of ON-Ru-O-V chain, leading to the NO release, which is confirmed by the DFT. The quantum yield of the Ru-NO photo-cleavage is $0.57\pm 0.05\%$. The products of the photolysis (NO and paramagnetic Ru^{III} complex) are confirmed by the Griess test and EPR-spectroscopy. On the other hand, the irradiation of the complex in the solid phase at 10 K results in the formation of the metastable bond isomer Ru-ON (MS1), which is detected by the infrared spectroscopy. The stretching vibration of the $\nu(\text{NO})$ band of MS1 (1750 cm^{-1}) is shifted by 150 cm^{-1} to lower energy with respect to the $\nu(\text{NO})$ band of the ground state GS (1900 cm^{-1}). The population of the MS1 is about 5%. MS1 thermally decays at 120-140 K back to the GS. Hence, this complex represents a bifunctional platform, which can release nitric oxide in solution and reversibly switch the NO ligand coordination in the solid state. It is shown, that the presence of vanadium strongly influences the photochemical properties of ruthenium nitrosyl both in the solid phase and in solution.

Keywords: ruthenium, vanadium, oxidovanadium complexes, nitrosyl, metastable states, isomerization

1. Introduction

One of the remarkable properties of nitrosyl ruthenium complexes is the ability to labilize the nitrosyl (NO) ligand under photoexcitation. Interestingly, that the outcome of NO labilization depends on the environment: in solution, light excitation of nitrosyl ruthenium leads predominantly to NO release [1], whereas in the solid state (crystal or powder) the formation of linkage isomers Ru-ON or Ru-(η^2 -(NO)) can be observed [2]. In some cases, both NO release and NO isomerization was observed in the solid state [3].

The NO release in solution is an appealing option for medical applications. It is known, that nitric oxide is a biological active molecule, which participates in many physiological processes, such as neurotransmission, blood pressure control, immunological responses, and antioxidant action [4–6]. The biologically relevant lifetime of the nitric oxide was estimated to be in the 0.09 - 2 s range depending on the distance from the blood vessels [7]. In this regard, ruthenium nitrosyl complexes are NO-bearing platforms enabling

phototriggered nitric oxide release, i.e. they can be applied in photodynamic therapy for targeted NO delivery. Moreover, ruthenium complexes can interact with DNA repair enzymes, thus, ruthenium nitrosyl complexes are considered as double bioactive species [8]. On the other hand, light irradiation of ruthenium nitrosyl complexes in solid phase induces the formation of metastable state isomers Ru-ON (MS1) or Ru-(η^2 -(NO)) (MS2) from the ground state Ru-NO (GS). Such isomerization is a reversible process – it is possible to drive MS1/MS2 back to the GS by heating or light irradiation [9–12]. It was shown, that the isomerization can find application in data storage based on holography technique [13].

Furthermore, the combination of ruthenium nitrosyl with a magnetic/optic/red-ox/catalytic building block leads to functional materials with photo-triggered properties. Particularly, mononuclear oxidovanadium complexes [14–18] are attractive species and can be used as building blocks for the design of bi- and polynuclear structures [19]. Oxidovanadium complexes attract considerable attention primarily due to their catalytic properties in diverse organic reactions and biological activity (insulin-enhancing effect, antidiabetic and antitumor activities) [20–24]. Complexes with V=O moiety have high activity in homo- and heterogeneous catalysis, for instance, oxidations of alkanes, alkenes, arenes, alcohols, aldehydes, ketones, and sulfur species, as well as oxidative C–C and C–O bond cleavage, carbon–carbon bond formation, deoxydehydration, haloperoxidase, cyanation, hydrogenation, dehydrogenation, ring-opening metathesis polymerization, and oxo/imido heterometathesis, etc [25–34]. Oxidovanadium complexes with N-donor heterocycle ligands show activity towards DNA cleavage upon near-IR irradiation [35–37]. In some cases, selective binding to cancer cell DNA is observed [37–41]. Thus, such complexes can be used in cancer photodynamic therapy. Furthermore, in nature, vanadium-dependent haloperoxidases (VHPO) catalyze the oxidation of halides with hydrogen peroxide [42–44], while vanadium-dependent nitrogenases are involved in nitrogen fixation [45,46].

Heterometallic complexes combining both 3d-V and 4d-Ru metals are extremely rare. According to the Cambridge Crystallographic Data Centre (CCDC), there are 6 known mixed vanadium-ruthenium complexes including only one heterometallic complex: $[L'Ru(\mu-O)(\mu-CH_3CO_2)_2VL](PF_6)_2$, where L' and L are N,N',N''-trimethyl-1,4,7-triazacyclononan and 1,4,7-triazacyclononane, respectively [47]. Since both metals, ruthenium and vanadium, poses biological activity, the combination of such metals in one complex can increase the biological and catalytic activity of the complex through a synergistic effect. The combination of nitrosyl photoisomerization with a vanadium center might lead to new materials with photo-triggered properties, where the type of NO coordination affects the properties of the heterometallic complex [48].

Thus, this work is devoted to the preparation of the heterometallic complex combining nitrosyl ruthenium and oxidovanadium. The photochemical properties of the obtained complex were thoroughly studied by the combined spectroscopic (UV/vis, IR, EPR) and calculation (DFT) methods - the nitric oxide release during irradiation in solution and the formation of metastable state isomer Ru-ON (MS1) in solid state under irradiation have been investigated.

2. Materials and methods

2.1. Synthesis of $[Ru^{II}(NO)(NO_2)_2(\mu-NO_2)(\mu-CH_3COO)(\mu-O)V^VO(dbppy)]CH_3CN$ (I)

The complexes $[VO(dbppy)(H_2O)Cl_2]$ and $Na_2[Ru(NO)(NO_2)_4(OH)] \cdot 2H_2O$ were synthesized according to the methods described in [16] and [49], respectively.

A mixture of 42 mg (100 μ mol) of the complex $[VO(dbppy)(H_2O)Cl_2]$ and 41 mg (100 μ mol) of the complex $Na_2[Ru(NO)(NO_2)_4(OH)] \cdot 2H_2O$ in a 1:1 ratio was stirred in 3 ml of CH_3CN for 30 minutes with moderate heating (60°C). The initially formed brown precipitate readily dissolved during the reaction. Then the solution was filtered off from NaCl and evaporated in vacuum. As a result, a fine brown powder was obtained with a quantitative yield. Dark red crystals were obtained from a mixture of CH_3CN/CH_2Cl_2 (1/10) by the slow diffusion of hexane. IR-spectra at room temperature (KBr, cm^{-1}): 2967 (m), 1900 (vs), 1619 (m), 1585 (w), 1463 (s), 1450 (m), 1415 (s), 1326 (m), 1270 (m), 1252 (m), 1036 (m), 976 (s), 901 (w), 821 (s). UV-vis: $12400 M^{-1}cm^{-1}$ (298 nm). Elemental analysis for $C_{20}H_{28}N_6O_{11}RuV$, the calculated %: C 35.3; N 12.4; H 4.1; obtained %: C 35.0; N 12.2; H 4.2. The structure model was determined by single crystal X-ray diffraction: $P 2_1/n$; $a = 6.24 \text{ \AA}$, $b = 16.60 \text{ \AA}$, $c = 28.27 \text{ \AA}$, $\alpha = 90^\circ$, $\beta = 92.30^\circ$, $\gamma = 90^\circ$.

2.2. Instrumental techniques

IR spectroscopic measurements with irradiation were performed using a Nicolet 5700 FT-IR spectrometer with a resolution of $2 cm^{-1}$ in the range $400\text{--}4000 cm^{-1}$. The sample was ground, mixed with KBr and pressed into pellets. The KBr pellets were bonded by silver paste onto the cold finger of a closed-cycle cryostat (Oxford Optistat V01) and irradiated through KBr windows by LED light of different wavelengths in the range $365\text{--}405 nm$ and $70\text{--}200 mW$ optical power (Thorlabs L and LP series). The cryostat has the temperature range of $9\text{--}320 K$.

UV-vis spectra were recorded on a PG Instruments T60 UV-vis single-beam spectrophotometer. UV-vis spectra of the complex were obtained in DMSO and acetonitrile in a 1 cm cell. The absorbance of the pure solvents was taken in account. The evolution of the spectra in time was monitored during perpendicular exposure by the LED at 445 nm, 100 mW.

Griess reagent was prepared as an equimolar ($5 \cdot 10^{-5}$ mole) solution of 1-naphthylamine and sulfanilamide in acetic acid/acetonitrile (1:4) mixture. The solution of the complex ($\approx 10^{-4}$ M) and Griess reagent (10^{-2} M) in acetic acid/acetonitrile (1:4) mixture was irradiated by LED 445 nm, 100 mW in a 1 cm cuvette. After the light exposure, the red area was observed at the place of the light spot.

The EPR spectra were obtained at 77 K on a Varian E-109 spectrometer operating at X-band. g-values were calculated using 2,2-diphenyl-1-picrylhydrazil (DPPH) with $g = 2.0036$ as a reference [50]. For the study of the photolysis product, on the first stage, the solution of the complex in acetonitrile (0.05 M) was irradiated at room temperature during 60 min by LED 445 nm, 100 mw, similar to UV-vis investigation. Then, the irradiated solution was cooled at 77 K and the EPR spectra was obtained.

Single-crystal X-ray diffraction data for the best crystal of **1** we have were collected using the graphite monochromatized MoK α -radiation ($\lambda=0.71073$ Å) at 150(2) K on a Bruker APEX DUO diffractometer equipped with a 4K CCD area detector. The φ - and ω -scan technique was employed to measure intensities. Absorption corrections were applied empirically using the SADABS program [51]. Structure was solved by the direct methods of the difference Fourier synthesis and further refined by the full-matrix least squares method using the SHELXTL package [52]. Atomic thermal parameters for non-hydrogen atoms were refined anisotropically. Atomic displacement parameters for some terminal carbon atoms in tert-butyl substituents and in acetonitrile solvent molecule were restrained with the ISOR command. The positions of hydrogen atoms were calculated corresponding to their geometrical conditions and refined using the riding model. Two nitro-groups were restrained with the N-O distances. The experimental and refinement details are shown in Table S1. CIF-file of the complex has been deposited into CCDC with the numbers 2027275.

2.3.DFT Computational details

The molecular geometry of [Ru(NO)(NO₂)₂(μ -NO₂)(μ -CH₃CO₂)(μ -O)VO(bpy)] was fully optimized in the acetonitrile liquid phase at the Density Functional Theory (DFT) level. All calculations were performed using the ADF-2017 program package [53–55]. The hybrid B3LYP [56–59] or VWN [56] functionals were used coupled with the triple- ζ with two polarization functions all-electron TZ2P uncontracted Slater Type Orbitals (STOs) basis set for all elements [60]. The inner shells were included in calculations. The relativistic effects were taken into account at default scalar level in Zero Order Regular Approximation (ZORA) formalism [61–63]. Solvent effects were modeled via the implicit Conductor like Screening Model (COSMO) of solvation with acetonitrile as solvent [64]. For geometry optimizations and UV-vis absorption spectrum calculations, the COSMO molecular cavity was built according to the van der Waals radii from MM3 method [65] scaled down by 1.2. The standard values for dielectric constant and refractive indexes were always assumed.

The optimized geometries were submitted to the time-dependent DFT calculations [66]. The same basis sets were used as for the optimization. The first 400/150 excited states were included in the calculation of the UV-vis absorption spectrum (VWN/B3LYP). Only singlet-singlet excitations were computed.

The convergence criteria for Self-Consistent Field were used at default 10⁻⁶ settings for the error of the commutator of the Fock matrix and the P-matrix, which is the density matrix in the representation of the basis functions. The rest of SCF setting were the default ones as well. The convergence criteria for geometry optimizations were set to default values of 10⁻³ Hartree for energy change, 10⁻³ Hartree Å⁻¹ for nuclear gradients, 10⁻² of the Cartesian displacement, and 0.5 degree for change in angles.

3. Results and discussion

3.1.Synthesis and structure description

The oxidovanadium(IV) complex [VO(dbbpy)(H₂O)Cl₂] was obtained from vanadium trichloride by reaction with 4,4'-di-*tert*-butyl-2,2'-bipyridine in acetonitrile in the ratio 1:1. The mixture was refluxed for 4 hours in air. The resulting solution was evaporated to dryness and was recrystallized from CH₂Cl₂/hexane mixture [16].

The nitrosyl ruthenium complex $\text{Na}_2[\text{Ru}(\text{NO})(\text{NO}_2)_4(\text{OH})]\cdot 2\text{H}_2\text{O}$ was obtained from ruthenium(III) chloride hydrate. Its synthesis consists of the interaction of RuCl_3 with sodium nitrite in boiling hydrochloric acid [49].

The binuclear $[\text{Ru}(\text{NO})(\text{NO}_2)_2(\mu\text{-NO}_2)(\mu\text{-CH}_3\text{COO})(\mu\text{-O})\text{VO}(\text{dbbpy})]\cdot \text{CH}_3\text{CN}$ (**I**) complex was obtained from the pre-organized ruthenium $\text{Na}_2[\text{Ru}(\text{NO})(\text{NO}_2)_4(\text{OH})]\cdot 2\text{H}_2\text{O}$ and vanadium $[\text{VO}(\text{dbbpy})(\text{H}_2\text{O})\text{Cl}_2]$ complexes (Fig. 1). The complex $[\text{VO}(\text{dbbpy})(\text{H}_2\text{O})\text{Cl}_2]$ has one facet of an octahedron formed by labile ligands, which are replaced during the reaction in acetonitrile. This approach yielded a rare example of heterometallic nitrosyl ruthenium complex in quantitative yield. The +5 oxidation state of vanadium is in agreement with the complex **I** being EPR silent in dark. Similar to the synthesis of parent vanadium(IV) complex, vanadium center was oxidized by oxygen to give vanadium(V).

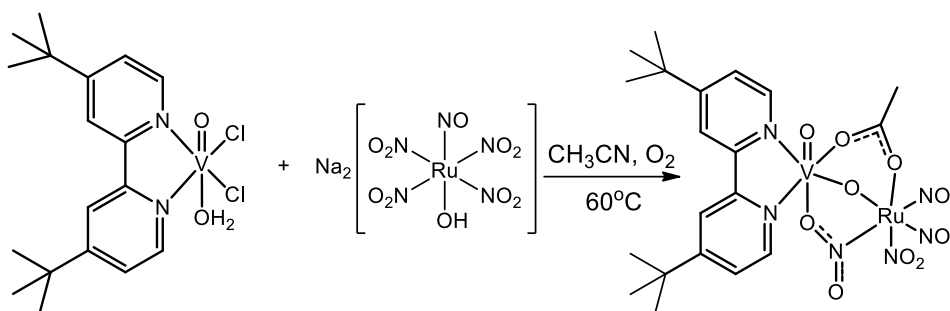


Fig. 1. The scheme of synthesis of $[\text{Ru}(\text{NO})(\text{NO}_2)_2(\mu\text{-NO}_2)(\mu\text{-CH}_3\text{COO})(\mu\text{-O})\text{VO}(\text{dbbpy})]\cdot \text{CH}_3\text{CN}$ (**I**).

Single crystals of **I** were obtained by recrystallization of **I** from a mixture $\text{CH}_3\text{CN}/\text{CH}_2\text{Cl}_2/\text{C}_6\text{H}_{12}$ (1:10:30 ratio). Unfortunately, no high quality crystals could be obtained. These thin-plate shaped crystals diffracted only weakly leading to rather poor diffraction data. Therefore, the structure model found for this compound exhibits rather large agreement factors *R*. Nevertheless, this crystal model shows the interesting features in this bimetallic complex, and it is supported by DFT calculations.

The experimentally determined molecular structure of **I** is shown in Fig. 2. Selected bond distances are listed in Table 1. Each metal atom has a distorted octahedral environment. In the case of vanadium, the octahedral environment is defined by two N atoms from dbbpy and four O atoms from the bridging groups CH_3COO^- , NO_2^- , O^{2-} and the terminal oxo ligand. In the case of ruthenium, it is defined by four N atoms from NO_2^- and NO^+ ligands and two O atoms from the bridging CH_3COO^- and O^{2-} ligands. The metal atoms share a triangular face formed by the bridging groups CH_3COO^- , NO_2^- and O^{2-} . We propose that the bridging acetate-ion was formed during the hydrolysis of acetonitrile during the reaction. Unexpected emergence of the coordinated acetate could be explained as intricate result of interaction of coordinated nitro group with acetonitrile solvent. A reaction of that kind was not reported for acetonitrile solution of starting $[\text{Ru}(\text{NO})(\text{NO}_2)_4(\text{OH})]^{2-}$ complex, thus, we assume that the vanadium complex is involved in this transformation. In the starting vanadium complex $[\text{VO}(\text{dbbpy})(\text{H}_2\text{O})\text{Cl}_2]$, the $\text{V-O}_{\text{terminal}}$ bond length is 1.589 Å. In the binuclear complex **I** this bond is the same and equals 1.57(1) Å. The $\text{V-}\mu\text{-O}$ bond length equals 1.70(1) Å indicating the coordination of the oxo ligand, instead of hydroxo. In $[\text{VO}(\text{dbbpy})(\text{H}_2\text{O})\text{Cl}_2]$, the dbbpy ligand is symmetrically coordinated with V-N distance 2.128(3)

Å, whereas in the case of **I**, dbbpy is asymmetrically coordinated with V-N distances 2.11(1) Å and 2.17(1) Å due to the different *trans* influence of the μ_2 -oxo, and μ_2 -acetate ligands.

In order to support experimental X-Ray diffraction data, we performed quantum mechanical calculations, which provide a detailed picture of bonding and electronic structure in the studied complex. The initial structure for the calculations was based on the bonding pattern from single crystal X-ray studies. The geometry optimization was carried out at density functional theory (DFT) level with local density approximation functional (VWN) or in hybrid B3LYP functional. The basis set was TZ2P for all atoms. The solvation shell of acetonitrile was modeled as the implicit Conductor like Screening Model (COSMO). The coordination spheres are distorted octahedral for vanadium and ruthenium atoms (Table 1, Figure 2). The ruthenium atom is shifted from {N₃O} equatorial plane (nitro groups and acetate) toward the nitrosyl group in the axial position at 0.1 Å for VWN calculations (or 0.08 Å for B3LYP). The magnitude and direction of the shift is in agreement with the X-ray structural data of other known complexes [67,68]. Nitrosyl group and bridging oxo ligand occupy the axial positions. The VWN distances (1.74 (Ru-NO), 1.14 (N-O_{NO}) and 1.94 (Ru- μ -O) Å) are close to the experimental ones of related complexes [69–75], as well as the B3LYP data (1.76 (Ru-NO), 1.13 (N-O_{NO}) and 1.99 (Ru- μ -O) Å). In case of vanadium coordination sphere, the equatorial plane with dbbpy, μ_2 -oxo, and μ_2 -acetate has bond lengths varying from 1.71_O to 2.12_N Å. The axial positions are occupied by the terminal oxo and bridging nitrito groups. The vanadium-oxygen distance of the bridging nitrito ligand is noticeably elongated due to the *trans* influence of the terminal oxo ligand. This is in agreement with previous studies of VO³⁺ complexes [76–78] and our X-ray data.

Table 1

Selected computed and experimental bond distances of the studied complex.

Functional/ bond length (Å)	VWN	B3LYP	Exp.
Ru-N_{NO}	1.74	1.76	1.73(1)
N-O_{NO}	1.14	1.13	1.16(2)
avg. Ru-NO₂ (terminal)	2.04	2.10	2.21(2)
avg. ON-O (terminal)	1.23	1.23	1.14(3)
Ru-μ-NO₂	2.06	2.13	2.07(1)
V-μ-ONO	2.26	2.43	2.26(1)
O-N-(μ-O)	1.21 (1.26)	1.22 (1.26)	1.19(2) (1.31(1))
Ru(V)-OCOCH₃	2.09 (1.90)	2.14 (1.93)	2.10(1) (1.90(1))
Ru(V)-μ-O	1.94 (1.71)	1.99 (1.70)	2.00(1) (1.70(1))
V-O (terminal)	1.59	1.58	1.57(1)
V-dbbpy	2.06; 2.12	2.11; 2.18	2.10(1); 2.17(1)

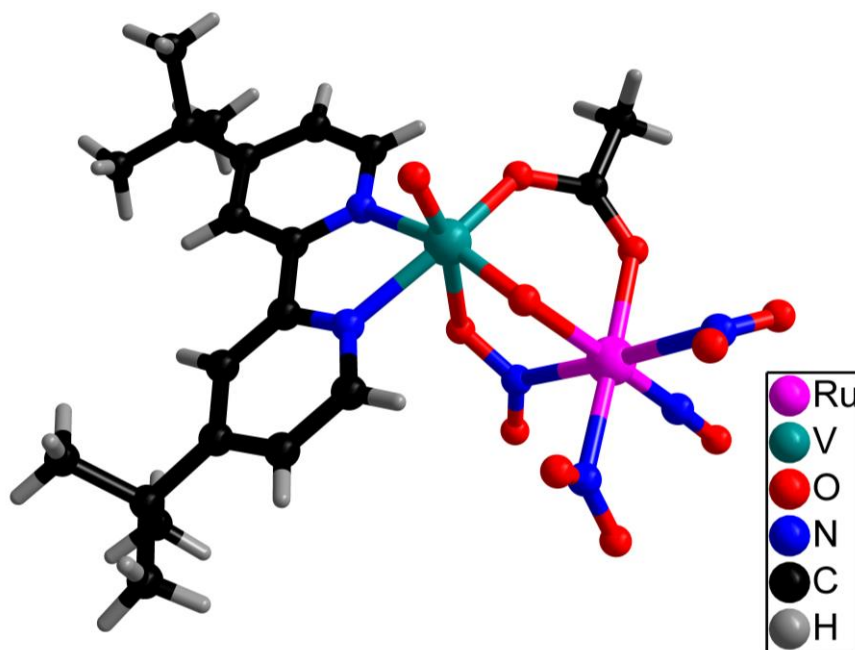


Fig. 2. The structure of the complex I determined by the single crystal X-Ray diffraction.

3.2. NO release in solution

The unique feature of the metal nitrosyl complexes is the metal-to-ligand charge transfer (MLCT) from the t_{2g} -like d orbitals of d^6 ruthenium to the π^* antibonding nitrosyl orbital [79,80]. After the excitation, the relaxation of the MLCT state leads to metastable states (side-on and κ O-coordination of the nitrosyl [10]) or to nitric oxide being released from the complex [1]. In the case of the studied ruthenium-vanadium complex, the MLCT transition is enhanced by antibonding interactions with bridging oxo ligand and vanadium. Thus, the electron density is transferred to the antibonding MO of ON-Ru-O-V or ON-Ru-O-V-O chains. Intense transitions promote the electron density from lone pairs in the two *trans* nitro groups or π -orbitals of the dbbpy ligand (Tables S2-S4) to the antibonding orbitals of the ON-Ru-O-V chain. These key transitions for NO labilization correspond to the 400-500 nm range of the spectrum, which causes the choice of 445 nm light source.

From the orbital point of view (Tables S2-S4), the lowest unoccupied molecular orbital (LUMO) (Fig. 3) contains atomic orbitals of nitrosyl group, ruthenium, bridging oxo ligand, and vanadium interacting in the antibonding fashion on the curved ON-Ru-O-V chain. Unoccupied orbitals involving orbitals of the whole ON-Ru-O-V-O chain are located next in energy (LUMO+1 and LUMO+2). Unoccupied orbitals with contributions of nitro, acetate, and dbbpy ligands are found at even higher energy. However, these orbitals do not play a role in the visible transitions. The nature of the highest occupied orbital (HOMO) (Fig. 3) depends on the functional choice. Oxygens' lone pairs in the two *trans* nitro groups are the HOMO-1 and HOMO for VWN and B3LYP functionals, respectively. For the VWN functional, the HOMO orbital is only 0.025 eV higher than HOMO-1 and it is constructed from the π -orbitals of the dbbpy ligand. For the B3LYP data, the occupied orbitals with

contribution from dbbpy π -system are lower in energy (HOMO-3, HOMO-4). The ruthenium t_{2g} -like d orbitals play an important role in the HOMO-2 orbital.

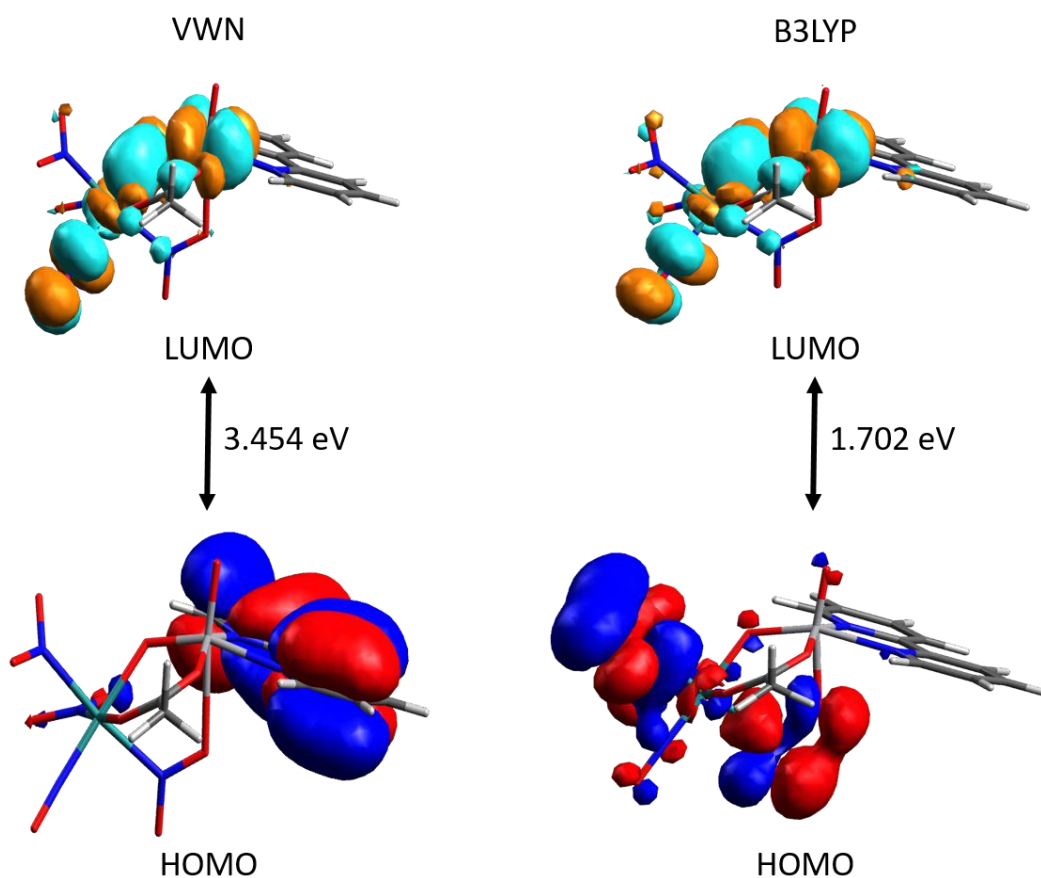


Fig. 3. The HOMO and LUMO orbitals by DFT calculations using VWN and B3LYP functionals.

The experimental absorption spectrum of the compound **I** in the acetonitrile solution is shown in Fig. 4. The compound **I** strongly absorbs in the UV region with the band maxima at 308 nm ($13700 \pm 500 \text{ M}^{-1} \cdot \text{cm}^{-1}$, Fig. 4). According to the DFT calculations the band corresponds to the inter- and intra-ligand transitions. Low-energy shoulder at 400-500 nm corresponds to the charge transfer from NO_2 and dbbpy ligands to the orbitals of the ON-Ru-O-V chain. The acetonitrile solution of **I** is stable in time, while a decomposition of **I** occurred in DMSO solution (Fig. S1).

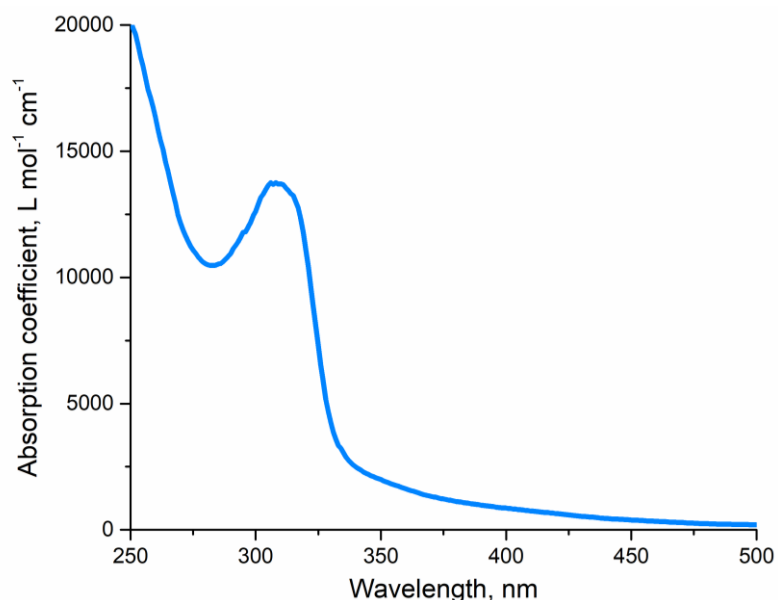
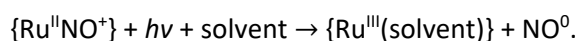


Fig. 4. The absorption spectrum of the compound **I** in the acetonitrile solution.

Ruthenium nitrosyl complexes release coordinated nitrogen monooxide upon photolysis according to the equation:



Regardless of the ligand environment, the $\{\text{Ru}^{\text{II}}\text{NO}^+\}$ species are shown as promising NO donors [1][81]. Commonly, in the absorption spectrum the decrease in the UV-blue range and the corresponding increase of the absorption in red range after light exposure of the complexes in solutions is observed [8,50,82,83]. Since five-coordinated ruthenium complexes are not stable, the free coordination place after NO photo-release is occupied by the solvent molecule [1]. In some cases, the structures determined by the single crystal X-ray diffraction of the photo-products with the coordinated acetonitrile ligand were obtained [84,85].

The photolysis of **I** in acetonitrile solution is promoted by the 445 nm irradiation (Fig. 5). Unlike the case of decomposition of **I** in DMSO solution, the 308 nm absorption peak had no significant change through the photolysis in acetonitrile solution. The spectral differences are manifested as decrease in the ultraviolet absorption and the formation of the 388 nm band. The latter slightly loses intensity in the dark.

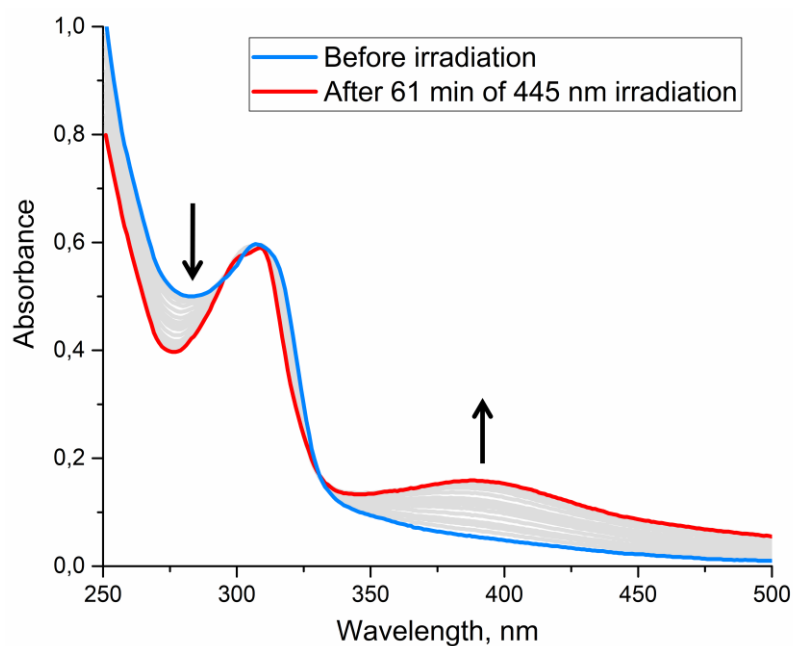
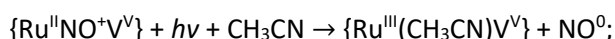


Fig. 5. Photolysis of the $4.35 \cdot 10^{-5}$ M solution of I in acetonitrile under 445 nm irradiation: blue line – before irradiation; red line – after 61 min of irradiation.

The spectral change of the freshly photolyzed solution stored in the dark resembles the nitrogen dioxide spectrum [86] (Fig. S2). This band undergoes single-exponential decay with the kinetic constant equal to $1.6 \pm 0.5 \cdot 10^{-3} \text{ s}^{-1}$. It is known, that NO_2 is in the equilibrium with N_2O_4 [87,88]. Nevertheless, reported rate constant of NO_2 disproportionation in water is significantly greater than $1.6 \pm 0.5 \cdot 10^{-3} \text{ s}^{-1}$ [89]. Hence, the assignment of the spectral evolution of the irradiated sample to the NO_2 is doubtful.

Additionally, the photolysis of the I in the presence of the Griess reagent (the reagent for the nitrite ion detection) was performed (Fig. S3) [90]. The oxidation of the photogenerated NO gives the nitrite ion via the quantitative reaction $4\text{NO} + \text{O}_2 + 2\text{H}_2\text{O} = 4\text{HNO}_2$ [91] or disproportionation reaction $2\text{NO}_2 + \text{H}_2\text{O} = \text{HNO}_2 + \text{HNO}_3$ [92]. The reaction of nitrite with the reagent produce the dye, characterized by the absorption band at around 500 nm (Fig. S3).

Hence, we propose the following scheme of the compound I photolysis:



The coordination of acetonitrile is not explicitly demonstrated, however its coordination is very likely due to previous reports and low stability of five-coordinated ruthenium species [1]. Thus, the absorbance at a given time and wavelength can be expressed as $A = \epsilon_{\text{RuNOV}} \cdot I \cdot C_{\text{RuNOV}} + \epsilon_{\text{RuV}} \cdot I \cdot (C_0 - C_{\text{RuNOV}})$. Concentrations of ruthenium complexes are derived from the photolysis equation. In the model, the quantum yield and extinction coefficients are refined by means of the least squares method to fit the experimental data. The quantum yield value is $0.57 \pm 0.05\%$.

Earlier, ruthenium nitrosyl complexes $[\text{RuNOL}_2(\text{NO}_2)_2\text{OH}]$ ($L = \text{pyridine}, \beta\text{-picoline}$) have been studied on the NO release in solution upon irradiation [8,50]. It was shown, the quantum yield of the nitric oxide release reaction was 6-20% depending on the solvent and the excitation wavelength. In the current case, the presence of vanadium sufficiently decreases the efficiency of NO photo-release, which is in an agreement with DFT calculations: the light excitation induces the charge transfer to the antibonding orbitals of ON-Ru-O-V chain, in which the presence of vanadium (LUMO occupancy is about 70%) decreases the probability of a distortion of the Ru-NO bond.

We used EPR spectroscopy to detect the paramagnetic photolysis products in the solution after light irradiation. The light exposure of the acetonitrile solution of the I by the 445 nm light for 60 min induce the formation of the paramagnetic species. The EPR spectrum after irradiation is presented in the Fig. 6. The spectrum presents a characteristic signal for paramagnetic Ru(III) complex with parameters $g_1 = 2.627, g_2 = g_3 = 2.20$ [93,94], which is consistent with the proposed photolysis scheme in which a ruthenium(III) complex with the $\{\text{V}^{\text{V}}\text{-Ru}^{\text{III}}(\text{solvent})\}$ fragment is formed. Thereby, the vacant coordination site after NO release is apparently occupied by the solvent molecule.

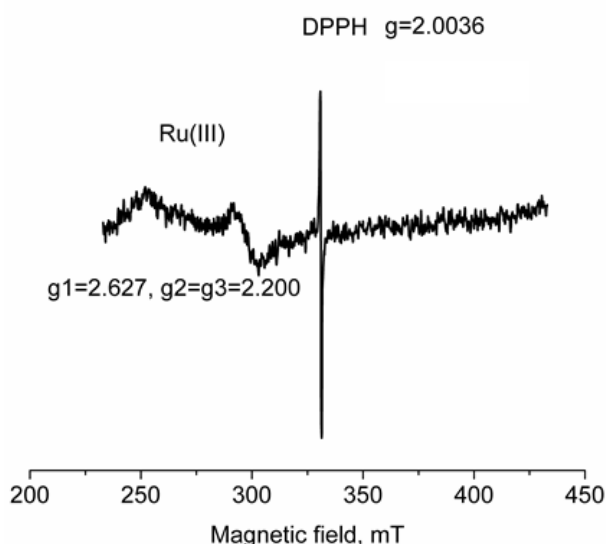


Fig. 6. EPR spectrum of complex I in acetonitrile after 60 min of 445 nm irradiation.

3.3. Photo-induced nitrosyl isomerization in solid state

The light irradiation of I in solution leads to the labilization of the NO^+ ligand followed by NO^0 release, whereas at temperatures below 273 K the bond isomers of nitrosyl ligand could exist. IR spectroscopy is an extremely sensitive method to verify the appearance of such isomers (MS1 or/and MS2).

The IR spectrum of complex I at 10 K contains bands related to the $\delta(\text{NO}_2)$ frequency vibration at 821 cm^{-1} , $\nu(\text{V-O})$ band at 973 cm^{-1} , bands of $\nu(\mu\text{-NO}_2)$ bridge ligand at $1252, 1270$ and 1585 cm^{-1} , $\nu(\text{NO}_2)$ bands at $1326, 1416,$ and 1467 cm^{-1} , $\nu(\text{C-C})$ band of dbbpy ligand at 1618 cm^{-1} and the most intense $\nu(\text{NO})$ band at 1900 cm^{-1} .

(Fig. 7 and Fig. S4). Irradiation of the complex by light in the spectral range 365-405 nm results in the formation of a new band with maximum at 1750 cm^{-1} , assigned to the $\nu(\text{NO})$ stretching vibration of the MS1 isomer and accompanied by the decrease of the $\nu(\text{NO})$ band of GS (Fig. 7). The population of MS1 is about 5%. The band exhibits a shift to lower energies compared to the GS band by 150 cm^{-1} , which is characteristic for nitrosyl ruthenium complexes [2,12,71,95–97]. The concomitant decrease of intensities of the NO_2 bands is most probably related to the nitrosyl isomerization and partial NO release (see below) (Fig. S4). The sensitivity of NO_2 bands to the change of NO linkage was shown in [68].

According to DFT calculations, the formation of bond isomers can be described as follows. After the light excitation, the excited singlet state of MLCT nature tends to undergo inter-system crossing (ISC) to the triplet MLCT of the same nature [98,99]. The triplet as well as first excited singlet states are known to have bended Ru-N-O fragment [100]. The relaxation of triplet state ends up in a point on the ground state potential energy surface, which is far from equilibrium linear geometry. From here the majority of the population relaxes to the ground state, however, a small fraction of molecules can hop to the side-on coordinated nitrosyl state (MS2). This state can be excited in a similar fashion with two different triplets as a long-living intermediate; one is O-coordinated and another is N-coordinated. The N-coordinated triplet of MS2 relaxes to GS or MS2 while the O-coordinated triplet can end up as MS2 or as O-coordinated nitrosyl with an almost linear Ru-O-N fragment (MS1). The ratio of the ground state, metastable states and generated triplets depends on the relaxation dynamics on the triplet and singlet energy surfaces, ISC process, and absorptive properties of the metastable states. The MS2 needs a special protocol to be accumulated because it absorbs excitation more readily than O- or N-coordinated nitrosyl states. On the other hand, absorptive properties of the MS1 are similar to the GS absorption; thus, the MS1 can have a decent fraction [9] or even a dominative one [10] in a solid sample.

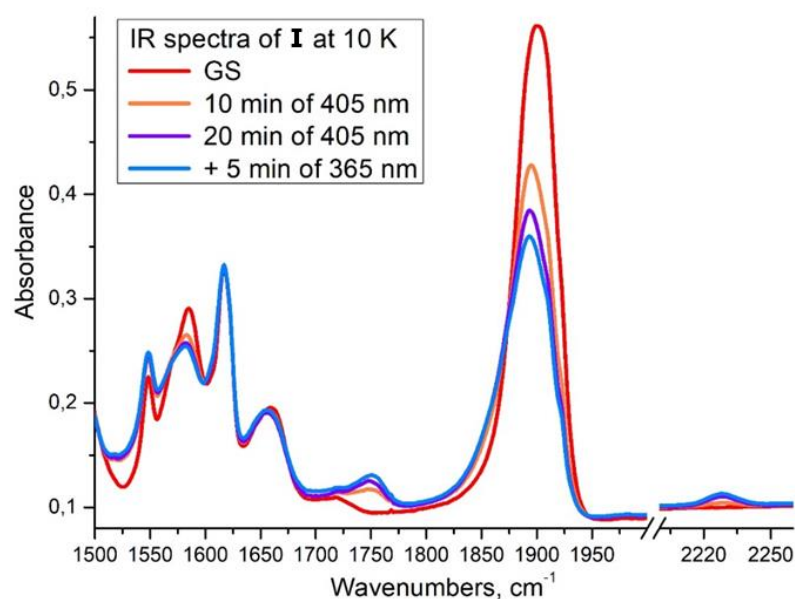


Fig. 7. IR spectra of **I** at 10 K in GS (red line), after 10 min of 405 nm irradiation (orange line), 20 min of 405 nm irradiation (purple line) and after subsequent 5 min of 365 nm irradiation (blue line).

The heating of MS1 from 10 to 140 K induces a decrease of the $\nu(\text{NO})$ band of MS1 and an increase of the corresponding GS band, indicating the complete decay of MS1 at 120-140 K (Fig. 8). The change of absorption bands corresponds to the back MS1→GS reaction [101]. Compared to related $\text{A}_2[\text{RuNO}(\text{NO}_2)_4\text{OH}]$ ($\text{A} = \text{NH}_4^+$ and K^+) and heterometallic $\{[\text{RuNO}(\text{NO}_2)_4\text{OH}]_2\text{Dy}_2(\text{H}_2\text{O})_2(\text{NO}_3)_2\}$ complexes [102–104], where MS1 decay occurs at 190-200 K, the thermal stability of MS1 isomer of **I** is much lower (120-140 K), which is likely due to presence of vanadium. An influence of a *trans*-to-NO ligand on the thermal stability of the MS1 was shown earlier [10,67,105]. According to that, higher electronegativity of *trans*-to-NO ligand increases the thermal stability of the MS1 isomer. On the other hand, a change of the ligands in *cis*-position to NO can lead to a decrease of the MS1 thermal stability as well. For example, the MS1 decay temperature of *trans*- $[\text{RuNOPy}_4\text{OH}](\text{PF}_6)_2$ (200-220 K) is much lower compared to *trans*- $[\text{RuNO}(\text{NH}_3)_4\text{OH}]\text{Cl}_2$ (260-280 K), in which pyridines (Py) are changed to ammine ligands [2,11]. Apparently, the decrease of the MS1 thermal stability of **I** is due to low activation energy of the MS1→GS transformation [9].

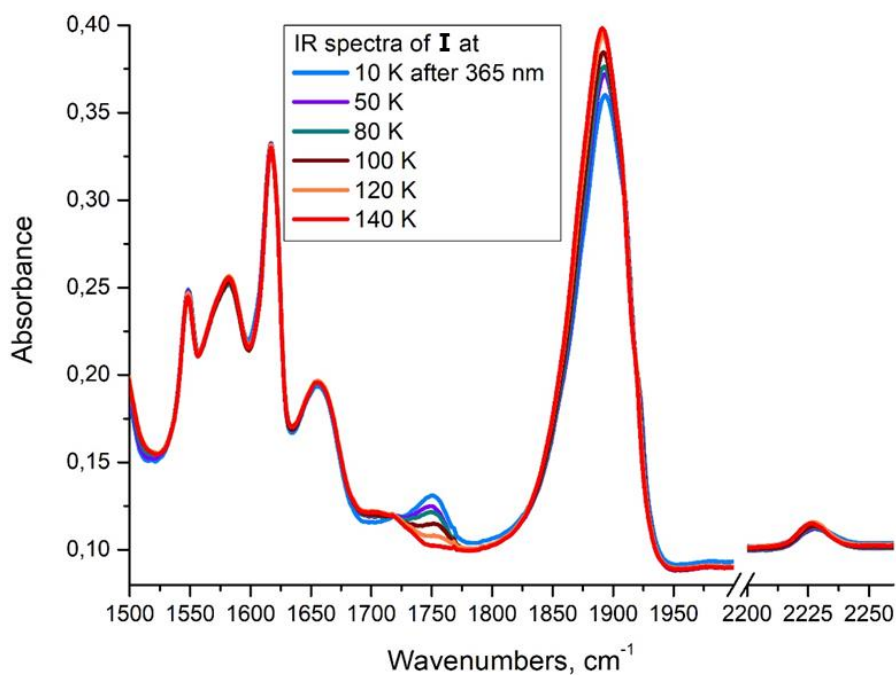


Fig. 8. IR spectra of **I** after MS1 generation (405 + 365 nm irradiation) at different temperatures: 10 K (blue line), 50 K (purple line), 80 K (green line), 100 K (brown line), 120 K (orange line) and 140 K (red line).

Besides of MS1 formation after light exposure, a band at 2228 cm^{-1} has appeared. The band reflects the formation of free nitrous oxide N_2O via NO release from the complex [106]. The N_2O formation after light exposure of nitrosyl ruthenium complexes in the solid state was reported earlier [10,69,107], however the mechanism of the formation is still obscure. The possible mechanism of N_2O formation in solution could comprise the formation of $\text{M}-(\kappa^2\text{-ONNO})$ intermediates (bonding through two oxygen atoms) [108]. In this regard, MS1 formation should favor $\text{M}-(\kappa^2\text{-ONNO})$ coordination, however further investigation is needed to clarify the mechanism.

It is worth mentioning that the $GS \leftrightarrow MS1$ reaction is a reversible process, meanwhile NO release with N_2O formation is an irreversible reaction. Thus, from the difference of the area under $\nu(NO)$ of GS before and after irradiation we estimated the amount of released NO, which is 40% from initial (Fig. S4). Complex I shows thus a noticeable sensitivity to the incident light. A similar behavior was found earlier in monomeric complexes $(PyH)[Ru(NO)(NO_2)_2(ONO)Py(OH)]$ and $[Ru(NO)(NO_2)(ONO)Py_2(OH)]$, where amount of NO release was found 50 and 20% respectively [69].

4. Conclusions

In this work, the binuclear $[Ru(NO)(NO_2)_3(CH_3COO)(O)VO(dbbpy)]$ complex is obtained from the pre-organized ruthenium $Na_2[Ru(NO)(NO_2)_4(OH)] \cdot 2H_2O$ and vanadium $[VO(dbbpy)(H_2O)Cl_2]$ precursors. This approach yielded a rare example of heterometallic nitrosyl ruthenium complex in quantitative yield. The complex is characterized by the single crystal X-ray diffraction and the structure of the complex is supported by the DFT calculations.

The complex is stable in acetonitrile solution, while light irradiation of the complex solution in the blue spectral range induces NO release. According to DFT, the light irradiation at 445 nm induces the charge transfer from NO_2 and dbbpy ligands to the antibonding orbitals of ON-Ru-O-V chain, which leads to the NO release reaction. The quantum yield of the Ru-NO photo-cleavage is $0.57 \pm 0.05\%$, which is relatively low with respect to the similar monomeric ruthenium nitrosyls. This peculiarity is due to the nature of antibonding orbitals, in which the presence of vanadium decreases the probability of a breaking of the Ru-NO bond, leading to a decrease of the efficiency of NO photo-release reaction. By the Griess test and EPR-spectroscopy the products of the photolysis (NO and paramagnetic Ru^{III} complex) are confirmed. The irradiation of the complex in a solid phase at 10 K results in the formation of a metastable bond isomer Ru-ON (MS1) as detected by IR-spectroscopy. The stretching vibration of $\nu(NO)$ band of MS1 (1750 cm^{-1}) is shifted by 150 cm^{-1} to lower energy with respect to the $\nu(NO)$ band of GS (1900 cm^{-1}). The population of the MS1 is about 5%. MS1 thermally decays at 120-140 K back to the GS, which is much lower compared to related monomeric complexes, in which MS1 decays at 190-200 K. Again, this feature is likely due to the presence of vanadium in the heterometallic complex. Besides of the MS1 formation, a partial formation of nitrous oxide N_2O via NO release is confirmed, however the mechanism of the reaction is uncertain.

In conclusion, the complex I represents a bifunctional platform, which can release nitric oxide in solution and reversibly switch the NO ligand coordination in the solid state. Though partial NO release in solid state is found, the degradation of the sample can be overcome by the adjustment of optical power. It is shown, that the presence of vanadium strongly influences the photochemical properties of ruthenium nitrosyl both in the solid phase and in solution. We suggest, that since unoccupied orbitals of an almost linear ON-Ru-O-V chain are found responsible for the efficiency of the nitric oxide release, the change of the arrangement of the vanadium center towards the Ru-N-O linkage will lead to the unprecedented change in the photochemical properties in any phase.

Declaration of Competing Interest

The authors declare no competing financial interest.

Acknowledgement

We thank Russian Foundation for Basic Research Grants No. 18-03-00155 for funding. Also we thank the Federal Agency for Scientific Organizations for funding. Artem Mikhailov is grateful for financial support from the Eiffel excellence bourse program (Grant P730329G).

Appendix A. Supplementary data

Supplementary material related to this article can be found, in the online version, at doi:<https://doi.org/10.1016/j.jphotochem.2018.12.037>.

References

- [1] M.J. Rose, P.K. Mascharak, Photoactive ruthenium nitrosyls: Effects of light and potential application as NO donors, *Coord. Chem. Rev.* 252 (2008) 2093–2114. doi:10.1016/j.ccr.2007.11.011.
- [2] P. Coppens, I. Novozhilova, A. Kovalevsky, Photoinduced linkage isomers of transition-metal nitrosyl compounds and related complexes, *Chem. Rev.* 102 (2002) 861–883. doi:10.1021/cr000031c.
- [3] H. Giglmeier, T. Kerscher, P. Klüfers, D. Schaniel, T. Woike, Nitric-oxide photorelease and photoinduced linkage isomerism on solid [Ru(NO)(terpy)(L)]BPh₄ (L = glycolate dianion), *Dalt. Trans.* 4 (2009) 9113. doi:10.1039/b912162e.
- [4] Z. Adhireksan, G.E. Davey, P. Campomanes, M. Groessler, C.M. Clavel, H. Yu, A.A. Nazarov, C.H.F. Yeo, W.H. Ang, P. Dröge, U. Rothlisberger, P.J. Dyson, C.A. Davey, Ligand substitutions between ruthenium-cymene compounds can control protein versus DNA targeting and anticancer activity, *Nat. Commun.* 5 (2014) 1–13. doi:10.1038/ncomms4462.
- [5] R.G. De Lima, B.R. Silva, R.S. Da Silva, L.M. Bendhack, Ruthenium complexes as NO donors for vascular relaxation induction, *Molecules.* 19 (2014) 9628–9654. doi:10.3390/molecules19079628.
- [6] E. Tfouni, D.R. Truzzi, A. Tavares, A.J. Gomes, L.E. Figueiredo, D.W. Franco, Biological activity of ruthenium nitrosyl complexes, *Nitric Oxide - Biol. Chem.* 26 (2012) 38–53. doi:10.1016/j.niox.2011.11.005.
- [7] D.D. Thomas, X. Liu, S.P. Kantrow, J.R. Lancaster, The biological lifetime of nitric oxide: implications for the perivascular dynamics of NO and O₂., *Proc. Natl. Acad. Sci. U. S. A.* 98 (2001) 355–360. doi:10.1073/pnas.98.1.355.
- [8] A.A. Mikhailov, D. V. Khantakova, V.A. Nichiporenko, E.M. Glebov, V.P. Grivin, V.F. Plyusnin, V. V. Yanshole, D. V. Petrova, G.A. Kostin, I.R. Grin, Photoinduced inhibition of DNA repair enzymes and the possible mechanism of photochemical transformations of the ruthenium nitrosyl complex [RuNO(β-Pic)₂(NO₂)₂OH], *Metallomics.* 11 (2019) 1999–2009. doi:10.1039/c9mt00153k.
- [9] A. Mikhailov, V. Vuković, C. Kijatkin, E. Wenger, M. Imlau, T. Woike, G. Kostin, D. Schaniel, Combining photoinduced linkage isomerism and nonlinear optical properties in ruthenium nitro-syl complexes, *Acta Crystallogr. Sect. B Struct. Sci. Cryst. Eng. Mater.* 75 (2019) 1152–1163. doi:10.1107/S205252061901357X.
- [10] A.A. Mikhailov, E. Wenger, G.A. Kostin, D. Schaniel, Room-Temperature Photogeneration of Nitrosyl Linkage Isomers in Ruthenium Nitrosyl Complexes, *Chem. – A Eur. J.* 25 (2019) 7569–7574. doi:10.1002/chem.201901205.

- [11] D. Schaniel, T. Woike, B. Delley, C. Boskovic, D. Biner, K.W. Krämer, H.U. Güdel, Long-lived light-induced metastable states in trans-[Ru(NH₃)₄(H₂O)NO]Cl₃·H₂O and related compounds, *Phys. Chem. Chem. Phys.* 7 (2005) 1164–1170. doi:10.1039/b415435e.
- [12] D. Schaniel, B. Cormary, I. Malfant, L. Valade, T. Woike, B. Delley, K.W. Krämer, H.U. Güdel, Photogeneration of two metastable NO linkage isomers with high populations of up to 76% in trans-[RuCl(py)₄(NO)][PF₆]₂·1/2H₂O, *Phys. Chem. Chem. Phys.* 9 (2007) 3717–3724. doi:10.1039/b704778a.
- [13] D. Schaniel, M. Imlau, T. Weisemoeller, T. Woike, K.W. Krämer, H.-U. Güdel, Photoinduced Nitrosyl Linkage Isomers Uncover a Variety of Unconventional Photorefractive Media, *Adv. Mater.* 19 (2007) 723–726. doi:10.1002/adma.200601378.
- [14] I.S. Fomenko, A.L. Gushchin, MONO- AND BINUCLEAR COMPLEXES OF 5 GROUP METALS WITH DIIMINE LIGANDS: SYNTHESIS, REACTIVITY AND PROSPECTS FOR APPLICATION, *Russ. Chem. Rev.* 89 (2020). doi:10.1070/rcr4949.
- [15] Y.S. Fomenko, A.L. Gushchin, A. V. Tkachev, E.S. Vasilyev, P.A. Abramov, V.A. Nadolinny, M.M. Syrokvashin, M.N. Sokolov, First oxidovanadium complexes containing chiral derivatives of dihydrophenanthroline and diazafluorene, *Polyhedron*. 135 (2017) 96–100. doi:10.1016/j.poly.2017.07.003.
- [16] I.S. Fomenko, S. Vincendeau, E. Manoury, R. Poli, P.A. Abramov, V.A. Nadolinny, M.N. Sokolov, A.L. Gushchin, An oxidovanadium(IV) complex with 4,4'-di-tert-butyl-2,2'-bipyridine ligand: Synthesis, structure and catalyzed cyclooctene epoxidation, *Polyhedron*. 177 (2020) 114305. doi:10.1016/j.poly.2019.114305.
- [17] I. Fomenko, A. Gushchin, P. Abramov, M. Sokolov, L. Shul'pina, N. Ikonnikov, M. Kuznetsov, A. Pombeiro, Y. Kozlov, G. Shul'pin, New Oxidovanadium(IV) Complexes with 2,2'-bipyridine and 1,10-phenanthroline Ligands: Synthesis, Structure and High Catalytic Activity in Oxidations of Alkanes and Alcohols with Peroxides, *Catalysts*. 9 (2019) 217. doi:10.3390/catal9030217.
- [18] I.S. Fomenko, A.L. Gushchin, L.S. Shul'pina, N.S. Ikonnikov, P.A. Abramov, N.F. Romashev, A.S. Poryvaev, A.M. Sheveleva, A.S. Bogomyakov, N.Y. Shmelev, M. V. Fedin, G.B. Shul'pin, M.N. Sokolov, New oxidovanadium(IV) complex with a BIAN ligand: synthesis, structure, redox properties and catalytic activity, *New J. Chem.* 42 (2018) 16200–16210. doi:10.1039/C8NJ03358G.
- [19] I.S. Fomenko, V.A. Nadolinny, N.N. Efimov, V. V. Kokovkin, A.L. Gushchin, Binuclear Oxidovanadium(IV) Complex with the Bridging Chloranilate Ligand: Synthesis and Magnetic Properties, *Russ. J. Coord. Chem. Khimiya*. 45 (2019) 776–781. doi:10.1134/S1070328419110022.
- [20] K.H. Thompson, C. Orvig, Coordination chemistry of vanadium in metallopharmaceutical candidate compounds, *Coord. Chem. Rev.* 219–221 (2001) 1033–1053. doi:10.1016/S0010-8545(01)00395-2.
- [21] K.H. Thompson, J.H. McNeill, C. Orvig, Vanadium Compounds as Insulin Mimics, *Chem. Rev.* 99 (1999) 2561–2571. doi:10.1021/cr980427c.
- [22] H. Sakurai, Y. Kojima, Y. Yoshikawa, K. Kawabe, H. Yasui, Antidiabetic vanadium(IV) and zinc(II) complexes, in: *Coord. Chem. Rev.*, Elsevier, 2002: pp. 187–198. doi:10.1016/S0010-8545(01)00447-7.
- [23] A. Bishayee, A. Waghray, M.A. Patel, M. Chatterjee, Vanadium in the detection, prevention and treatment of cancer: The in vivo evidence, *Cancer Lett.* 294 (2010) 1–12. doi:10.1016/j.canlet.2010.01.030.
- [24] D.C. Crans, A.M. Trujillo, P.S. Pharyzyn, M.D. Cohen, How environment affects drug activity: Localization, compartmentalization and reactions of a vanadium insulin-enhancing compound, dipicolinatooxovanadium(V), *Coord. Chem. Rev.* 255 (2011) 2178–2192. doi:10.1016/j.ccr.2011.01.032.
- [25] S. Takizawa, H. Gröger, H. Sasai, Vanadium in Asymmetric Synthesis: Emerging Concepts in Catalyst

- Design and Applications, Chem. - A Eur. J. 21 (2015) 8992–8997. doi:10.1002/chem.201406444.
- [26] G. Zhang, B.L. Scott, R. Wu, L.A.P. Silks, S.K. Hanson, Aerobic oxidation reactions catalyzed by vanadium complexes of bis(phenolate) ligands, *Inorg. Chem.* 51 (2012) 7354–7361. doi:10.1021/ic3007525.
- [27] S.K. Hanson, R. Wu, L.A. “Pete” Silks, C-C or C-O Bond Cleavage in a Phenolic Lignin Model Compound: Selectivity Depends on Vanadium Catalyst, *Angew. Chemie.* 124 (2012) 3466–3469. doi:10.1002/ange.201107020.
- [28] S.K. Hanson, R.T. Baker, J.C. Gordon, B.L. Scott, L.A.P. Silks, D.L. Thorn, Mechanism of alcohol oxidation by dipicolinate vanadium(V): Unexpected role of pyridine, *J. Am. Chem. Soc.* 132 (2010) 17804–17816. doi:10.1021/ja105739k.
- [29] J. Roček, D.E. Aylward, One-Electron vs. Two-Electron Oxidations. Vanadium(V) Oxidation of Cyclobutanols, *J. Am. Chem. Soc.* 97 (1975) 5452–5456. doi:10.1021/ja00852a021.
- [30] T. Hirao, M. Mori, Y. Ohshiro, VO(OR)Cl₂-Induced Oxidative Aromatization of α,β -Unsaturated Cyclohexenones, *J. Org. Chem.* 55 (1990) 358–360. doi:10.1021/jo00288a065.
- [31] K.I. Smith, L.L. Borer, M.M. Olmstead, Vanadium(IV) and Vanadium(V) Complexes of Salicyladimine Ligands, *Inorg. Chem.* 42 (2003) 7410–7415. doi:10.1021/ic034640p.
- [32] C.J. Chang, J.A. Labinger, H.B. Gray, Aerobic Epoxidation of Olefins Catalyzed by Electronegative Vanadyl Salen Complexes, *Inorg. Chem.* 36 (1997) 5927–5930. doi:10.1021/ic970824q.
- [33] R.R. Langeslay, D.M. Kaphan, C.L. Marshall, P.C. Stair, A.P. Sattelberger, M. Delferro, Catalytic Applications of Vanadium: A Mechanistic Perspective, *Chem. Rev.* 119 (2019) 2128–2191. doi:10.1021/acs.chemrev.8b00245.
- [34] G.B. Shul’pin, *Comprehensive Inorganic Chemistry II (Second Edition): From Elements to Applications*, in: J. Reedijk, K. Poeppelmeier, L. Casella (Eds.), *Compr. Inorg. Chem. II*, Elsevier, 2013: pp. 79–104.
- [35] P.K. Sasmal, S. Saha, R. Majumdar, R.R. Dighe, A.R. Chakravarty, Oxovanadium(IV)-based near-IR PDT agents: Design to biological evaluation, *Chem. Commun.* 0 (2009) 1703–1705. doi:10.1039/b822229k.
- [36] S. Banerjee, P. Prasad, A. Hussain, I. Khan, P. Kondaiah, A.R. Chakravarty, Remarkable photocytotoxicity of curcumin in HeLa cells in visible light and arresting its degradation on oxovanadium(IV) complex formation, *Chem. Commun.* 48 (2012) 7702–7704. doi:10.1039/c2cc33576j.
- [37] P. Prasad, I. Khan, P. Kondaiah, A.R. Chakravarty, Mitochondria-Targeting Oxidovanadium(IV) Complex as a Near-IR Light Photocytotoxic Agent, *Chem. – A Eur. J.* 19 (2013) 17445–17455. doi:10.1002/chem.201303487.
- [38] L. Li, Z. Guo, Q. Zhang, T. Xu, D. Wang, An unexpected oxovanadium(IV) complex with in situ generated lactone ligand: Synthesis, crystal structure and DNA-binding property, *Inorg. Chem. Commun.* 13 (2010) 1166–1169. doi:10.1016/j.inoche.2010.06.040.
- [39] S. Banerjee, A. Dixit, A.A. Karande, A.R. Chakravarty, Endoplasmic reticulum targeting tumour selective photocytotoxic oxovanadium(IV) complexes having vitamin-B6 and acridinyl moieties, *Dalt. Trans.* 45 (2016) 783–796. doi:10.1039/c5dt03412d.
- [40] H. Kumagai, S. Kitagawa, M. Maekawa, S. Kawata, H. Kiso, M. Munakata, Preparation, crystal structures and spectroscopic properties of vanadium(III) complexes with [V-O-V]⁴⁺ cores, *J. Chem. Soc. Dalt. Trans.* (2002) 2390–2396. doi:10.1039/b106517n.
- [41] S. Zhai, Q. Guo, J. Dong, T. Xu, L. Li, An oxovanadium(IV) complex of an l-serine Schiff base and 1,10-phenanthroline: Synthesis, crystal structure, and DNA and albumin-binding properties, *Transit. Met. Chem.* 39 (2014) 271–280. doi:10.1007/s11243-014-9800-6.

- [42] D. Wischang, O. Brücher, J. Hartung, Bromoperoxidases and functional enzyme mimics as catalysts for oxidative bromination-A sustainable synthetic approach, *Coord. Chem. Rev.* 255 (2011) 2204–2217. doi:10.1016/j.ccr.2011.04.003.
- [43] A. Butler, J.N. Carter-Franklin, The role of vanadium bromoperoxidase in the biosynthesis of halogenated marine natural products, *Nat. Prod. Rep.* 21 (2004) 180–188. doi:10.1039/b302337k.
- [44] A. Butler, Mechanistic considerations of the vanadium haloperoxidases, *Coord. Chem. Rev.* 187 (1999) 17–35. doi:10.1016/S0010-8545(99)00033-8.
- [45] B.J. Hales, E.E. Case, J.E. Morningstar, M.F. Dzeda, L.A. Mauterer, Isolation of a new vanadium-containing nitrogenase from *Azotobacter vinelandii*, *Biochemistry.* 25 (1986) 7251–7255. doi:10.1021/bi00371a001.
- [46] R.L. Robson, R.R. Eady, T.H. Richardson, R.W. Miller, M. Hawkins, J.R. Postgate, The alternative nitrogenase of *Azotobacter chroococcum* is a vanadium enzyme, *Nature.* 322 (1986) 388–390. doi:10.1038/322388a0.
- [47] R. Hotzelmann, K. Wieghardt, U. Flörke, H.-J. Haupt, Asymmetric Heterodinuclear[L’Ru(μ -O)(μ -CH₃CO₂)₂ML]²⁺ Complexes (M=Fe, Mn, V): Electronic Structure and Magnetic Properties, *Angew. Chemie Int. Ed. English.* 29 (1990) 645–647. doi:10.1002/anie.199006451.
- [48] G.A. Kostin, A.O. Borodin, N.A. Kryuchkova, N. V. Kurat’Eva, A.I. Boronin, R. V. Gulyaev, Electronic structures of heterometallic complexes [Ru(NO)(NO₂)₄(OH)ZnL_n] according to the data of quantum-chemical calculations and photoelectron spectroscopy, *Russ. J. Coord. Chem. Khimiya.* 38 (2012) 535–544. doi:10.1134/S107032841207007X.
- [49] N. M. Sinitsyn, V.N. Pichkov, O.E. Zvyagintsev, Extraction of ruthenium nitrosonitro complexes by amines, *Radiokhimiya.* 8 (1966) 545–555.
- [50] A.A. Mikhailov, V.A. Vorobyev, V.A. Nadolniny, Y. V. Patrushev, Y.S. Yudina, G.A. Kostin, Primary and secondary photochemical transformations of biologically active precursor - Nitro-Nitrosyl ruthenium complex, *J. Photochem. Photobiol. A Chem.* 373 (2019) 37–44. doi:10.1016/j.jphotochem.2018.12.037.
- [51] SHELDRICK, G. M., Program for Empirical Absorption Correction of Area Detector Data, SADABS. (1996). <https://ci.nii.ac.jp/naid/10011313791/> (accessed June 16, 2019).
- [52] G.M. Sheldrick, SHELXT – Integrated space-group and crystal-structure determination, *Acta Crystallogr. Sect. A Found. Adv.* 71 (2015) 3–8. doi:10.1107/S2053273314026370.
- [53] C. Fonseca Guerra, J.G. Snijders, G. Te Velde, E.J. Baerends, Towards an order-N DFT method, *Theor. Chem. Acc.* 99 (1998) 391–403. doi:10.1007/s002140050353.
- [54] G. te Velde, F.M. Bickelhaupt, E.J. Baerends, C. Fonseca Guerra, S.J.A. van Gisbergen, J.G. Snijders, T. Ziegler, Chemistry with ADF, *J. Comput. Chem.* 22 (2001) 931–967. doi:10.1002/jcc.1056.
- [55] ADF2016, *Theor. Chem.* (n.d.). <http://www.scm.com>.
- [56] S.H. Vosko, L. Wilk, M. Nusair, Accurate spin-dependent electron liquid correlation energies for local spin density calculations: a critical analysis, *Can. J. Phys.* 58 (1980) 1200–1211. doi:10.1139/p80-159.
- [57] C. Lee, W. Yang, R.G. Parr, Development of the Colle-Salvetti correlation-energy formula into a functional of the electron density, *Phys. Rev. B.* 37 (1988) 785–789. doi:10.1103/PhysRevB.37.785.
- [58] A.D. Becke, Density-functional thermochemistry. III. The role of exact exchange, *J. Chem. Phys.* 98 (1993) 5648–5652. doi:10.1063/1.464913.
- [59] P.J. Stephens, F.J. Devlin, C.F. Chabalowski, M.J. Frisch, Ab Initio calculation of vibrational absorption and circular dichroism spectra using density functional force fields, *J. Phys. Chem.* 98 (1994) 11623–11627. doi:10.1021/j100096a001.

- [60] E. Van Lenthe, E.J. Baerends, Optimized Slater-type basis sets for the elements 1-118, *J. Comput. Chem.* 24 (2003) 1142–1156. doi:10.1002/jcc.10255.
- [61] E. Van Lenthe, Geometry optimizations in the zero order regular approximation for relativistic effects, *J. Chem. Phys.* 110 (1999) 8943–8953. doi:10.1063/1.478813.
- [62] E. Van Lenthe, E.J. Baerends, J.G. Snijders, Relativistic total energy using regular approximations, *J. Chem. Phys.* 101 (1994) 9783–9792. doi:10.1063/1.467943.
- [63] E. Van Lenthe, E.J. Baerends, J.G. Snijders, Relativistic regular two-component Hamiltonians, *J. Chem. Phys.* 99 (1993) 4597–4610. doi:10.1063/1.466059.
- [64] C.C. Pye, T. Ziegler, An implementation of the conductor-like screening model of solvation within the Amsterdam density functional package, *Theor. Chem. Acc.* 101 (1999) 396–408. doi:10.1007/s002140050457.
- [65] N.L. Allinger, X. Zhou, J. Bergsma, Molecular mechanics parameters, *J. Mol. Struct. THEOCHEM.* 312 (1994) 69–83. doi:10.1016/S0166-1280(09)80008-0.
- [66] S.J.A. Van Gisbergen, J.G. Snijders, E.J. Baerends, Implementation of time-dependent density functional response equations, 1999.
- [67] G.A. Kostin, A.A. Mikhailov, N. V. Kuratieva, D.P. Pishchur, A.N. Makhinya, High thermal stability of the Ru-ON (MS1) linkage isomer of the ruthenium nitrosyl complex $[\text{RuNO}(\text{Py})_4\text{F}](\text{ClO}_4)_2$ with the trans NO-Ru-F coordinate, *New J. Chem.* 42 (2018) 18928–18934. doi:10.1039/c8nj04620d.
- [68] G.A. Kostin, A.O. Borodin, A.A. Mikhailov, N. V. Kuratieva, B.A. Kolesov, D.P. Pishchur, T. Woike, D. Schaniel, Photocrystallographic, Spectroscopic, and Calorimetric Analysis of Light-Induced Linkage NO Isomers in $[\text{RuNO}(\text{NO}_2)_2\text{-(pyridine)}_2\text{OH}]$, *Eur. J. Inorg. Chem.* 2015 (2015) 4905–4913. doi:10.1002/ejic.201500702.
- [69] G.A. Kostin, A.A. Mikhailov, N. V. Kuratieva, S. V. Tkachev, D. Schaniel, T. Woike, Reaction of $[\text{RuNO}(\text{NO}_2)_4\text{OH}]^{2-}$ with Sulfamic Acid as a Pathway to Mixed Nitro Pyridine Ruthenium Nitrosyl Complexes, *Eur. J. Inorg. Chem.* 2016 (2016) 4045–4053. doi:10.1002/ejic.201600477.
- [70] G.A. Kostin, A.A. Mikhailov, N. V. Kuratieva, D.P. Pischur, D.O. Zharkov, I.R. Grin, Influence of pyridine-like ligands on the structure, photochemical and biological properties of nitro-nitrosyl ruthenium complexes, *New J. Chem.* 41 (2017) 7758–7765. doi:10.1039/c7nj01602f.
- [71] G.A. Kostin, V. Vorobyev, A.A. Mikhailov, N. V. Kuratieva, Ruthenium nitrosyl complexes $[\text{RuNOL}_2(\text{NO}_2)_2\text{OH}]$ with ethyl isonicotinate and pyrazine: Synthesis, structure and formation of metastable linkage isomers, *J. Mol. Struct.* 1193 (2019) 334–341. doi:10.1016/j.molstruc.2019.05.012.
- [72] V. Vorobyev, E. V. Kabin, V.A. Emelyanov, I.A. Baidina, I. V. Korolkov, Synthesis and crystal structure of mer-nitroaquatriamminenitrosylruthenium(II) nitrate $[\text{RuNO}(\text{NH}_3)_3(\text{NO}_2)(\text{H}_2\text{O})](\text{NO}_3)_2$, *Inorg. Chem. Commun.* 68 (2016) 1–3. doi:10.1016/j.inoche.2016.03.019.
- [73] V. Vorobyev, V.A. Emelyanov, O.A. Plusnina, E.M. Makarov, I.A. Baidina, A.I. Smolentsev, S. V. Tkachev, T.I. Asanova, Triamine *fac* and *mer* Coordination for Ruthenium-Nitrosyl Complexes: Synthesis and Characterization of $[\text{RuNO}(\text{NH}_3)_3\text{Cl}_2]\text{Cl}$, *Eur. J. Inorg. Chem.* 2017 (2017) 971–978. doi:10.1002/ejic.201601233.
- [74] V. Vorobyev, V.A. Emelyanov, I.A. Valuev, I.A. Baidina, Nitrosyl cis-dichlorodiammine ruthenium complex with bridging H_3O_2^- ligand, *Inorg. Chem. Commun.* 76 (2017) 40–43. doi:10.1016/j.inoche.2016.12.004.
- [75] V.A. Vorobyev, V.A. Emelyanov, I.A. Baidina, D.A. Piryazev, First example of crystal structure of the nitrosoruthenium(II) trinitrato complex, *J. Struct. Chem.* 58 (2017) 975–982. doi:10.1134/S0022476617050171.

- [76] M. Sutradhar, L.M.D.R.S. Martins, M.F.C. Guedes da Silva, A.J.L. Pombeiro, Oxidovanadium complexes with tridentate aroylhydrazone as catalyst precursors for solvent-free microwave-assisted oxidation of alcohols, *Appl. Catal. A Gen.* 493 (2015) 50–57. doi:10.1016/j.apcata.2015.01.005.
- [77] W. Plass, Synthesis and characterization of a VO³⁺ complex of a pentadentate amine alcohol ligand: Towards hydrolytically stable ligands forming model complexes for vanadium-dependent haloperoxidases, *Inorganica Chim. Acta.* 244 (1996) 221–229. doi:10.1016/0020-1693(95)04778-6.
- [78] G.J. Colpas, B.J. Hamstra, J.W. Kampf, V.L. Pecoraro, Preparation of VO³⁺ and VO²⁺ Complexes Using Hydrolytically Stable, Asymmetric Ligands Derived from Schiff Base Precursors, *Inorg. Chem.* 33 (1994) 4669–4675. doi:10.1021/ic00099a017.
- [79] M. Tassé, H.S. Mohammed, C. Sabourdy, S. Mallet-Ladeira, P.G. Lacroix, I. Malfant, Synthesis, crystal structure, spectroscopic, and photoreactive properties of a ruthenium(II)-mononitrosyl complex, *Polyhedron.* 119 (2016) 350–358. doi:10.1016/j.poly.2016.09.010.
- [80] V. Vorobyev, D.S. Budkina, A.N. Tarnovsky, Femtosecond Excited-State Dynamics and Nitric Oxide Photorelease in a Prototypical Ruthenium Nitrosyl Complex, *J. Phys. Chem. Lett.* 11 (2020) 4639–4643. doi:10.1021/acs.jpcllett.0c01105.
- [81] E. Tfouni, M. Krieger, B.R. McGarvey, D.W. Franco, Structure, chemical and photochemical reactivity and biological activity of some ruthenium amine nitrosyl complexes, *Coord. Chem. Rev.* 236 (2003) 57–69. doi:10.1016/S0010-8545(02)00177-7.
- [82] J. Bordini, D.L. Hughes, J.D. Da Motta Neto, C.J. Da Cunha, Nitric oxide photorelease from ruthenium salen complexes in aqueous and organic solutions, *Inorg. Chem.* 41 (2002) 5410–5416. doi:10.1021/ic011273d.
- [83] M. Bocé, M. Tassé, S. Mallet-Ladeira, F. Pillet, C. Da Silva, P. Vicendo, P.G. Lacroix, I. Malfant, M.P. Rols, Effect of trans(NO, OH)-[RuFT(Cl)(OH)NO](PF₆) ruthenium nitrosyl complex on methicillin-resistant *Staphylococcus epidermidis*, *Sci. Rep.* 9 (2019) 1–8. doi:10.1038/s41598-019-41222-0.
- [84] I. Sasaki, S. Amabilino, S. Mallet-Ladeira, M. Tassé, A. Sournia-Saquet, P.G. Lacroix, I. Malfant, Further studies on the photoreactivities of ruthenium-nitrosyl complexes with terpyridyl ligands, *New J. Chem.* 43 (2019) 11241–11250. doi:10.1039/c9nj02398d.
- [85] J. Akl, I. Sasaki, P.G. Lacroix, V. Hugues, P. Vicendo, M. Bocé, S. Mallet-Ladeira, M. Blanchard-Desce, I. Malfant, Trans - And cis -(Cl,Cl)-[Ru^{II}(FT)Cl₂(NO)](PF₆): Promising candidates for NO release in the NIR region, *Photochem. Photobiol. Sci.* 15 (2016) 1484–1491. doi:10.1039/c6pp00181e.
- [86] W. Schneider, G.K. Moortgat, G.S. Tyndall, J.P. Burrows, Absorption cross-sections of NO₂ in the UV and visible region (200 - 700 nm) at 298 K, *J. Photochem. Photobiol. A Chem.* 40 (1987) 195–217. doi:10.1016/1010-6030(87)85001-3.
- [87] T.F. Redmond, B.B. Wayland, Dimerization of nitrogen dioxide in solution: A comparison of solution thermodynamics with the gas phase, *J. Phys. Chem.* 72 (1968) 1626–1629. doi:10.1021/j100851a040.
- [88] P. Neta, R.E. Huie, A.B. Ross, Rate Constants for Reactions of Inorganic Radicals in Aqueous Solution, *J. Phys. Chem. Ref. Data.* 17 (1988) 1027–1284. doi:10.1063/1.555808.
- [89] M. Ottolenghi, J. Rabani, Photochemical generation of nitrogen dioxide in aqueous solutions, *J. Phys. Chem.* 72 (1968) 593–598. doi:10.1021/j100848a600.
- [90] K. Ghosh, S. Kumar, R. Kumar, U.P. Singh, Ruthenium(III) Cyclometalates Obtained by Site-Specific Orthometallation and Their Reactivity with Nitric Oxide: Photoinduced Release and Estimation of NO Liberated from the Ruthenium Nitrosyl Complexes, *Eur. J. Inorg. Chem.* 2012 (2012) 929–938. doi:10.1002/ejic.201101026.
- [91] R. Oliveira, C. Sella, C. Souprayen, E. Ait-Yahiatene, C. Slim, S. Griveau, L. Thouin, F. Bedioui, Development of a flow microsensor for selective detection of nitric oxide in the presence of hydrogen

- peroxide, *Electrochim. Acta.* 286 (2018) 365–373. doi:10.1016/j.electacta.2018.07.158.
- [92] R.E. Huie, The reaction kinetics of NO₂, *Toxicology.* 89 (1994) 193–216. doi:10.1016/0300-483X(94)90098-1.
- [93] T.D. Thangadurai, K. Natarajan, Tridentate Schiff base complexes of ruthenium(III) containing ONS/ONO donor atoms and their biocidal activities, *Transit. Met. Chem.* 26 (2001) 717–722. doi:10.1023/A:1012081112872.
- [94] N. Dharmaraj, K. Natarajan, Synthesis, characterisation, electrochemistry and biological activity of ruthenium(III) complexes containing N, S donor ligands and triphenylphosphine or triphenylarsine, *Synth. React. Inorg. Met. Chem.* 27 (1997) 601–618. doi:10.1080/00945719708000213.
- [95] V. Vorobyev, N.I. Alferova, V.A. Emelyanov, Infrared Detection with Temperature Sweep for Stability Determination of Ru-ON Metastable States, *Inorg. Chem.* 58 (2019) 1007–1011. doi:10.1021/acs.inorgchem.8b03067.
- [96] V. Vorobyev, G.A. Kostin, N. V. Kuratieva, V.A. Emelyanov, Two oxygen-coordinated metastable Ru-ON states for ruthenium mononitrosyl complex, *Inorg. Chem.* 55 (2016) 9158–9161. doi:10.1021/acs.inorgchem.6b01818.
- [97] V. Vorobyev, G.A. Kostin, I.A. Baidina, A.A. Mikhailov, I. V. Korolkov, V.A. Emelyanov, Synthesis of the Ruthenium Nitrosyl Complex with Coordinated Ammonia and Pyridine at Room Temperature, *Zeitschrift Für Anorg. Und Allg. Chemie.* 646 (2020) 58–64. doi:10.1002/zaac.201900246.
- [98] J. Sanz García, F. Alary, M. Boggio-Pasqua, I.M. Dixon, I. Malfant, J.L. Heully, Establishing the Two-Photon Linkage Isomerization Mechanism in the Nitrosyl Complex $\text{trans-}[\text{RuCl}(\text{NO})(\text{py})_4]^{2+}$ by DFT and TDDFT, *Inorg. Chem.* 54 (2015) 8310–8318. doi:10.1021/acs.inorgchem.5b00998.
- [99] F. Talotta, J.L. Heully, F. Alary, I.M. Dixon, L. González, M. Boggio-Pasqua, Linkage Photoisomerization Mechanism in a Photochromic Ruthenium Nitrosyl Complex: New Insights from an MS-CASPT2 Study, *J. Chem. Theory Comput.* 13 (2017) 6120–6130. doi:10.1021/acs.jctc.7b00982.
- [100] M. Kaneko, A. Kato, S. Nakashima, Y. Kitatsuji, Density Functional Theory (DFT)-Based Bonding Analysis Correlates Ligand Field Strength with 99Ru Mössbauer Parameters of Ruthenium-Nitrosyl Complexes, *Inorg. Chem.* 58 (2019) 14024–14033. doi:10.1021/acs.inorgchem.9b02024.
- [101] Y. Morioka, A. Ishikawa, H. Tomizavva, E.I. Miki, Light-induced metastable states in nitrosyl-ruthenium complexes containing ethylenediamine and oxalate ion ligands, *J. Chem. Soc. Dalton Trans.* (2000) 781–786. doi:10.1039/a906429j.
- [102] G.A. Kostin, A.O. Borodin, N. V. Kuratieva, A.S. Bogomyakov, A.A. Mikhailov, Tetranuclear Ru₂Ln₂ complexes of heavier lanthanides (Gd, Tb, Dy, Ho, Lu) with $[\text{RuNO}(\text{NO}_2)_4\text{OH}]^{2-}$ anion, combining SMM properties and photoswitchable Ru-NO group, *Inorganica Chim. Acta.* 479 (2018) 135–140. doi:10.1016/j.ica.2018.04.006.
- [103] G.A. Kostin, A.O. Borodin, N. V. Kuratieva, A.A. Mikhailov, P.E. Plusnin, Synthesis, structure and properties of $(\text{NH}_4)_2[\text{RuNO}(\text{NO}_2)_4\text{OH}]$ and $\text{NH}_4[\text{RuNO}(\text{L})(\text{NO}_2)_3\text{OH}]$ (L = NH₃, Py), *J. Mol. Struct.* 1176 (2019) 402–407. doi:10.1016/j.molstruc.2018.08.105.
- [104] T. Woike, S. Haussühl, Infrared-spectroscopic and differential scanning calorimetric studies of the two light-induced metastable states in $\text{K}_2[\text{Ru}(\text{NO}_2)_4(\text{OH})(\text{NO})]$, *Solid State Commun.* 86 (1993) 333–337. doi:10.1016/0038-1098(93)90384-Y.
- [105] R.D. Yamaletdinov, I.L. Zilberberg, The Effect of *trans* Ligands in the NO-Linkage Reverse Isomerization for Ruthenium-Nitrosyl-Tetraammine Complexes: A DFT Study, *Eur. J. Inorg. Chem.* 2017 (2017) 2951–2954. doi:10.1002/ejic.201700138.
- [106] R.L. Hudson, M.J. Loeffler, P.A. Gerakines, Infrared spectra and band strengths of amorphous and crystalline N₂O, *J. Chem. Phys.* 146 (2017) 024304. doi:10.1063/1.4973548.

- [107] E. Orłowska, M. V. Babak, O. Dömötör, E.A. Enyedy, P. Rapta, M. Zalibera, L. Bučinský, M. Malček, C. Govind, V. Karunakaran, Y.C.S. Farid, T.E. McDonnell, D. Luneau, D. Schaniel, W.H. Ang, V.B. Arion, NO Releasing and Anticancer Properties of Octahedral Ruthenium-Nitrosyl Complexes with Equatorial 1 H-Indazole Ligands, *Inorg. Chem.* 57 (2018) 10702–10717. doi:10.1021/acs.inorgchem.8b01341.
- [108] C. Gaviglio, J. Pellegrino, D. Milstein, F. Doctorovich, NO disproportionation by a {RhNO}₉ pincer-type complex, *Dalt. Trans.* 46 (2017) 16878–16884. doi:10.1039/c7dt03944a.

Solution and solid-state light-induced transformations in heterometallic vanadium-ruthenium nitrosyl complex

Iakov S. Fomenko^a, Artem A. Mikhailov^a, Vasily Vorobyev^a, Natalia V. Kuratieva^a, Gennadiy A. Kostin^a,
Dominik Schaniel^b, Vladimir A. Nadolnny^a, Artem L. Gushchin^a

^a Nikolaev Institute of Inorganic Chemistry SB RAS, 3 Acad. Lavrentiev Ave., Novosibirsk, 630090, Russia

^b Université de Lorraine, CNRS, CRM2, UMR 7036, Nancy 54000, France

Quantum yield calculation

DMSO solutions:

In the dissociative model for the DMSO dark case, the unimolecular kinetic was implemented as the reagent's concentration depends on time $C = C_0 \cdot e^{-kt}$. Total absorbance is equal to the sum of reagent (A) and products (B) absorbances:

$$A_{\text{tot}} = \varepsilon_a \cdot l \cdot C_a + \varepsilon_b \cdot l \cdot C_b \text{ (Eq. 1)}$$

Taking in account mentioned time-dependency, one can derive the following:

$$A_{\text{tot}} = \varepsilon_a \cdot l \cdot C_0 \cdot e^{-kt} + \varepsilon_b \cdot l \cdot C_0 \cdot (1 - e^{-kt}) = \varepsilon_b \cdot l \cdot C_0 + (\varepsilon_a - \varepsilon_b) \cdot l \cdot C_0 \cdot e^{-kt} \text{ (Eq. 2)}$$

The data were fitted at 283 and 318 nm where located the most pronounced changes. The best fit was achieved with the following parameters: $\varepsilon_a(318) = \varepsilon_a(283) = 12790$, $\varepsilon_b(318) = 6300$, $\varepsilon_b(283) = 18200 \text{ M}^{-1} \cdot \text{cm}^{-1}$, $k = 3.4 \pm 0.1 \cdot 10^{-4} \text{ s}^{-1}$.

Acetonitrile solutions:

In order to investigate dark reaction, firstly the acetonitrile solution was irradiated for several minutes in the spectrometer. The spectral changes were monitored during irradiation, Fig. 5. After that, the solution was kept in the instrument without irradiation and the spectral evolution was monitored over 0 - 50 minutes. The model absorbance for each data point in the 350-450 nm range was calculated from equation 2 of the Supplemental Information. The unknown spectrum at infinite time was fitted as four-polynomial function and it was different for different preparatory irradiation time. The first-order kinetic constant was wavelength independent. Thus, total 4040 experimental data points were fitted using six parameters only, which were five absorptions at 350, 375, 400, 425, and 450 nm at infinite time and one kinetic constant. These parameters were adjusted to minimize sum of squared residuals. The loss of absorbance as first experimental spectrum minus modeled spectrum at infinite time was plotted in Fig. S2.

The photolysis equation of the compound I as $\{\text{RuNOV}\} + h\nu \Rightarrow \{\text{RuV}\} + \text{NO}$ can be kinetically described as:

$$-\frac{d\{\text{RuNOV}\}}{dt} = q \cdot I_{\text{abs}} \cdot \varepsilon_{\text{RuNOV}} \cdot l \cdot \{\text{RuNOV}\} / (A_{\text{total}} \cdot V_{\text{total}}) = q \cdot \varepsilon_{\text{RuNOV}} \cdot l \cdot \{\text{RuNOV}\} \cdot I \cdot (1 - 10^{-A_{\text{total}}}) / (A_{\text{total}} \cdot V_{\text{total}})$$

where q is quantum yield, $\varepsilon_{\text{RuNOV}}$ is extinction coefficient of the compound I at the excitation wavelength, l is light pass length, I_{abs} is amount of absorbed light, I is light intensity, A_{total} is total absorbance at the excitation wavelength. The term $\frac{1 - 10^{-A_{\text{total}}}}{A_{\text{total}}}$ was approximated based on the experimental data as $f(t) = a_1 \cdot e^{-b_1 t} + a_2 \cdot e^{-b_2 t} + a_3 \cdot (t - b_3)^2 - a_4 \cdot (t - b_3) + c$ with 99% accuracy which is better than numerical error of absorbance values at excitation wavelength. Solving the differential equation gives the compound I concentration:

$\{\text{RuNOV}\} = C_0 \cdot \exp(-q \cdot \varepsilon_{\text{RuNOV}} \cdot l \cdot I \cdot (t \cdot (c + a_3 \cdot b_3^2 + a_4 \cdot b_3) - t^2 \cdot (a_3 \cdot b_3 + a_4/2) + a_3 \cdot t^3/3 + a_1 \cdot (1 - e^{-b_1 t})/b_1 + a_2 \cdot (1 - e^{-b_2 t})/b_2) / V_{\text{total}})$, where C_0 is the initial concentration of the complex I. The product concentration is $\{\text{RuV}\} = C_0 - \{\text{RuNOV}\}$.

Table S1. Experimental and refinement details of the [Ru(NO)(NO₂)₂(μ-NO₂)(μ-CH₃COO)(μ-O)VO(dbbpy)]·CH₃CN.

Empirical formula	C ₂₂ H ₃₀ N ₇ O ₁₁ RuV
Formula weight	720.54
Temperature/K	150(2)
Crystal system	monoclinic
Space group	P2 ₁ /n
a/Å	6.2399(12)
b/Å	16.601(3)
c/Å	28.271(5)
α/°	90
β/°	92.297(6)
γ/°	90
Volume/Å ³	2926.2(9)
Z	4
ρ _{calc} /g/cm ³	1.636
μ/mm ⁻¹	0.903
F(000)	1464.0
Crystal size/mm ³	0.140 × 0.140 × 0.010
Radiation	MoKα (λ = 0.71073)
2θ range for data collection/°	3.786 to 55.388
Index ranges	-8 ≤ h ≤ 7, -21 ≤ k ≤ 21, -35 ≤ l ≤ 36
Reflections collected	23713
Independent reflections	6761 [R _{int} = 0.0807, R _{sigma} = 0.0994]
Data/restraints/parameters	6761/58/387
Goodness-of-fit on F ²	1.163
Final R indexes [I ≥ 2σ (I)]	R ₁ = 0.1590, wR ₂ = 0.3298
Final R indexes [all data]	R ₁ = 0.1995, wR ₂ = 0.3434
Largest diff. peak/hole / e Å ⁻³	2.27/-1.82

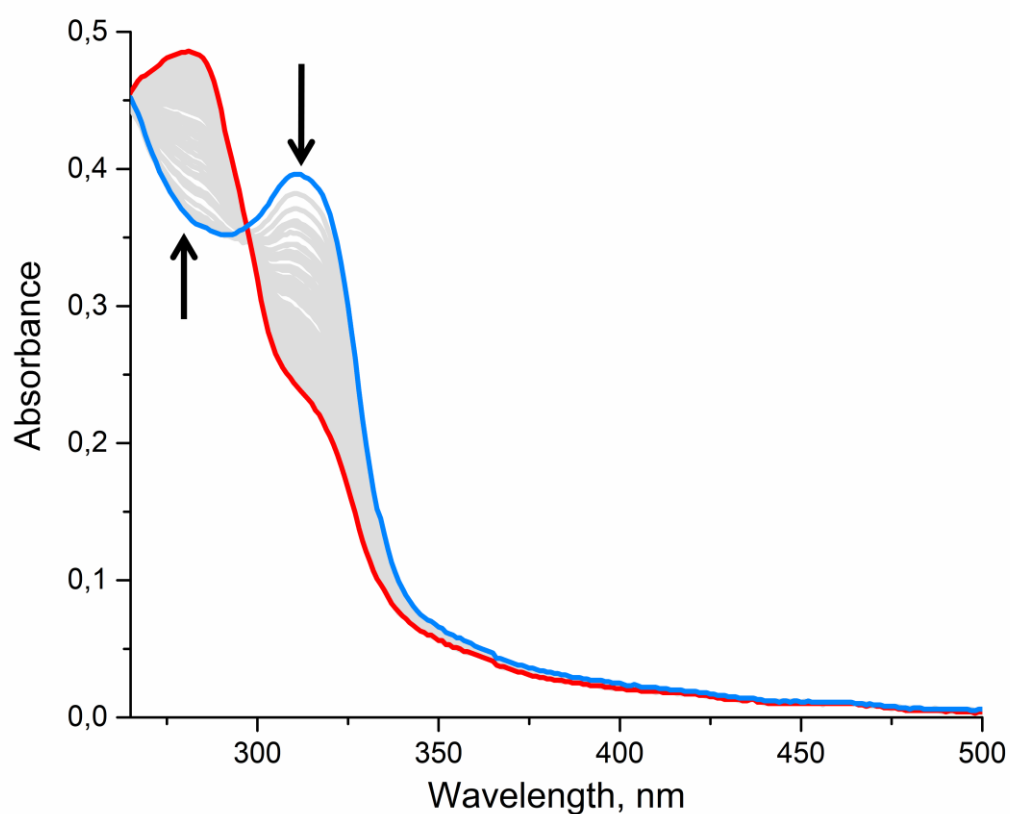


Fig. S1. The evolution of the $2.83 \cdot 10^{-5}$ M I in DMSO. Time interval between spectra is 77 seconds. The isosbestic point is observable at 298 nm with $12,400 \pm 400 \text{ M}^{-1} \cdot \text{cm}^{-1}$ molar absorptivity. For the decomposition process, the highest degree of change occurred at 318 nm for depression and at 283 nm for suppression of the absorbance. Implemented kinetic model took in account a unimolecular decomposition reaction fitted by a single exponential term. Estimated characteristic first-order constant was $3.4 \pm 0.1 \cdot 10^{-4} \text{ s}^{-1}$.

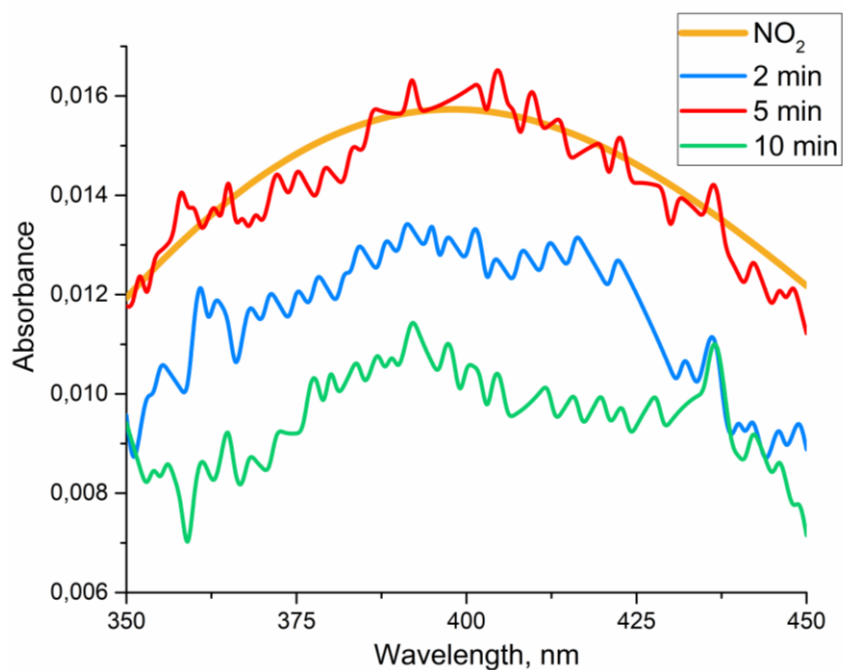


Fig. S2. The absorbance's loss of the solution kept in the dark, which was photolysed I for 2, 5, or 10 minutes. The smoothed data is scaled gas phase absorption data of nitrogen dioxide.

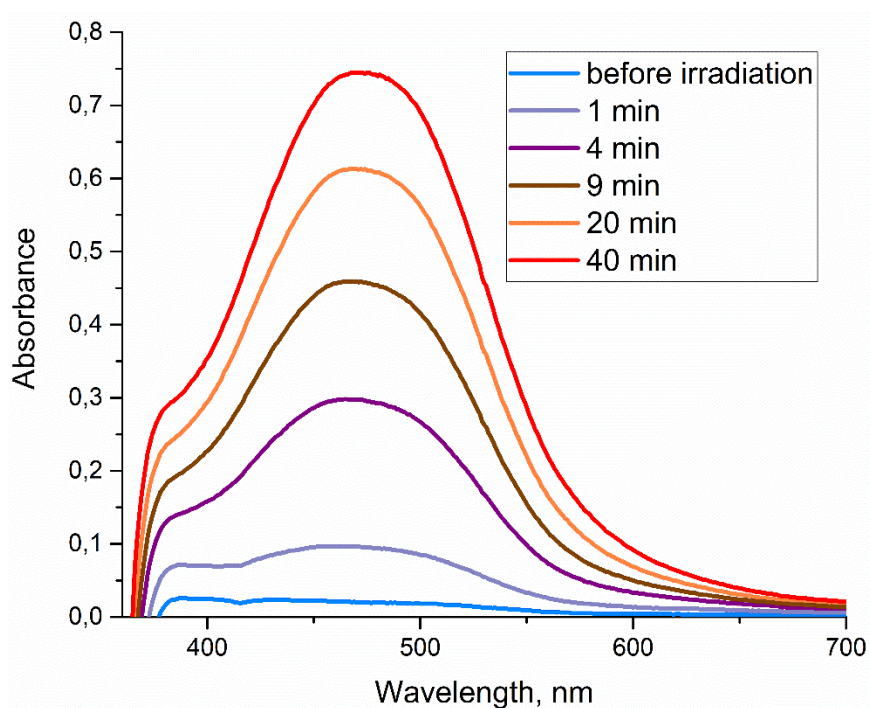


Fig. S3. The photolysis of the I ($4.8 \cdot 10^{-5}$ M) in the presence of Griess reagent after 445 nm light exposure.

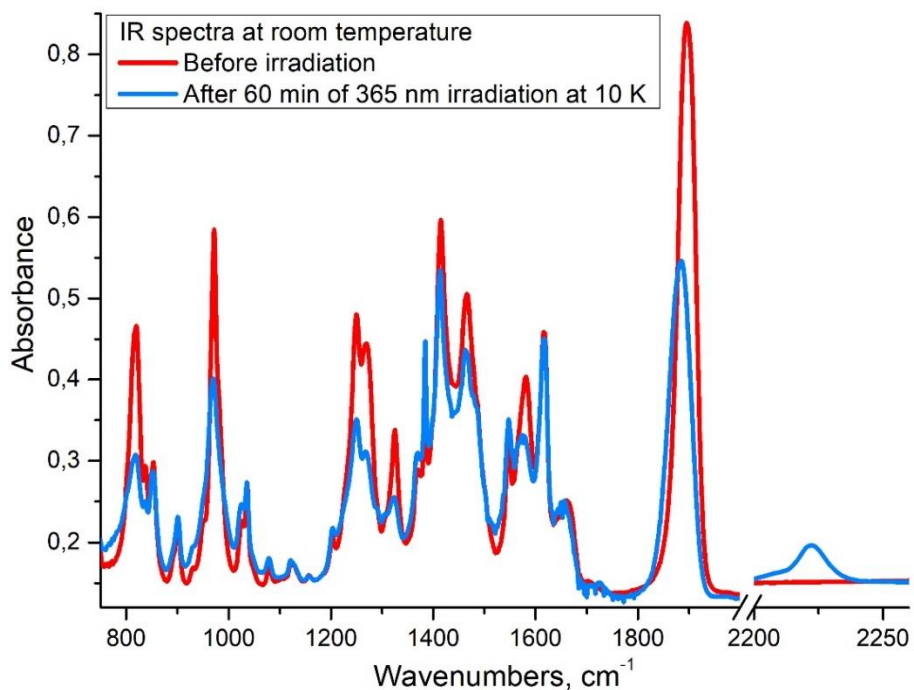
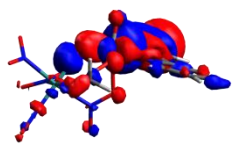
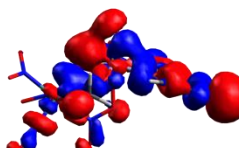
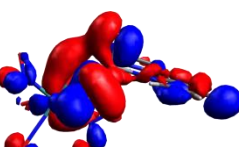
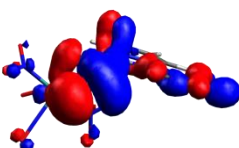
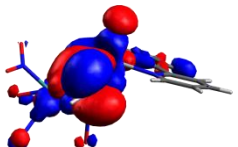
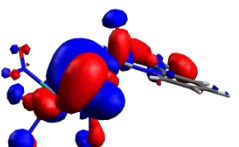
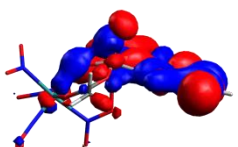
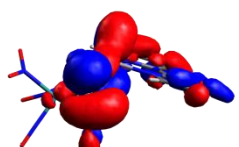
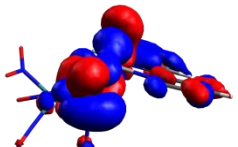
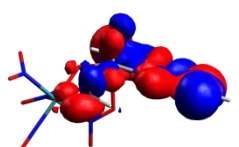
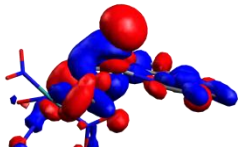
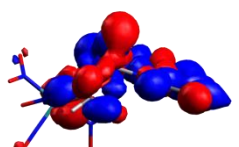
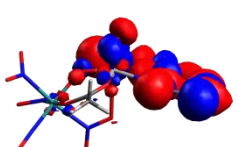
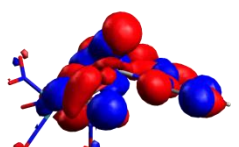
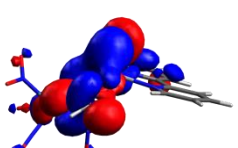
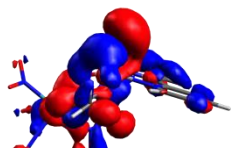


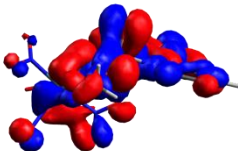
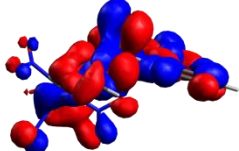
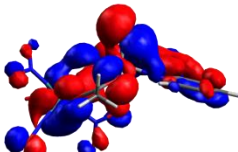
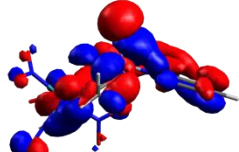
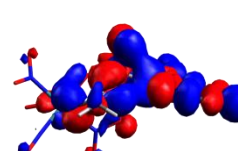
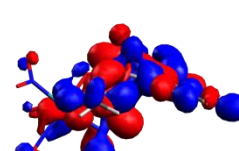
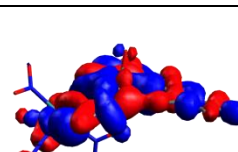
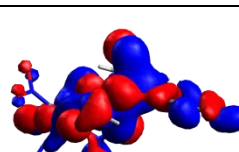
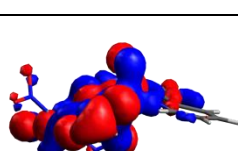
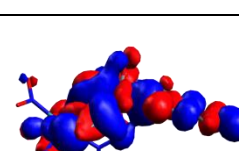
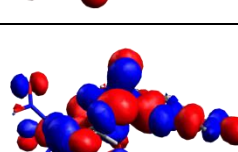
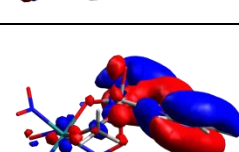
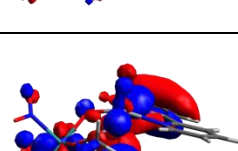
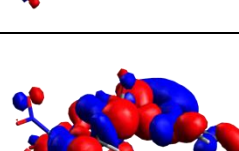
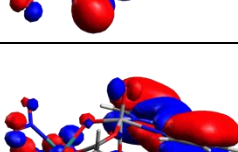
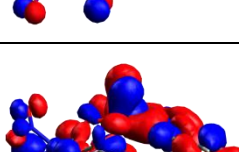
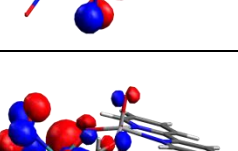
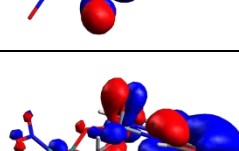
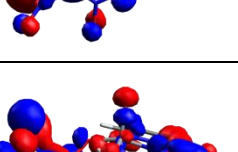
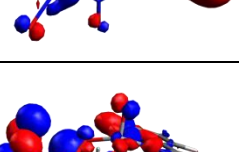
Fig. S4. IR spectra of I at room temperature (300 K) before (red line) and after 60 min 365 nm exposure at 10 K (blue line).

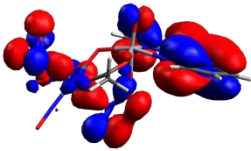
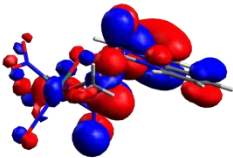
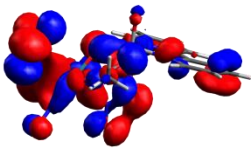
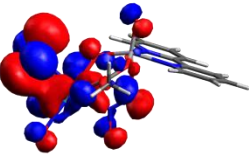
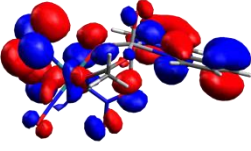
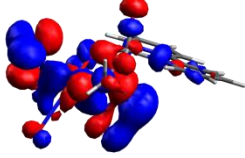
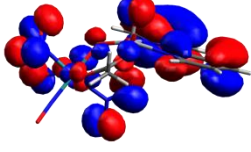
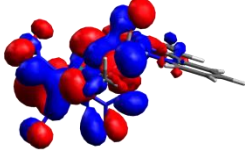
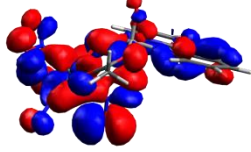
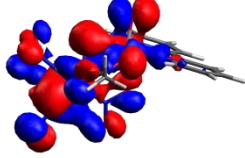
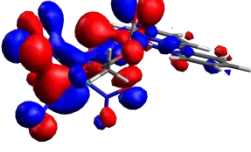
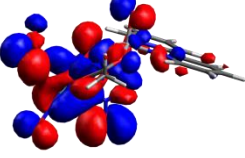
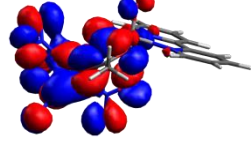
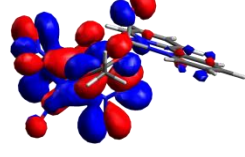
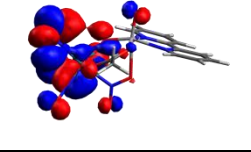
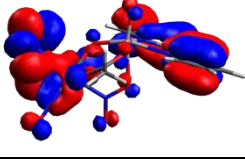
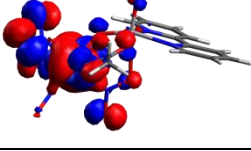
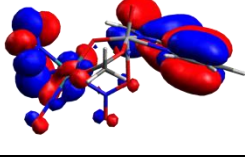
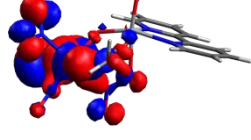
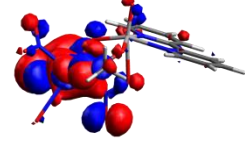
Table S2.

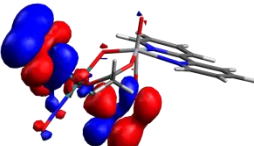
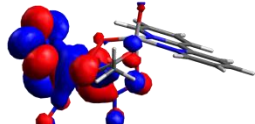
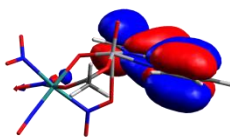
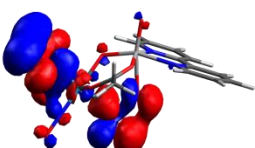
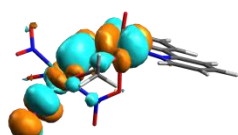
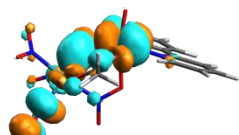
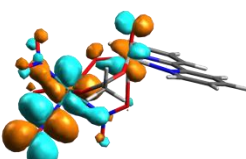
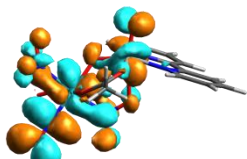
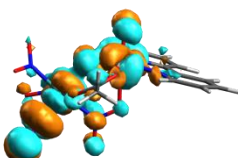
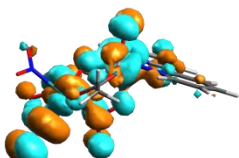
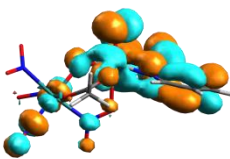
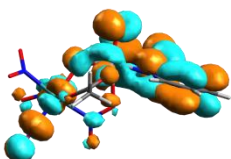
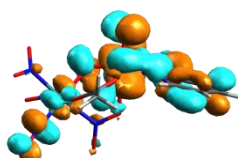
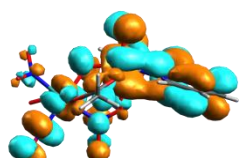
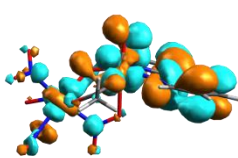
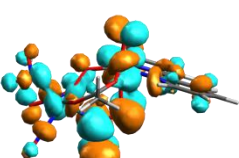
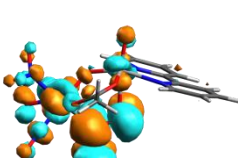
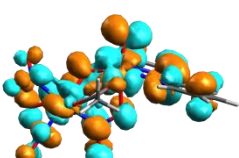
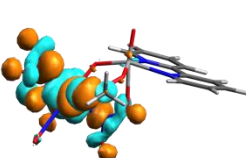
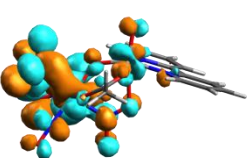
HOMO – 140, LUMO – 141. Zero energy – HOMO, shift is +6.517 eV for VWN, +7.457 eV for B3LYP

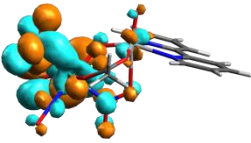
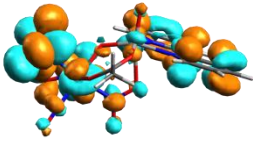
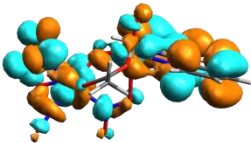
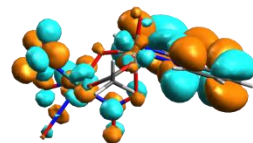
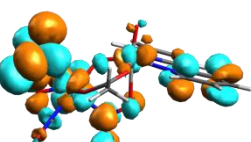
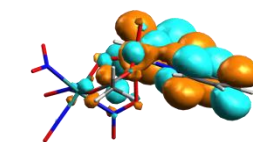
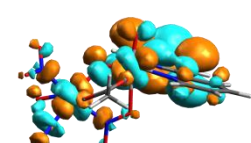
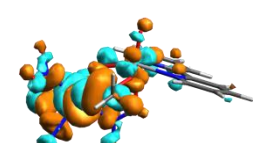
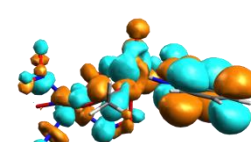
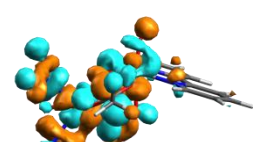
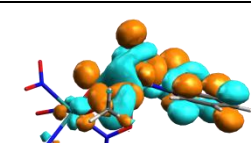
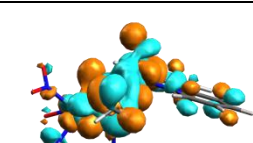
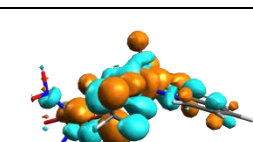
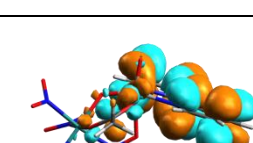
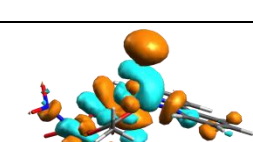
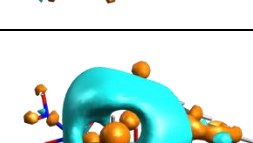
	B3LYP		VWN	
N	Energy, eV	MO	Energy, eV	MO
105			-5.116	
106			-5.02	
107			-4.896	
108			-4.717	

109			-4.607	
110			-4.192	
111			-4.016	
112			-3.876	
113	-3.816		-3.81	
114	-3.652		-3.504	
115	-3.605		-3.407	
116	-3.48		-3.29	
117	-3.416		-3.206	
118	-3.248		-3.145	

119	-2.773		-2.724	
120	-2.709		-2.695	
121	-2.37		-2.346	
122	-2.212		-2.299	
123	-2.194		-2.262	
124	-2.003		-2.104	
125	-1.795		-1.993	
126	-1.616		-1.943	
127	-1.565		-1.859	
128	-1.526		-1.783	

129	-1.421		-1.712	
130	-1.391		-1.632	
131	-1.383		-1.525	
132	-1.334		-1.336	
133	-1.189		-1.167	
134	-1.09		-1.12	
135	-0.977		-0.937	
136	-0.802		-0.689	
137	-0.537		-0.593	
138	-0.459		-0.495	

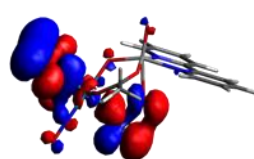
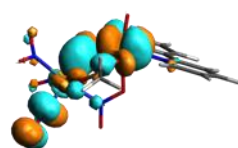
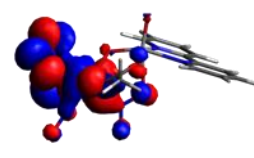
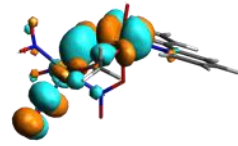
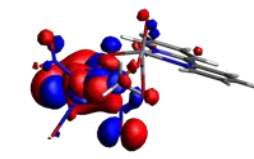
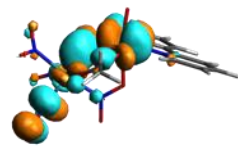
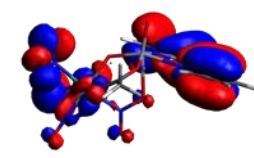
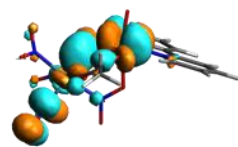
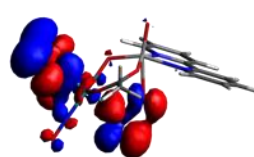
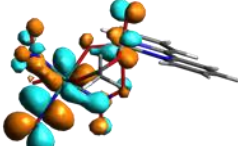
139	-0.025		-0.273	
140	0		0	
141	3.454		1.702	
142	3.928		2.318	
143	4.112		2.384	
144	4.333		2.537	
145	4.621		2.824	
146	4.915		3.046	
147	5.149		3.185	
148	5.414		3.376	

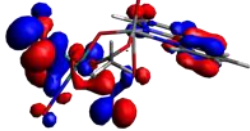
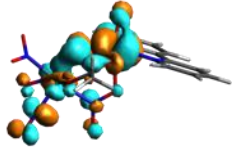
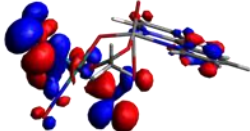
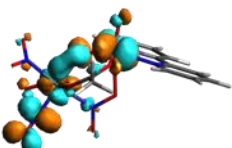
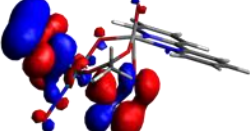
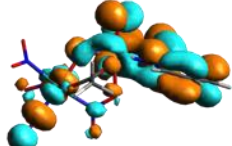
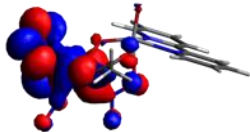
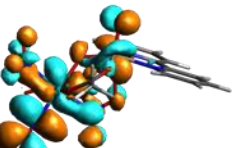
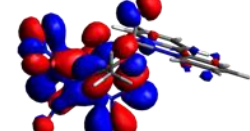
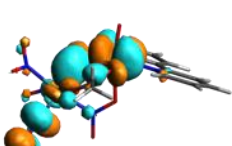
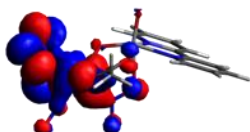
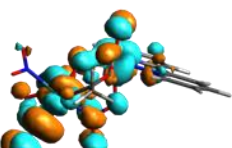
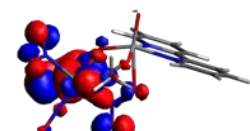
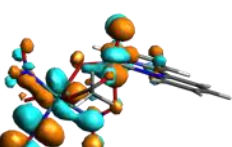
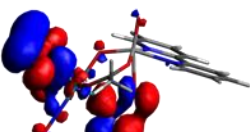
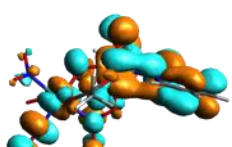
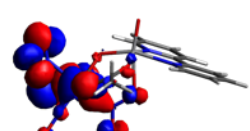
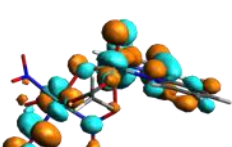
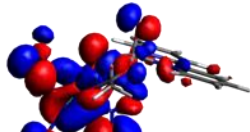
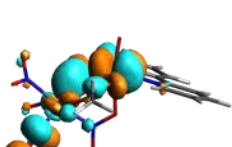
149	5.435		3.598	
150	5.586		3.686	
151	5.677		3.883	
152	5.775		3.958	
153	5.858		4.237	
154	6.165		4.443	
155			4.9	
156			5.11	
157			5.722	
158			6.016	

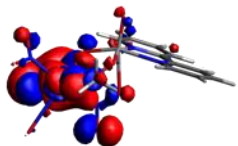
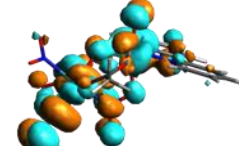
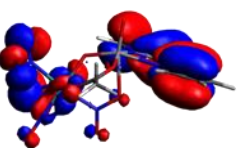
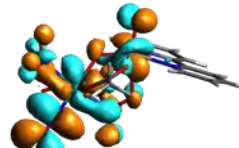
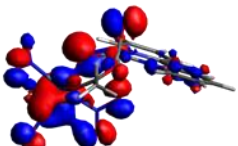
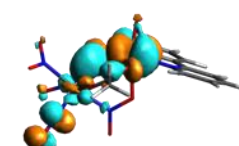
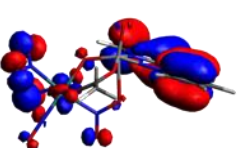
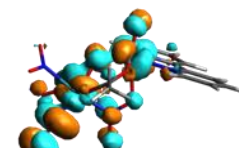
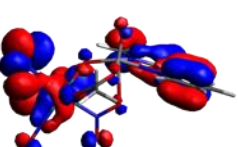
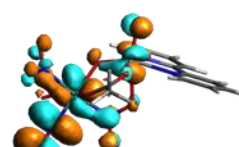
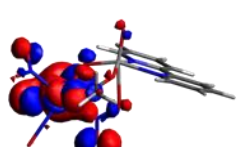
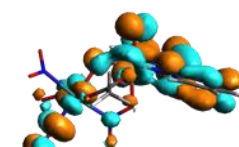
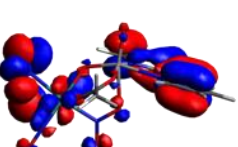
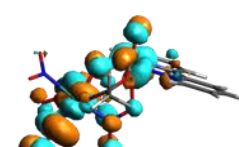
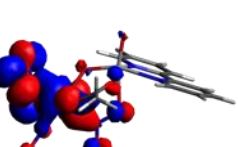
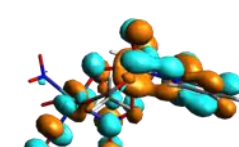
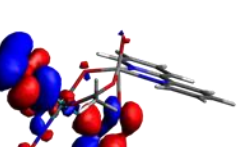
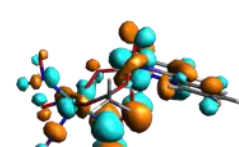
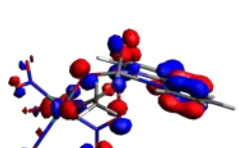
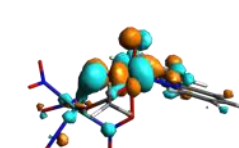
159			6.416	
160			6.576	

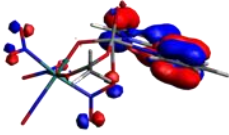
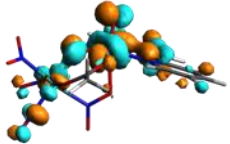
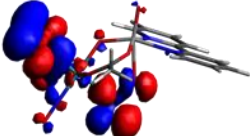
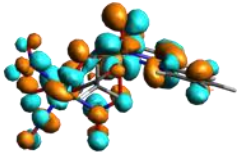
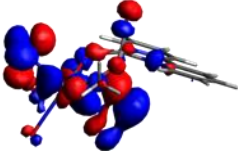
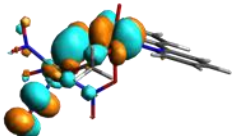
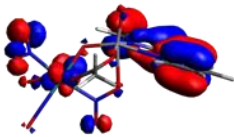
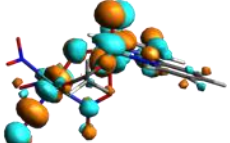
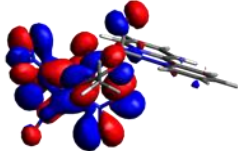
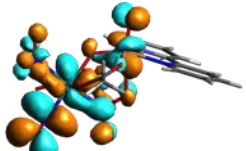
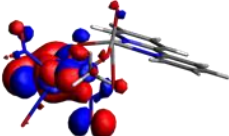
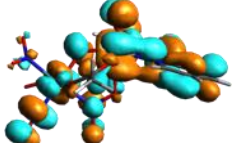
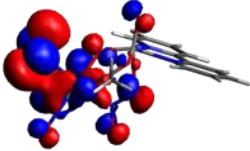
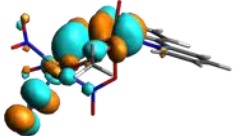
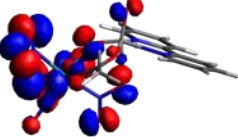
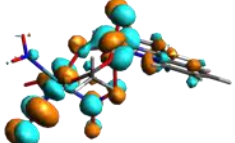
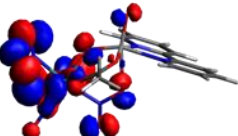
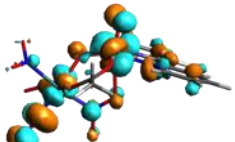
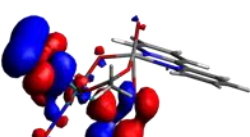
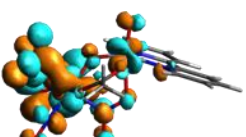
Table S3.

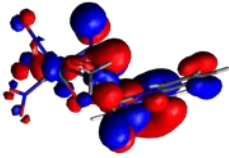
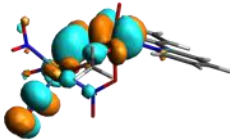
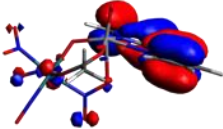
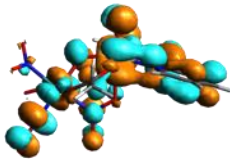
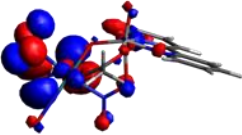
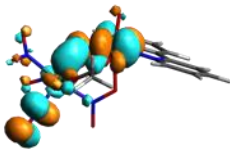
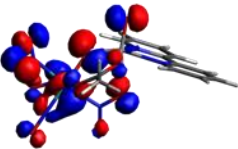
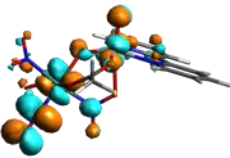
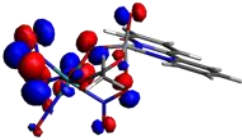
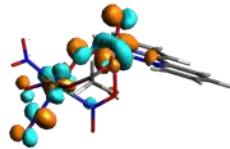
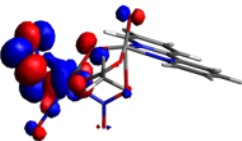
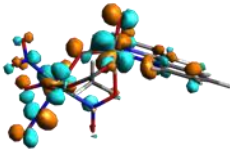
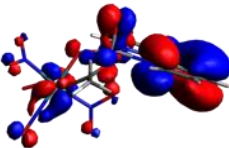
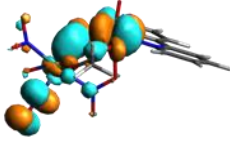
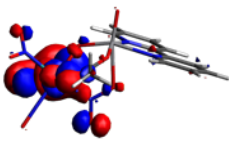
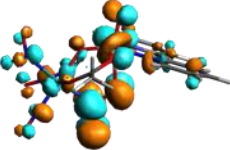
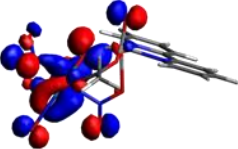
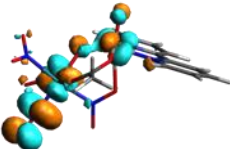
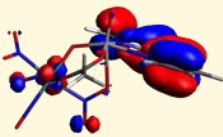
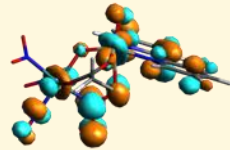
DFT calculations using VWN functional

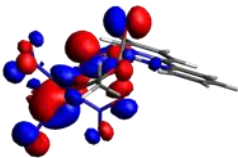
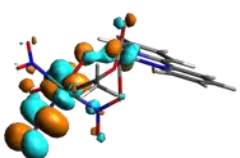
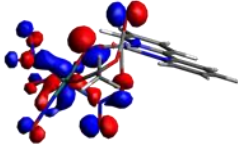
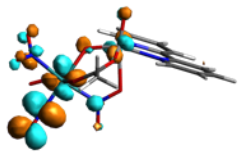
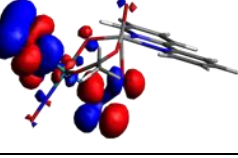
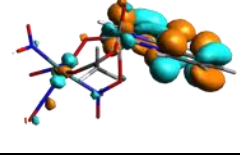
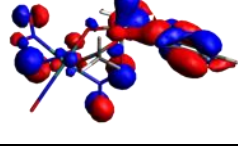
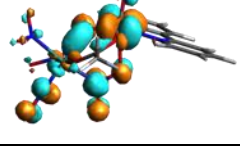
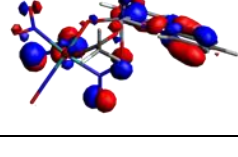
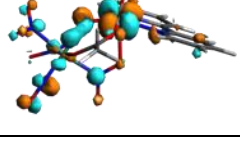
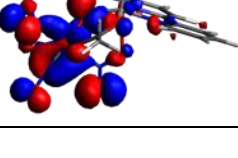
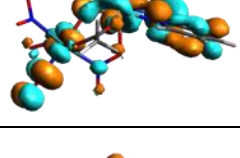
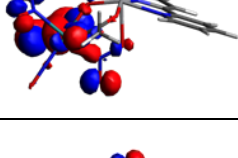
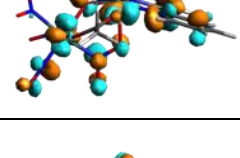
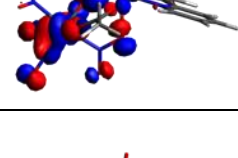
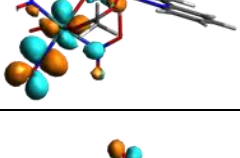
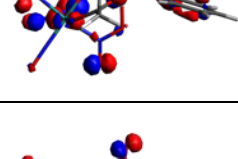
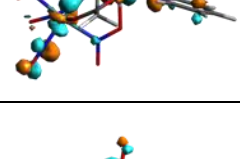
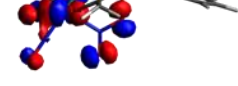
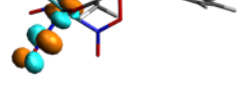
N	Transition Energy, eV	Oscillator strength, 10^3 a.u.	Origin of the transferred electron density, weighted sum of the occupied MO	Destination of the transferred electron density, weighted sum of the occupied MO
1	1.71347	0.0391		
2	1.99859	0.1850		
3	2.22164	0.2814		
4	2.30817	0.5378		
5	2.38746	0.3777		

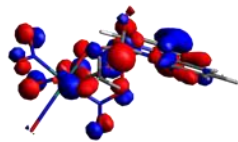
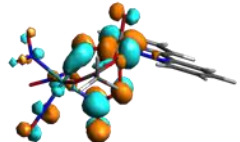
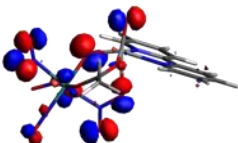
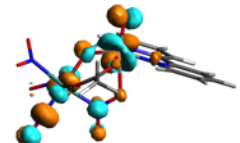
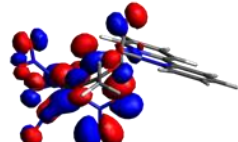
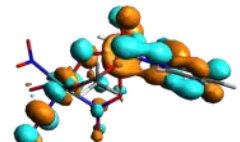
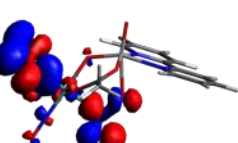
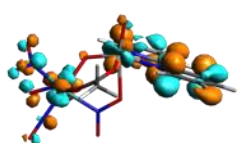
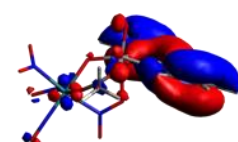
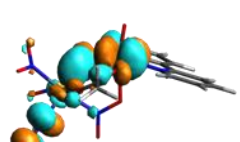
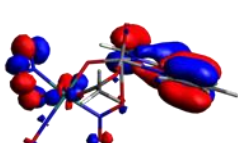
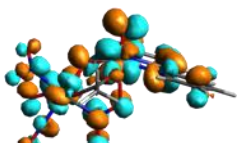
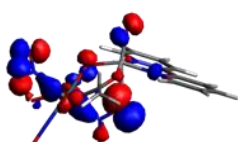
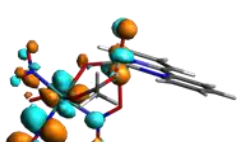
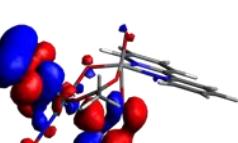
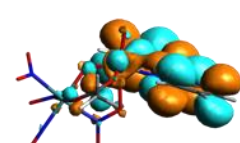
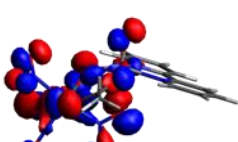
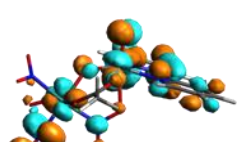
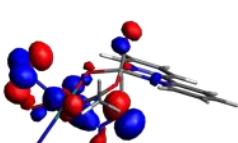
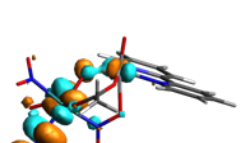
6	2.40292	0.1043		
7	2.41708	1.9290		
8	2.5455	1.0540		
9	2.6519	0.4587		
10	2.66393	0.0998		
11	2.71823	1.0170		
12	2.8282	0.1188		
13	2.8363	0.0536		
14	2.84837	0.7903		
15	2.85321	0.4501		

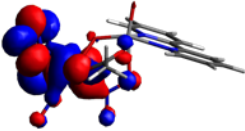
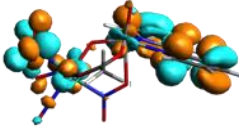
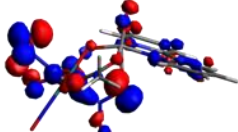
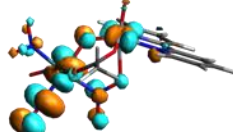
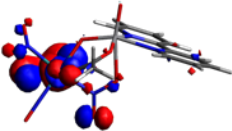
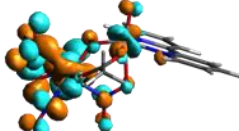
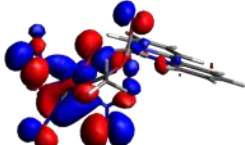
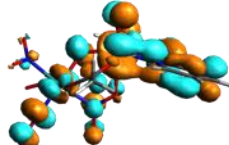
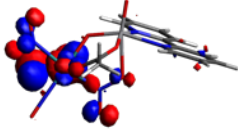
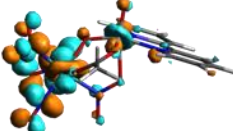
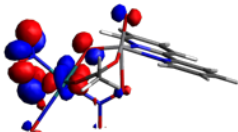
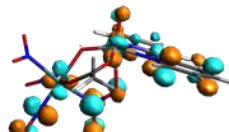
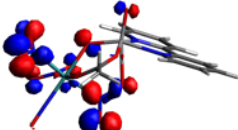
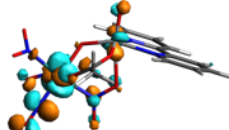
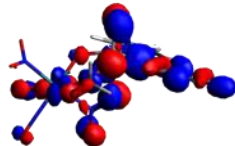
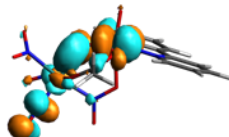
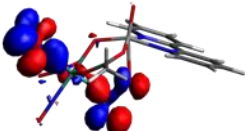
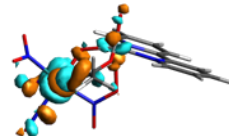
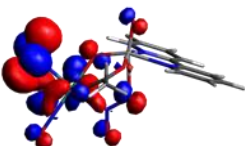
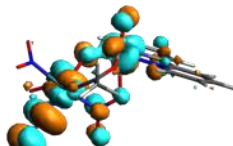
16	2.91382	1.0380		
17	2.92602	0.4158		
18	2.98006	4.0040		
19	3.00253	1.1710		
20	3.04135	0.0263		
21	3.04791	0.5007		
22	3.10168	1.2700		
23	3.12148	0.3191		
24	3.12395	1.7100		
25	3.1629	2.3240		

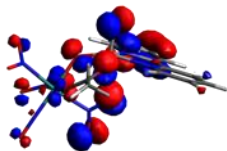
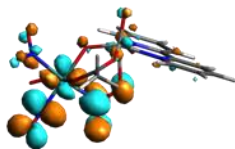
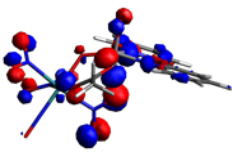
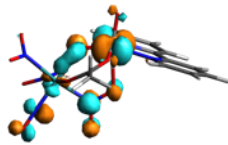
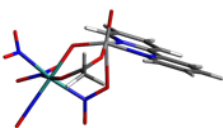
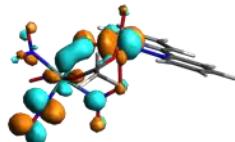
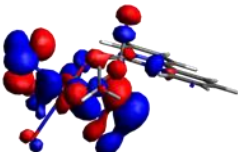
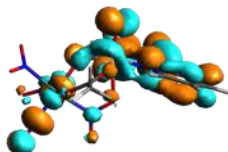
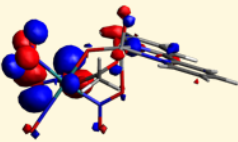
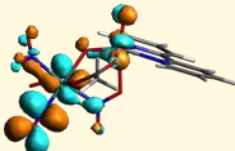
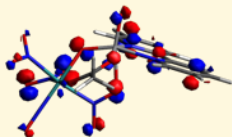
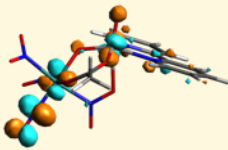
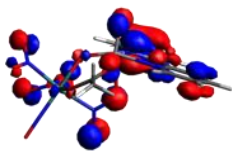
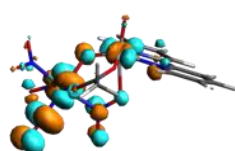
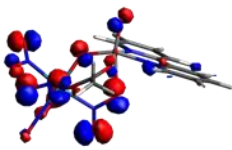
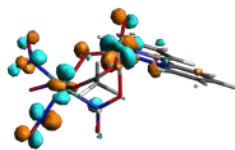
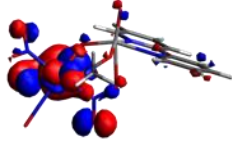
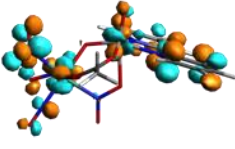
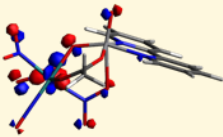
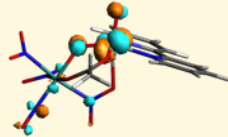
26	3.20248	6.1640		
27	3.22519	2.4640		
28	3.25845	2.8850		
29	3.30091	7.2760		
30	3.30522	1.5700		
31	3.33485	1.8990		
32	3.35779	0.6567		
33	3.37465	6.6350		
34	3.40264	1.9960		
35	3.4288	0.0595		

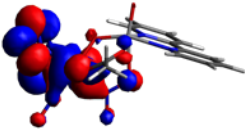
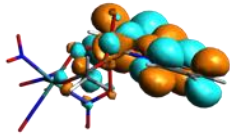
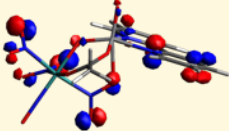
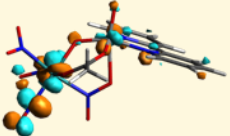
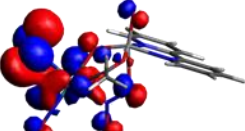
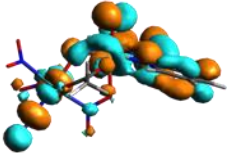
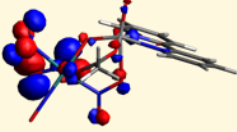
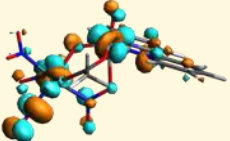
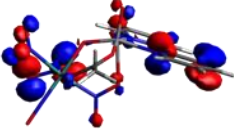
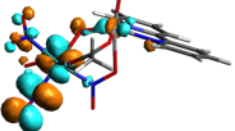
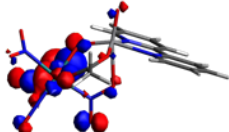
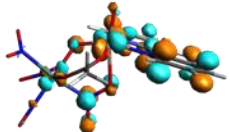
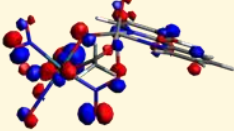
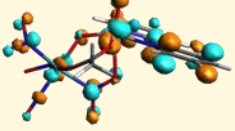
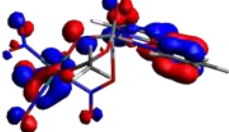
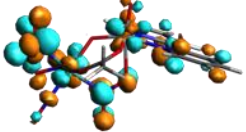
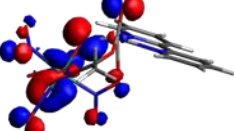
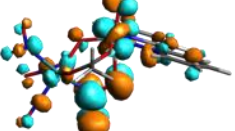
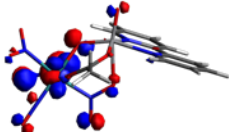
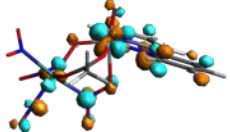
36	3.4311	1.6890		
37	3.47818	4.4030		
38	3.49581	0.1731		
39	3.50352	0.6918		
40	3.50718	2.5610		
41	3.52385	1.4740		
42	3.56766	0.2099		
43	3.57241	0.1837		
44	3.58107	0.2364		
45	3.61319	17.0800		

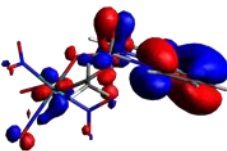
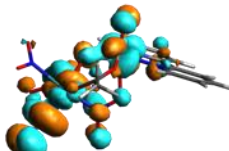
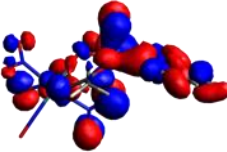
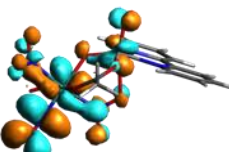
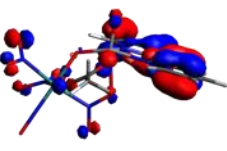
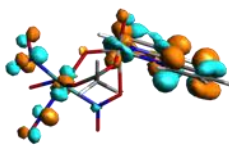
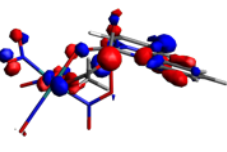
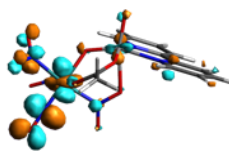
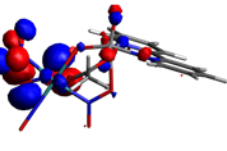
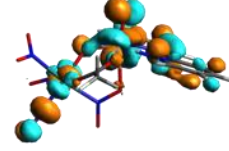
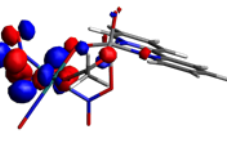
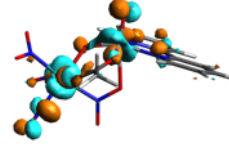
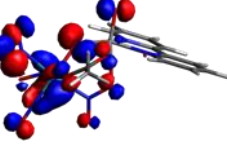
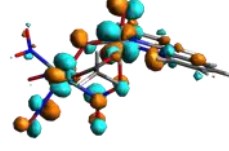
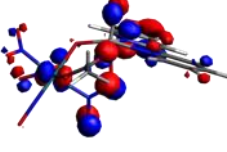
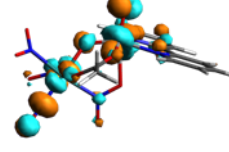
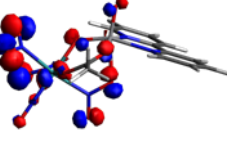
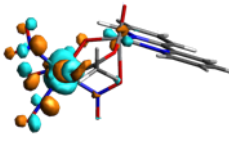
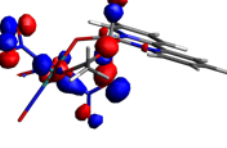
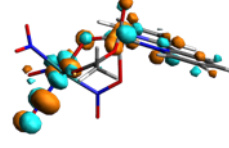
46	3.62025	3.7100		
47	3.66082	1.3040		
48	3.66495	0.2857		
49	3.66848	1.4770		
50	3.68113	1.9130		
51	3.69937	0.8175		
52	3.71321	0.6818		
53	3.72269	3.1150		
54	3.74347	2.1020		
55	3.7477	0.6063		

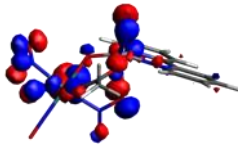
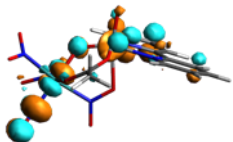
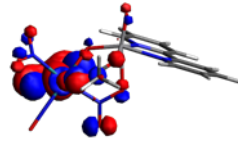
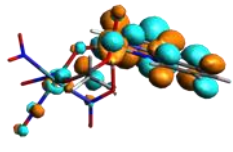
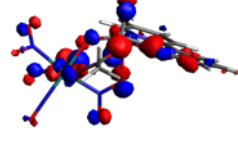
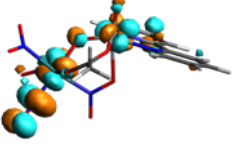
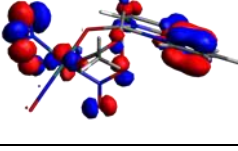
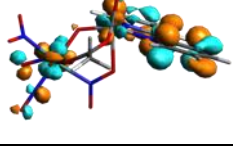
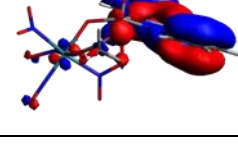
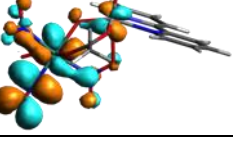
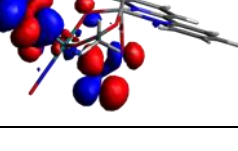
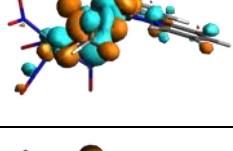
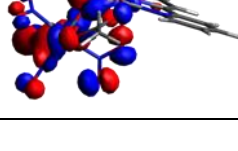
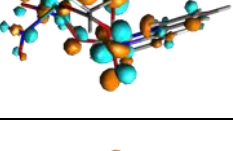
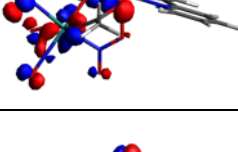
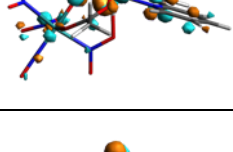
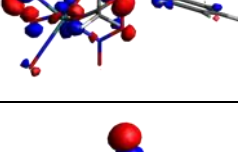
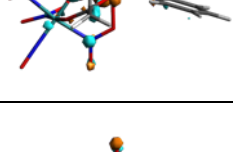
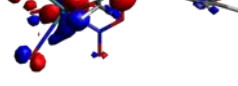
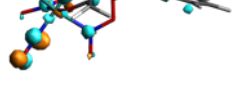
56	3.75255	1.1120		
57	3.76689	0.8562		
58	3.79063	1.2600		
59	3.80073	1.1430		
60	3.82054	1.8460		
61	3.8583	6.2920		
62	3.87532	6.5890		
63	3.88474	0.2443		
64	3.8975	4.3700		
65	3.92594	0.6206		

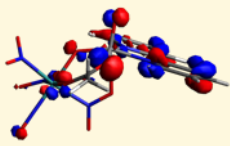
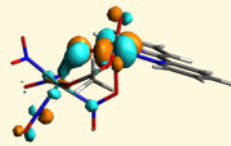
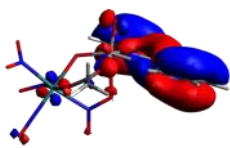
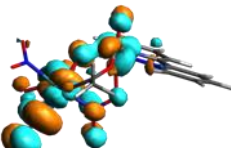
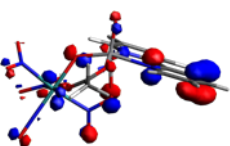
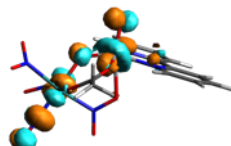
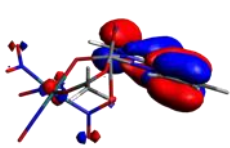
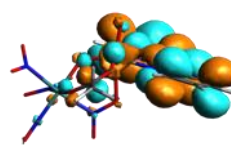
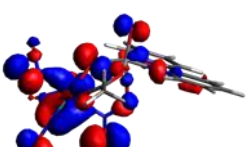
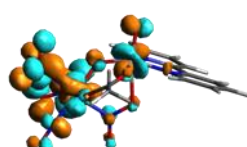
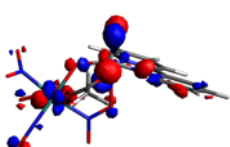
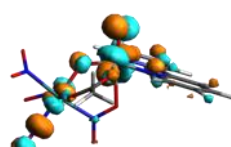
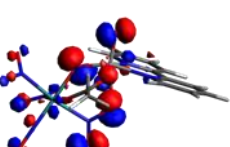
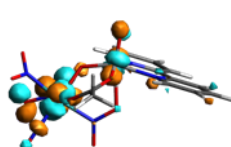
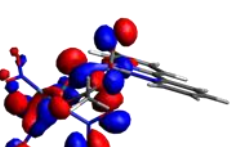
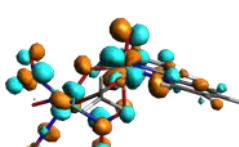
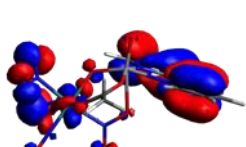
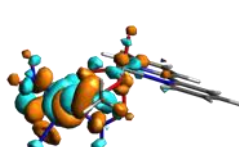
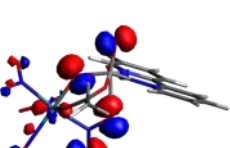
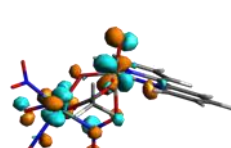
66	3.92726	0.4194		
67	3.96114	2.3220		
68	3.96488	2.0860		
69	3.97308	0.6956		
70	3.99173	2.4580		
71	3.99754	0.5430		
72	4.00683	3.5610		
73	4.02083	2.2990		
74	4.03145	2.9430		
75	4.03947	1.0040		

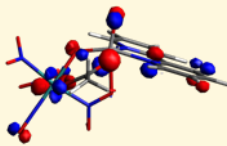
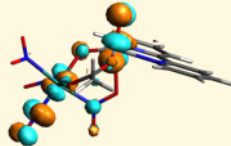
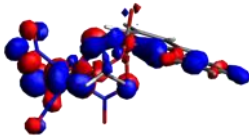
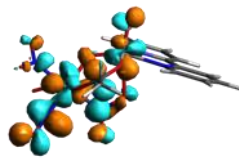
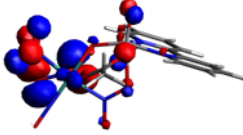
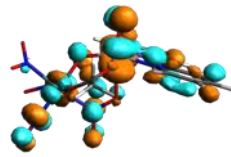
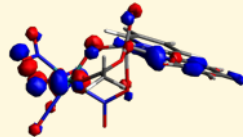
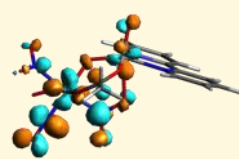
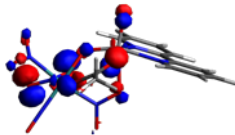
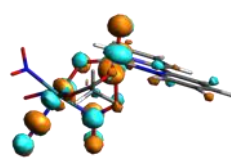
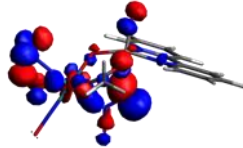
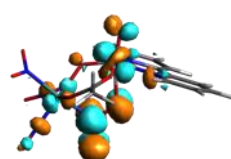

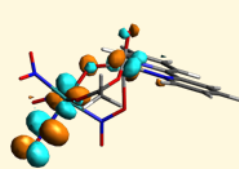
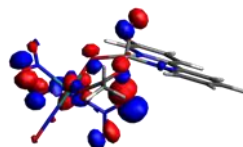
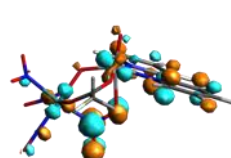
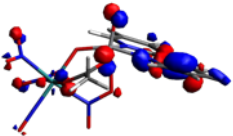
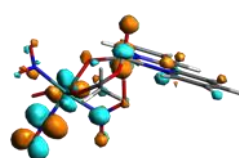
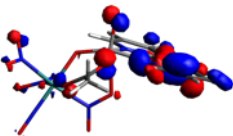
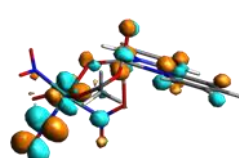
76	4.0509	1.8520		
77	4.06949	2.4350		
78	4.07501	3.5760		
79	4.09189	3.4030		
80	4.11126	17.3000		
81	4.11445	32.6700		
82	4.13764	1.8810		
83	4.14836	2.2550		
84	4.15646	3.6900		
85	4.15836	17.7700		

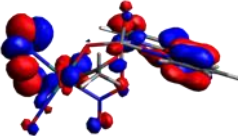
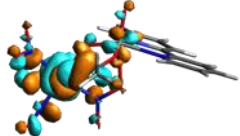
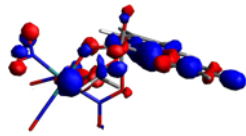
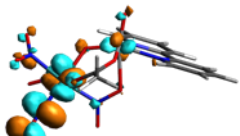
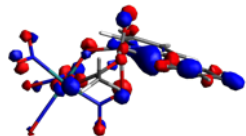
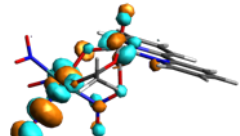
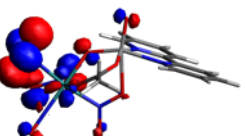
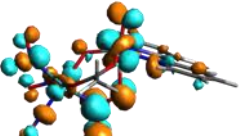
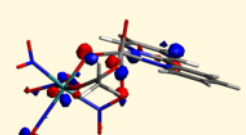
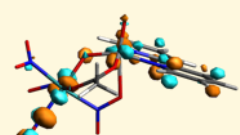
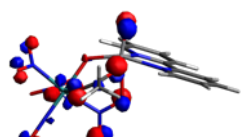
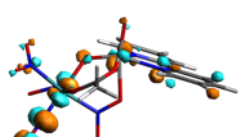
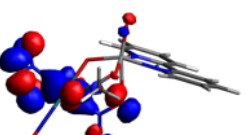
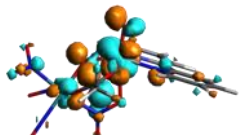
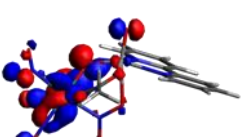
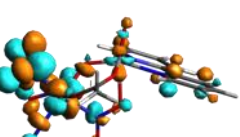
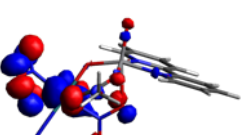
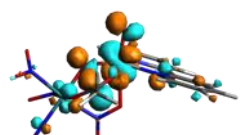
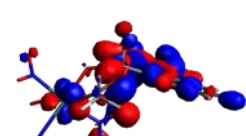
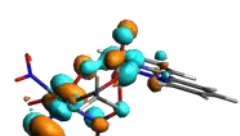
86	4.16081	1.5390		
87	4.16519	12.9900		
88	4.1805	0.8220		
89	4.19138	19.3600		
90	4.19984	9.1600		
91	4.20787	4.7700		
92	4.21936	10.0400		
93	4.23954	2.4150		
94	4.25104	2.1750		
95	4.25342	4.8840		

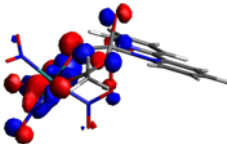
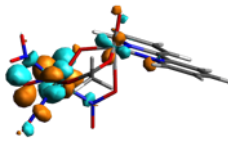
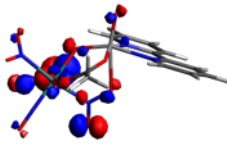
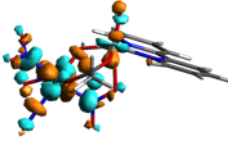
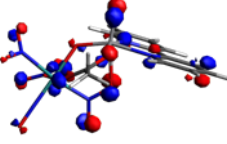
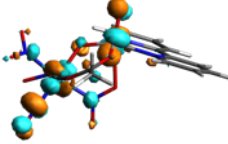
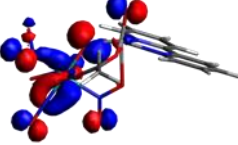
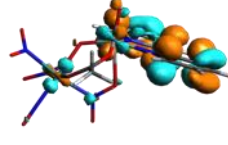
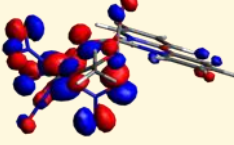
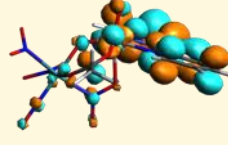
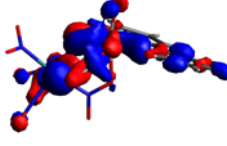
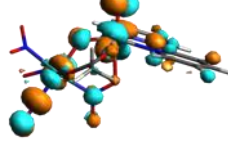
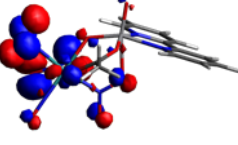
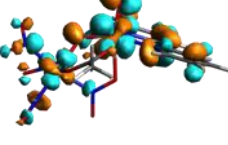
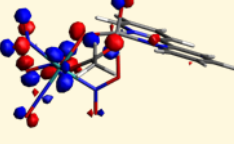
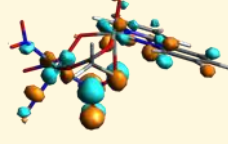
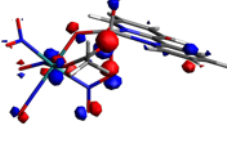
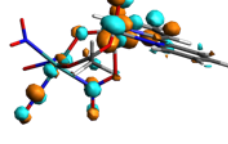
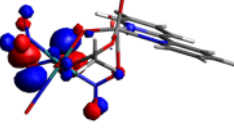
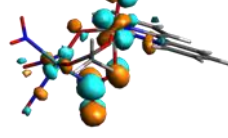
96	4.26417	1.1900		
97	4.28317	1.4010		
98	4.30866	3.7690		
99	4.31557	8.2490		
100	4.33144	1.2790		
101	4.33576	2.7060		
102	4.3519	3.9690		
103	4.35703	2.5900		
104	4.36737	3.1130		
105	4.37078	3.7020		

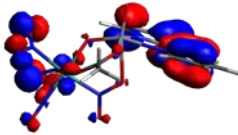
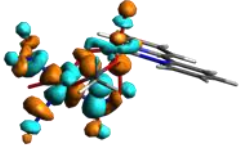
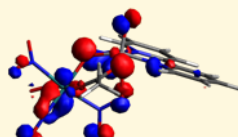
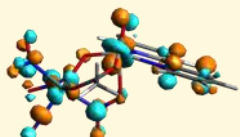
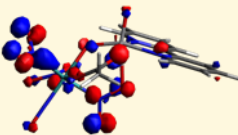
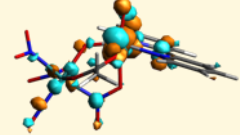
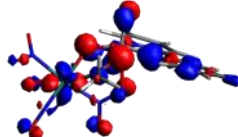
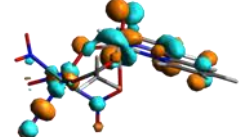
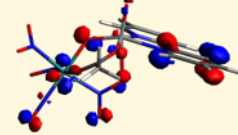
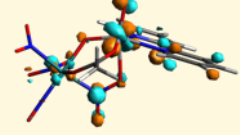
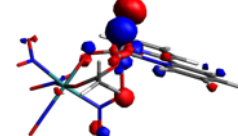
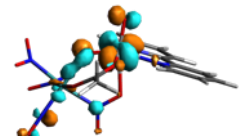
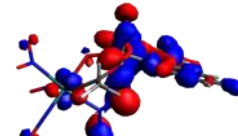
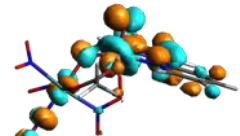
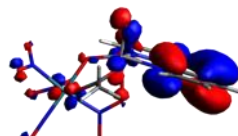
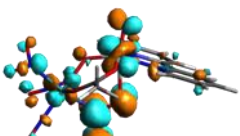
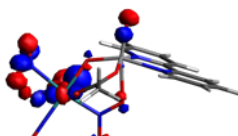
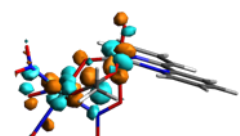
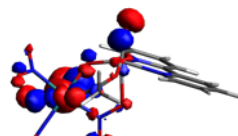
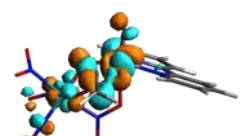
106	4.38133	0.3936		
107	4.38642	3.2920		
108	4.39375	8.4270		
109	4.4122	0.4537		
110	4.42809	0.6103		
111	4.43523	2.6310		
112	4.44059	1.9310		
113	4.45425	1.5520		
114	4.46475	0.5480		
115	4.47372	9.4660		

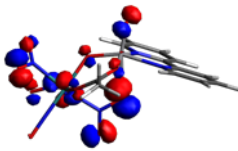
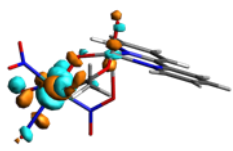
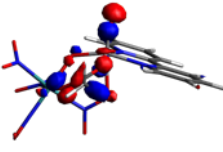
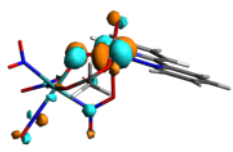
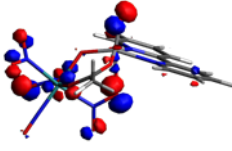
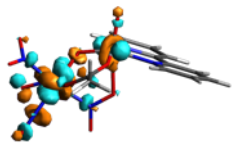
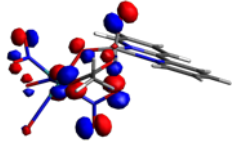
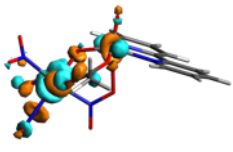
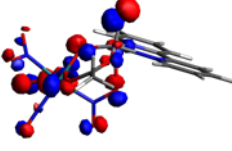
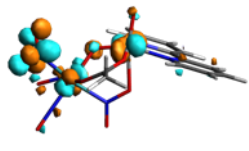
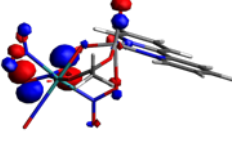
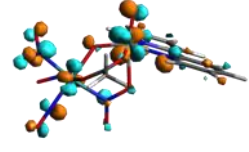
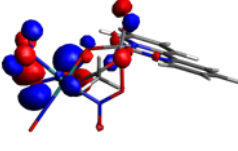
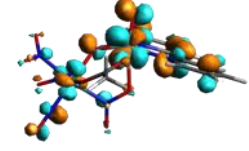
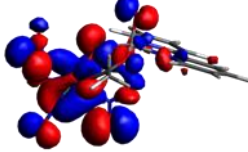
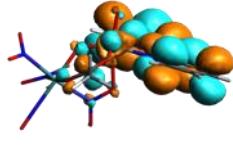
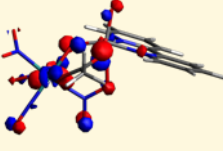
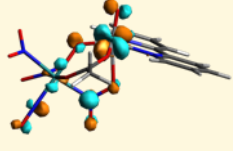
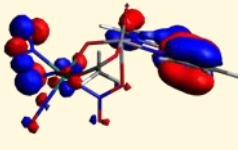
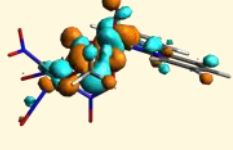
116	4.47614	21.8700		
117	4.50223	2.4860		
118	4.50906	1.7150		
119	4.53154	4.2940		
120	4.54227	0.6143		
121	4.54772	2.3430		
122	4.55669	7.2610		
123	4.56274	1.1540		
124	4.57053	5.4230		
125	4.57723	4.3300		

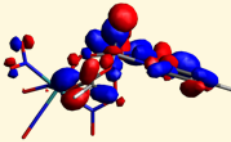
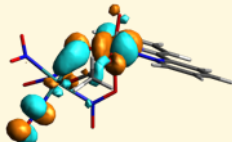
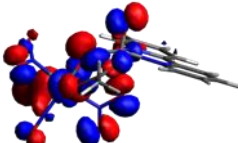
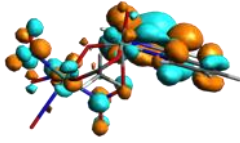
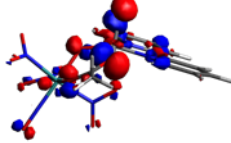
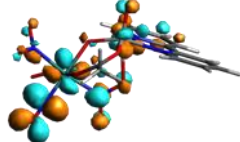
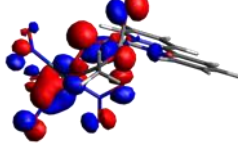
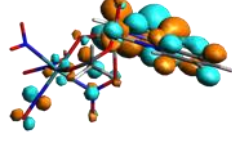
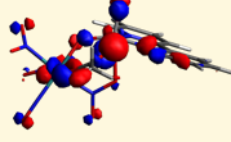
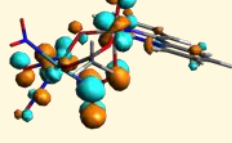
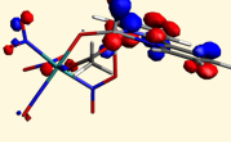
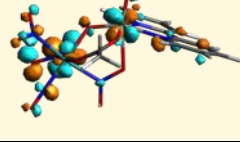
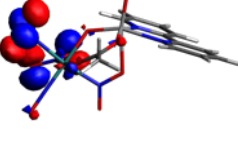
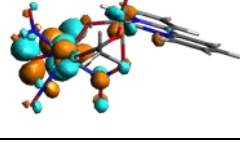
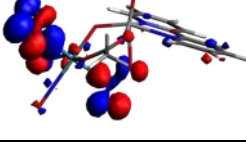
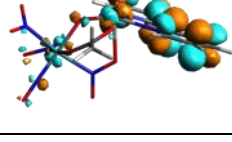
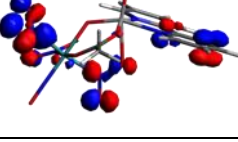
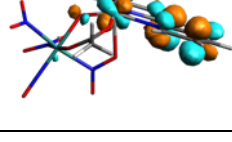
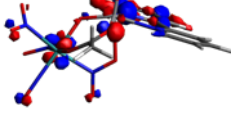
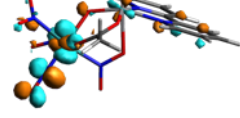
126	4.59628	11.1200		
127	4.60394	0.1766		
128	4.61264	1.0800		
129	4.61833	10.3300		
130	4.62446	2.3480		
131	4.6314	4.4820		
132	4.64339	33.2700		
133	4.6463	2.7030		
134	4.668	7.1220		
135	4.66909	2.8370		

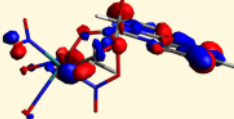
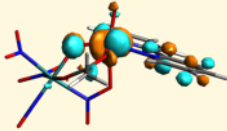
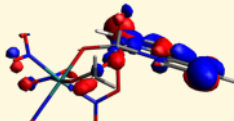
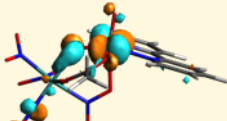
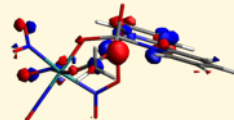
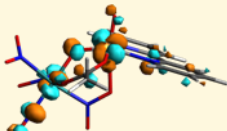
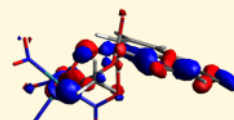
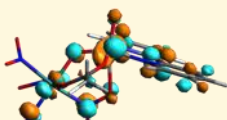
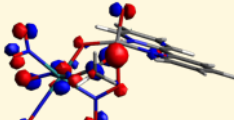
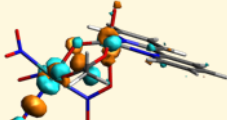
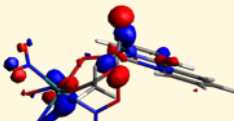
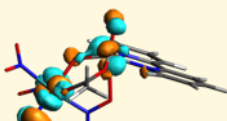
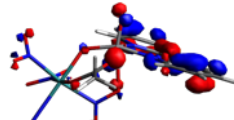
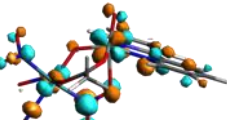
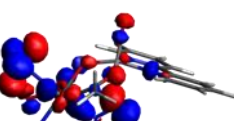
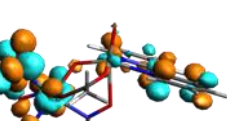
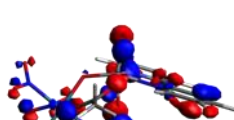
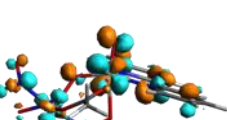
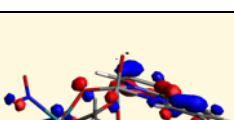
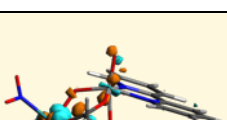
136	4.69017	3.3120		
137	4.69773	5.9620		
138	4.70379	6.6350		
139	4.7063	3.0790		
140	4.73491	11.2100		
141	4.74184	8.3360		
142	4.74926	1.2650		
143	4.75823	6.2460		
144	4.76271	0.3744		
145	4.76731	6.8130		

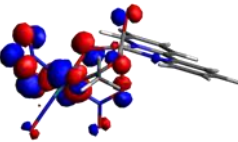
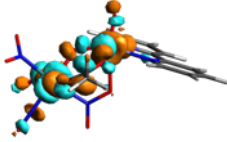
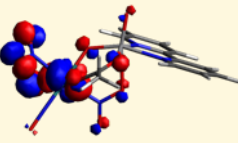
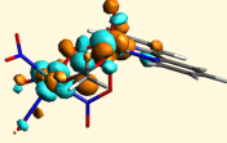
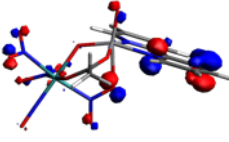
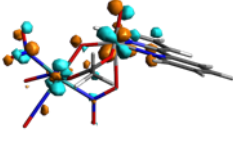
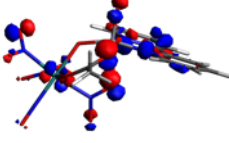
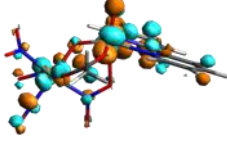
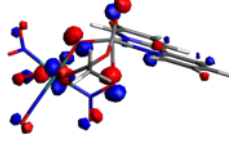
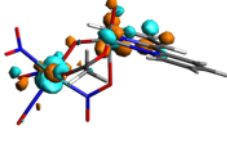
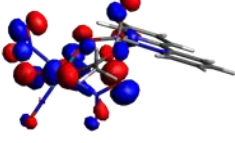
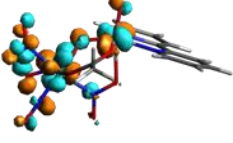
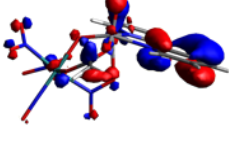
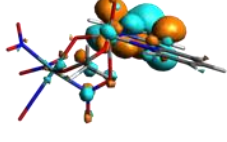
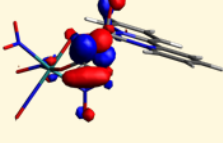
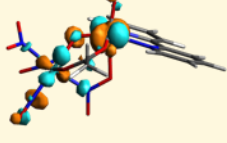
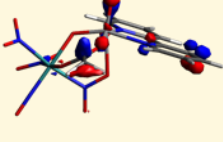
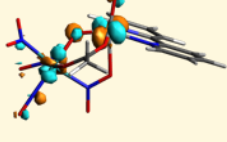
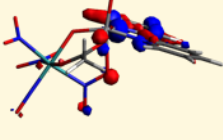
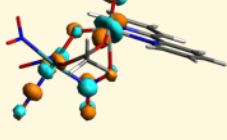
146	4.77428	7.0050		
147	4.79004	2.6250		
148	4.80325	3.8080		
149	4.81904	6.2560		
150	4.82127	31.9900		
151	4.82707	8.8710		
152	4.83208	3.4250		
153	4.83674	19.1900		
154	4.85106	7.2140		
155	4.85266	2.7500		

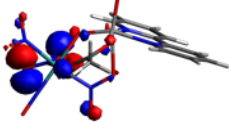
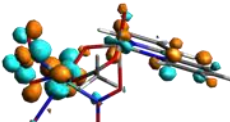
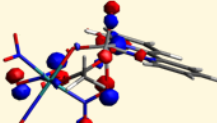

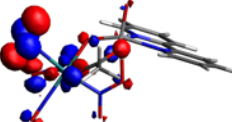
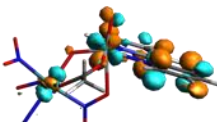
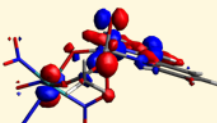
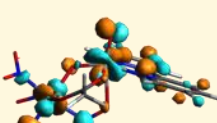
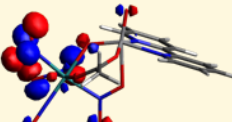
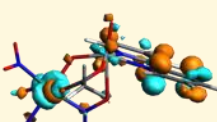
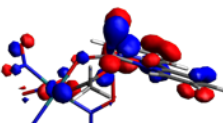
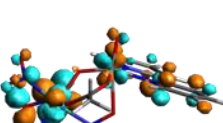
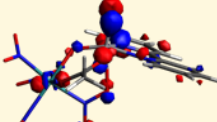

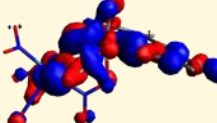
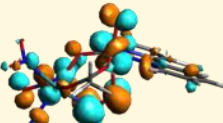
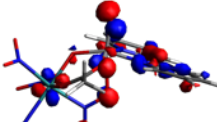
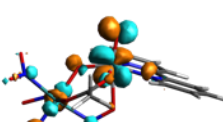
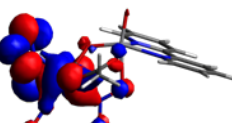
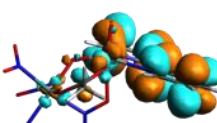
156	4.86146	5.3020		
157	4.86481	17.1800		
158	4.87592	27.0700		
159	4.88502	1.9120		
160	4.88781	10.0900		
161	4.91948	5.1520		
162	4.92304	4.3860		
163	4.93399	2.9740		
164	4.93768	3.4070		
165	4.94375	3.7140		

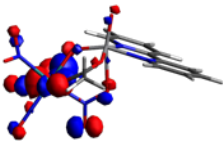
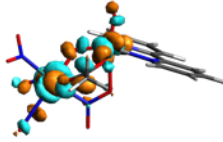
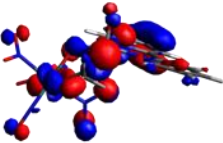
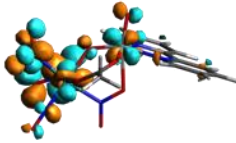
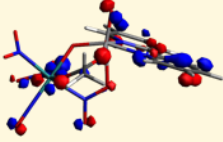
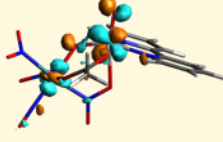
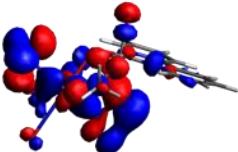
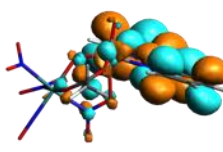
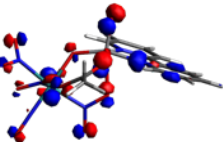
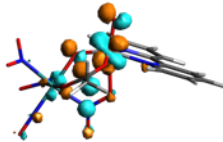
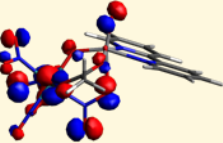
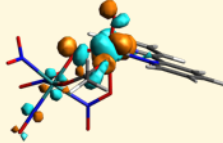
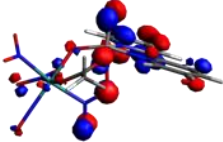
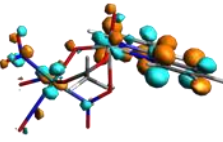
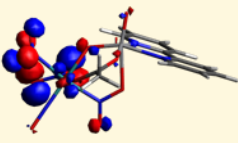
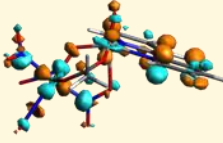
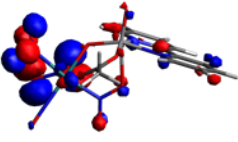
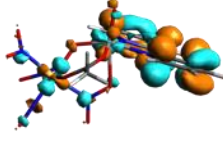
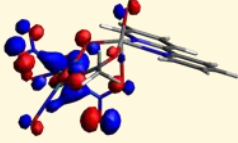
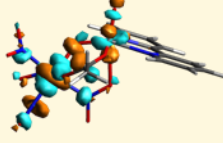
166	4.9493	7.7390		
167	4.95161	0.4532		
168	4.96404	1.5930		
169	4.97143	6.2600		
170	4.97681	4.8640		
171	4.98853	6.9910		
172	4.99737	7.2310		
173	5.01314	2.3630		
174	5.01837	17.9900		
175	5.0314	10.6600		

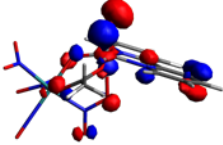
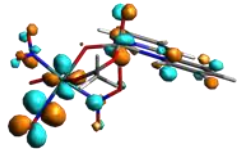
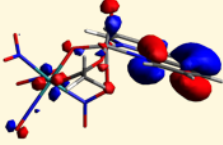
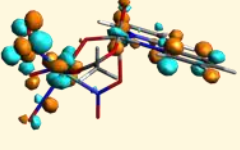
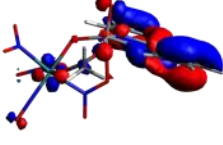
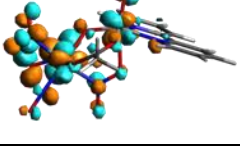
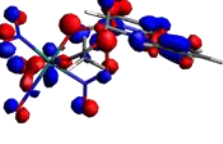
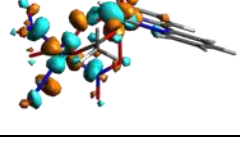
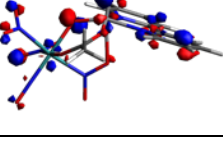
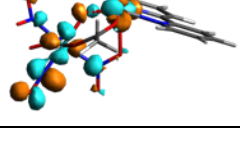
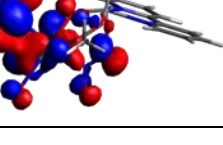
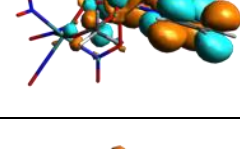
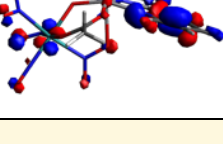
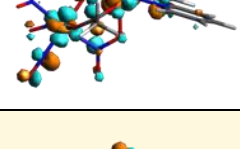
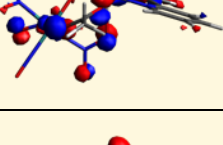
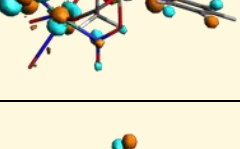
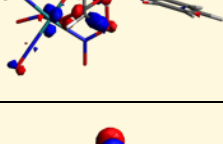
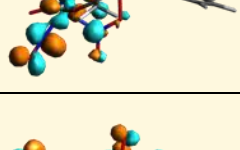
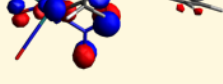
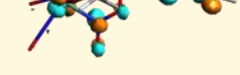
176	5.04054	12.2900		
177	5.04805	1.2490		
178	5.05507	4.2170		
179	5.05914	5.0880		
180	5.06758	10.0500		
181	5.08418	14.5500		
182	5.0953	7.1820		
183	5.10238	7.0900		
184	5.11337	4.3960		
185	5.11491	8.9450		

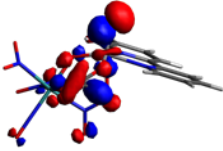
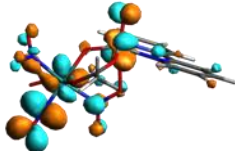
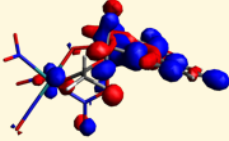
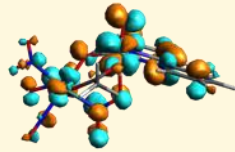
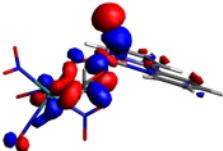
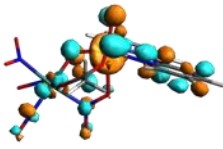
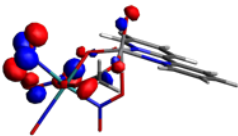
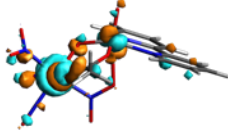
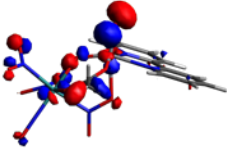
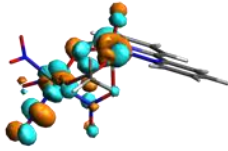
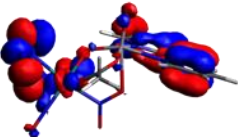
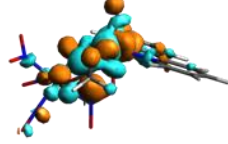
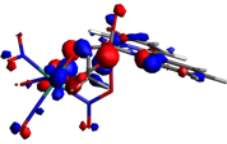
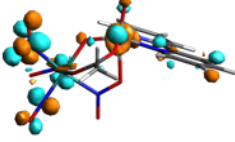
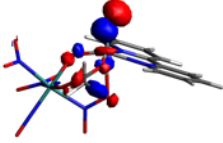
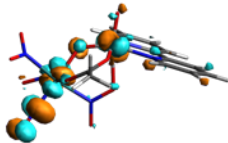
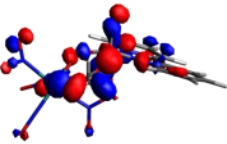
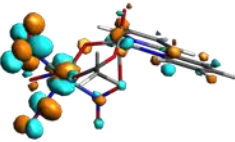
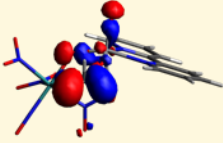

186	5.12045	16.4500		
187	5.13143	11.2500		
188	5.133	14.3300		
189	5.1476	33.9400		
190	5.15498	16.6400		
191	5.16087	20.0000		
192	5.16589	6.8760		
193	5.17107	4.2560		
194	5.1854	9.1980		
195	5.19623	35.1300		

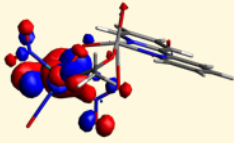
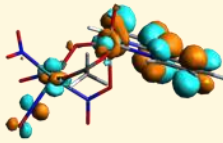
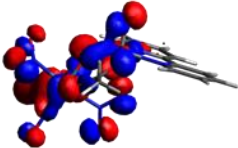
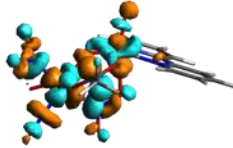
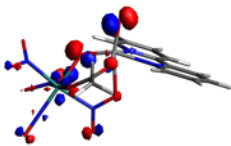
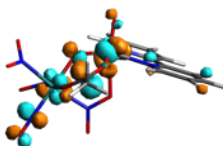
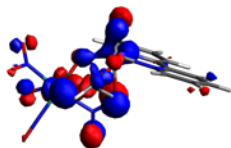
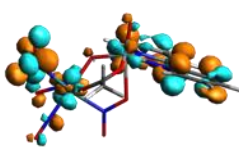
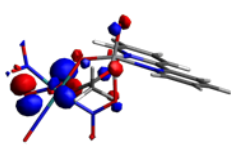
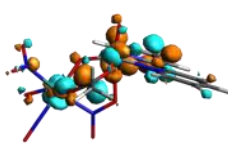
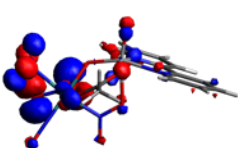
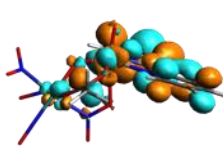
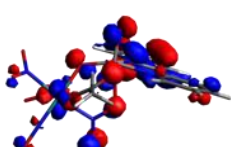
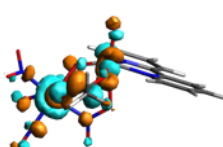
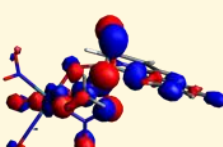
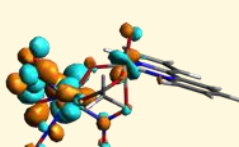
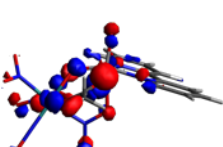
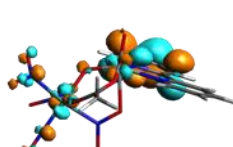
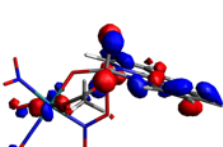
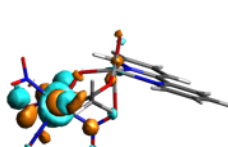
196	5.20446	3.5840		
197	5.21189	11.0700		
198	5.21971	3.8240		
199	5.22413	6.6020		
200	5.23457	5.0030		
201	5.24144	9.2540		
202	5.24638	1.5900		
203	5.25607	15.8300		
204	5.26327	27.7900		
205	5.27988	12.7400		

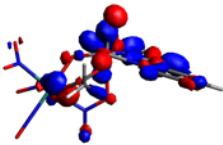
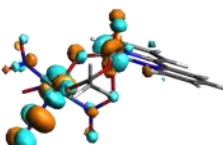
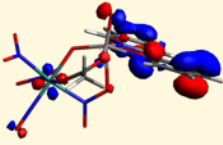
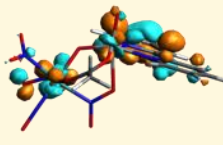
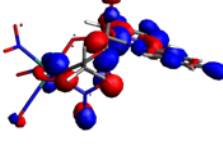
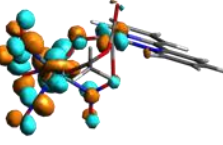
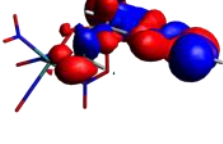
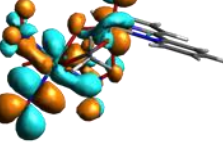
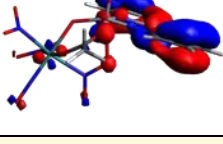
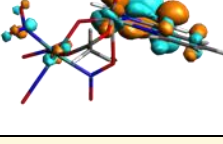
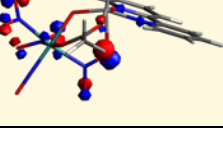
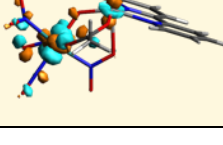
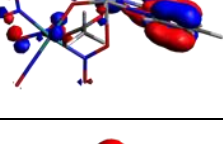
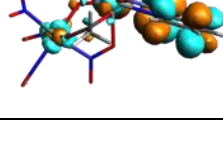
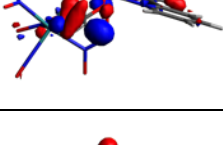
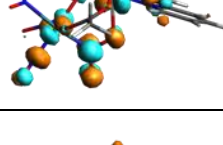
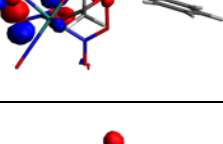
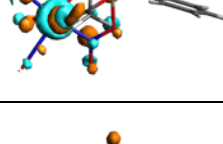
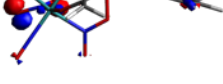
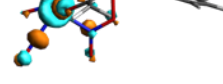
206	5.28741	2.4040		
207	5.28973	12.9600		
208	5.3056	3.6120		
209	5.31483	21.1100		
210	5.32824	20.8600		
211	5.33152	1.2560		
212	5.34293	14.6500		
213	5.34914	10.5200		
214	5.3647	4.4170		
215	5.3862	2.1460		

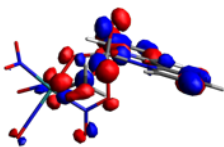
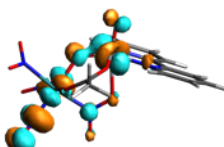
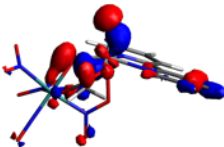
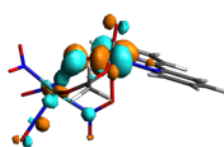
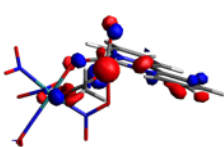
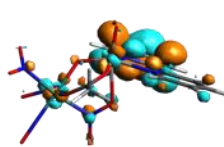
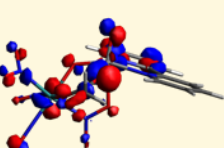
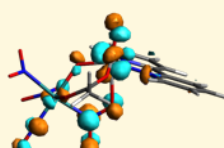
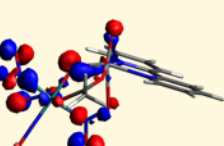
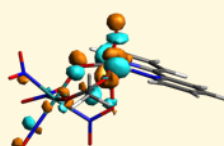
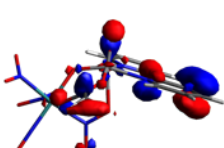
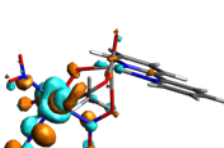
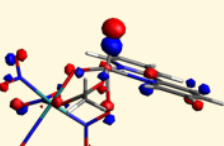
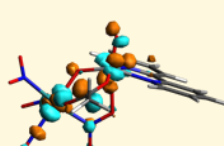
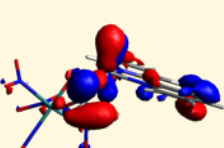
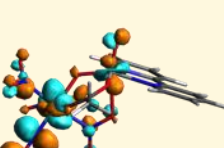
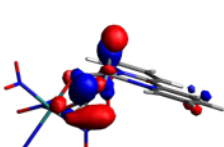
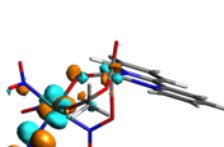
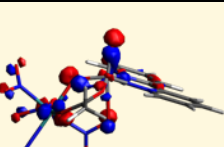
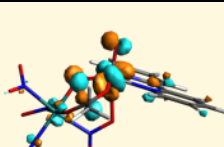
216	5.39497	3.1320		
217	5.39661	4.7920		
218	5.40194	11.7000		
219	5.41959	0.8911		
220	5.42945	5.7430		
221	5.43379	13.0100		
222	5.45299	8.0880		
223	5.45783	12.2600		
224	5.46139	8.9420		
225	5.46858	36.3900		

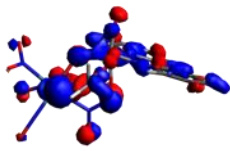
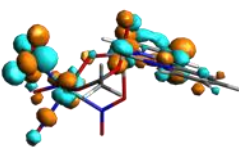
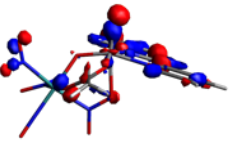
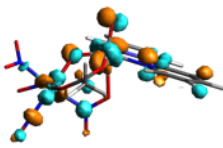
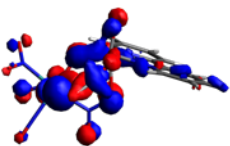
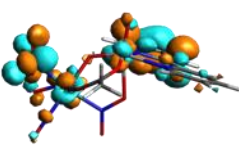
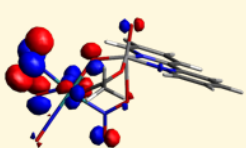
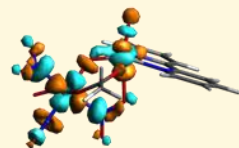
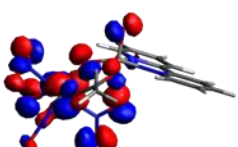
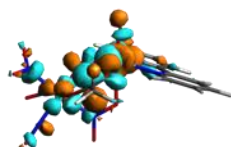
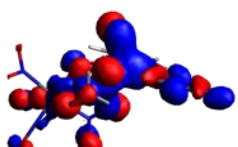
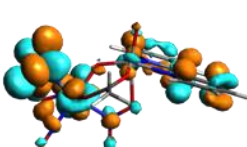
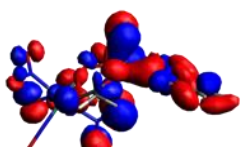
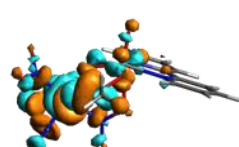
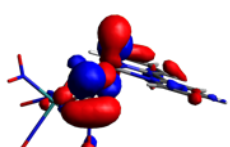
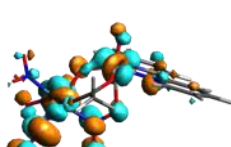
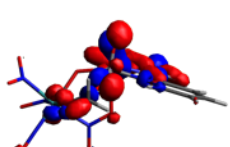
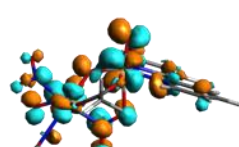
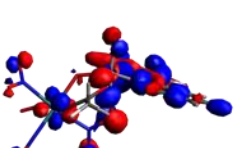
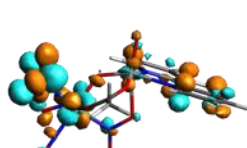
226	5.47757	7.5710		
227	5.48582	19.2100		
228	5.49784	6.7270		
229	5.50312	0.5587		
230	5.51156	2.3650		
231	5.51686	0.1053		
232	5.51801	1.4100		
233	5.52899	10.0900		
234	5.54183	16.3200		
235	5.55117	23.2200		

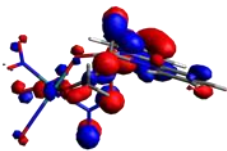
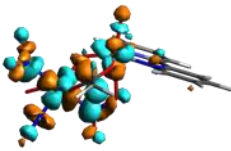
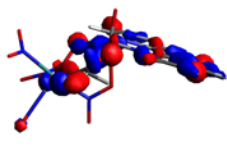
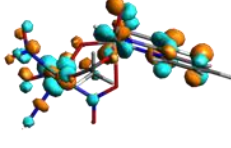
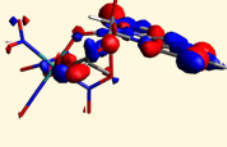
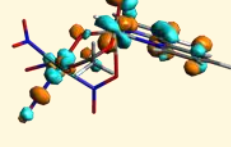
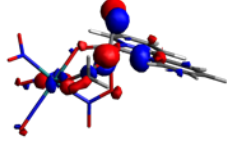
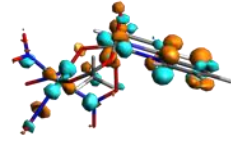
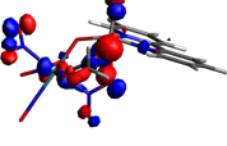
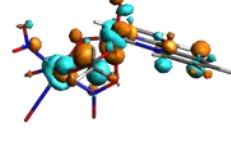
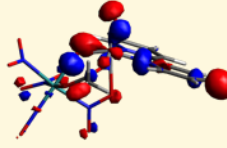
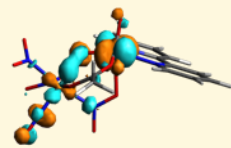
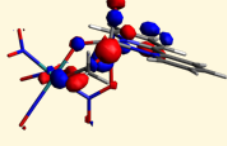
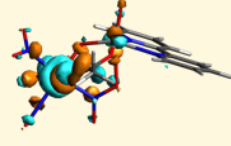
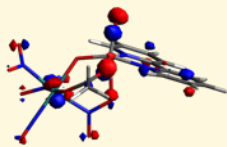
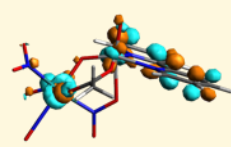
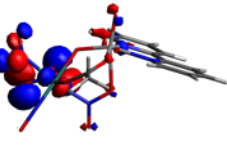
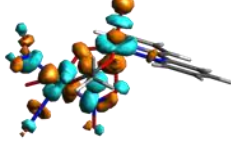
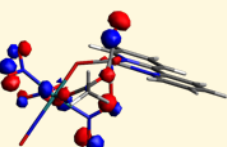
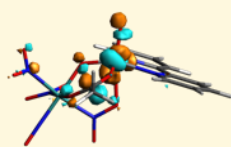
236	5.56196	9.6790		
237	5.5727	25.8700		
238	5.58456	0.8759		
239	5.58877	5.3380		
240	5.59819	4.9650		
241	5.60174	3.5430		
242	5.60883	9.6790		
243	5.61358	3.5700		
244	5.61547	3.6150		
245	5.62321	12.5000		

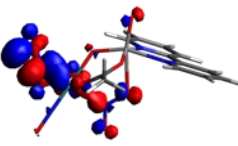
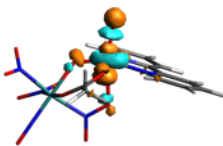
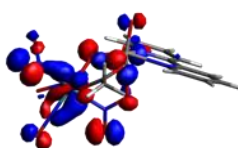
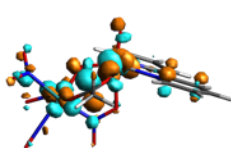
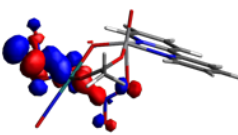
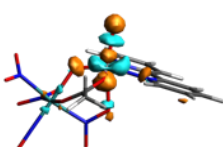
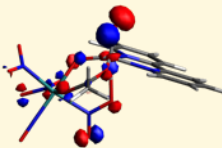
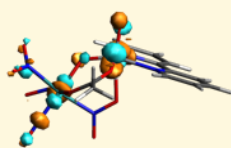
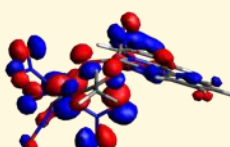
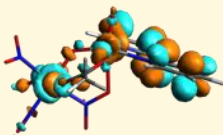
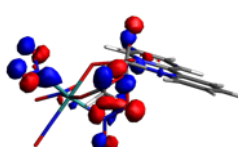
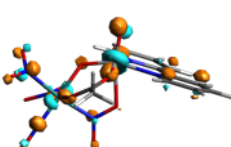
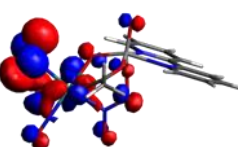
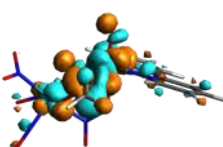
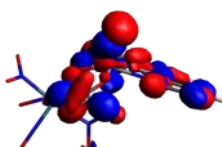
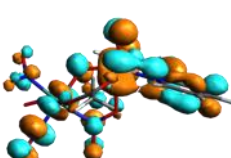
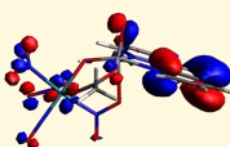
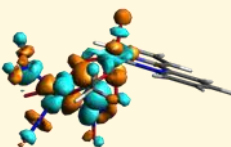
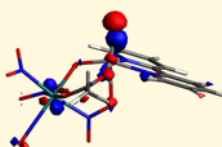
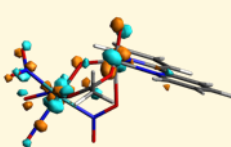
246	5.62776	13.4900		
247	5.63698	2.4730		
248	5.64353	7.6600		
249	5.65384	4.9460		
250	5.6645	1.1260		
251	5.67407	3.8100		
252	5.67714	7.7550		
253	5.6807	45.1500		
254	5.68773	0.3722		
255	5.70261	2.6770		

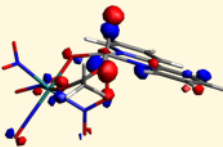
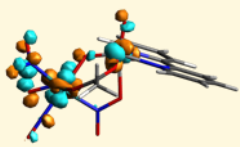
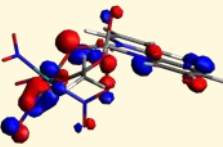
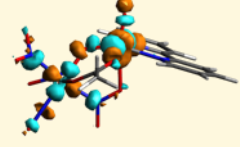
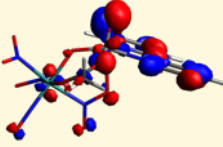
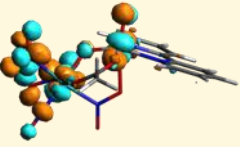
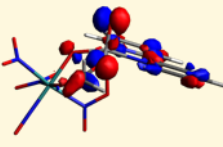
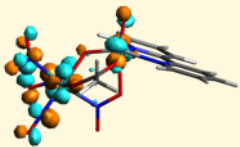
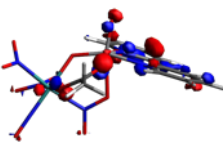
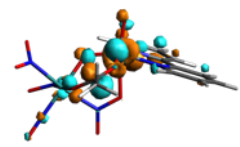
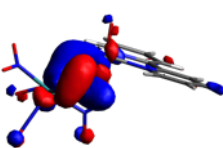
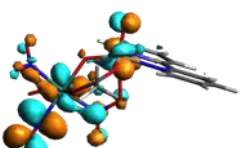
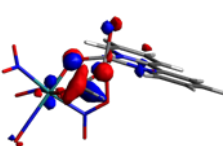
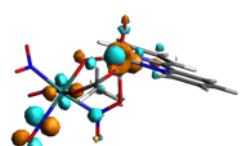
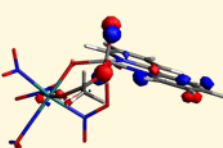
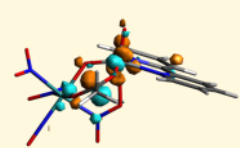
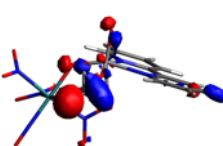
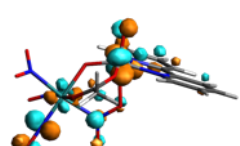
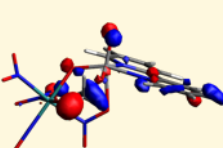
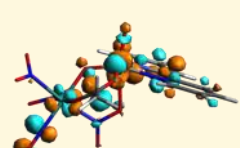
256	5.70593	3.2580		
257	5.7083	19.9400		
258	5.71601	9.7360		
259	5.72969	0.1579		
260	5.7321	9.4200		
261	5.74652	34.7800		
262	5.76432	2.1460		
263	5.76622	3.6220		
264	5.77716	1.7120		
265	5.78398	9.4840		


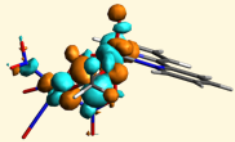
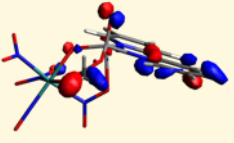
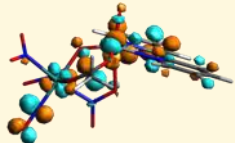
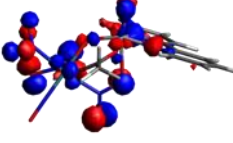
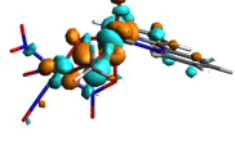
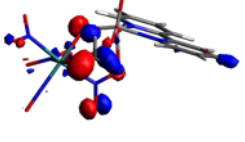
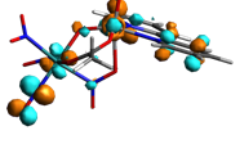
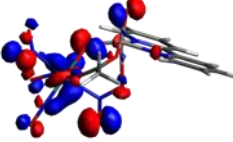
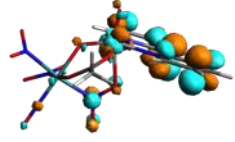
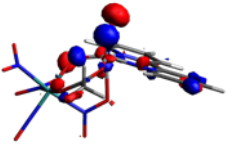
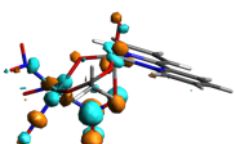
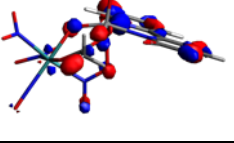
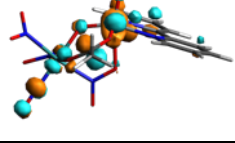
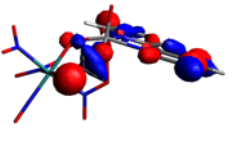
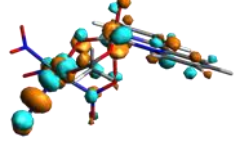
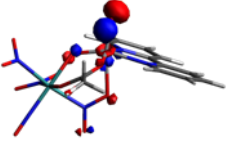
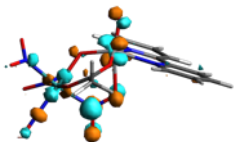
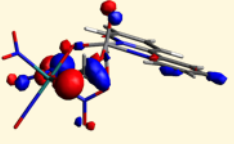
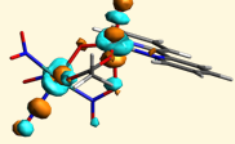
266	5.78983	1.1610		
267	5.79229	1.5980		
268	5.7986	4.7630		
269	5.80795	18.0700		
270	5.81664	36.9900		
271	5.82801	0.1630		
272	5.83657	37.7000		
273	5.838	11.3000		
274	5.8482	4.9450		
275	5.85404	27.1200		

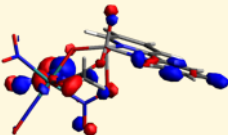
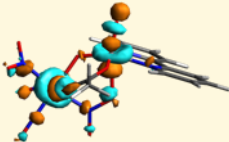
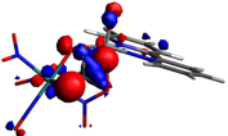
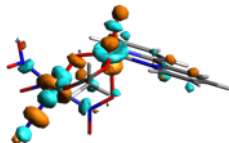
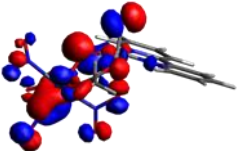
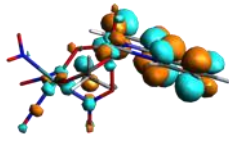
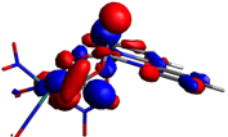
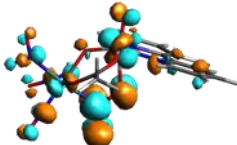
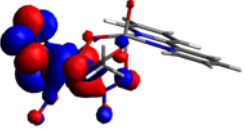
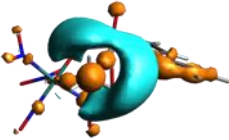
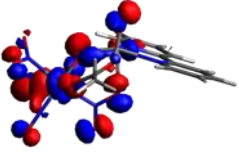
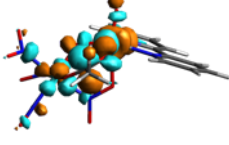
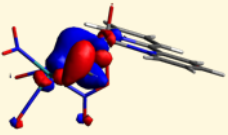
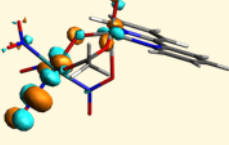
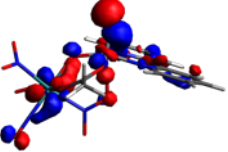
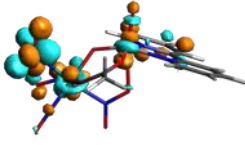
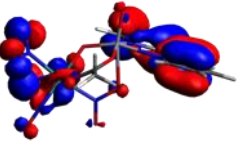
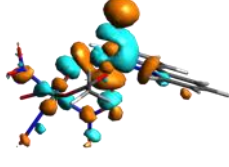

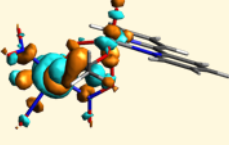
276	5.86551	4.0510		
277	5.86778	5.5150		
278	5.87831	5.3900		
279	5.88293	50.9100		
280	5.89113	0.5754		
281	5.90734	4.7300		
282	5.91813	0.5069		
283	5.92774	8.8390		
284	5.93757	3.8970		
285	5.95242	7.4660		

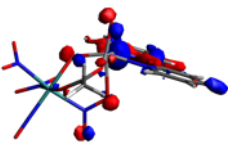
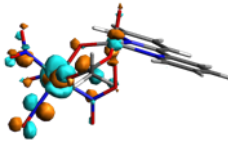
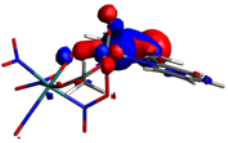
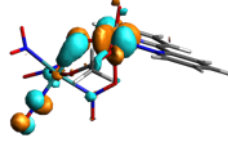

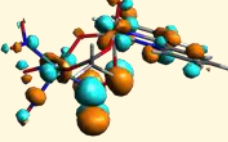
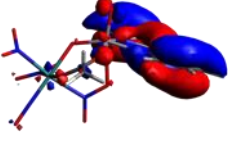
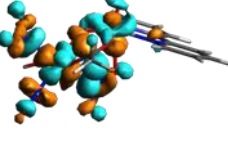
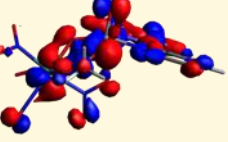
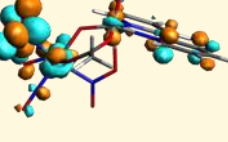
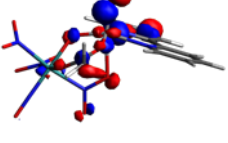
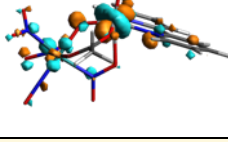
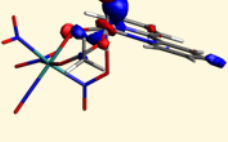
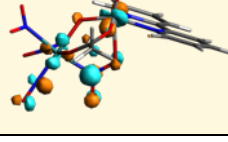
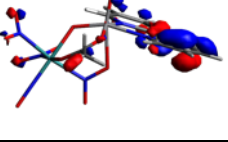
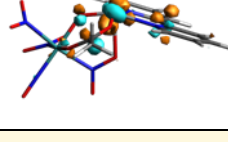
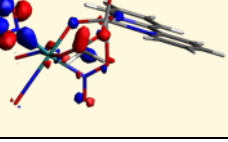
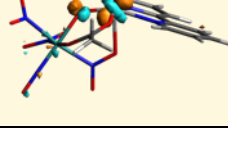
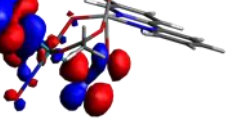
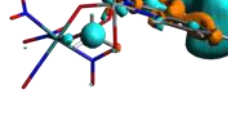
286	5.96015	0.3483		
287	5.96742	4.9390		
288	5.97237	12.4600		
289	5.9789	7.3860		
290	5.98538	0.8353		
291	5.99154	12.6300		
292	6.00288	12.7400		
293	6.01198	13.1700		
294	6.0163	3.0180		
295	6.02349	39.4800		

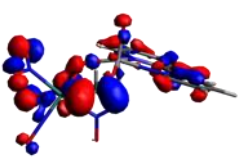
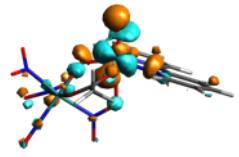
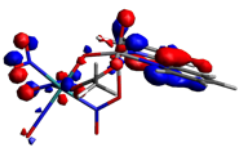
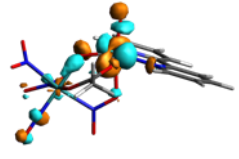
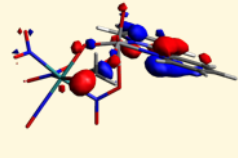
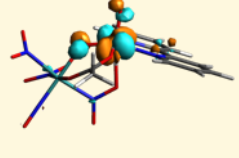
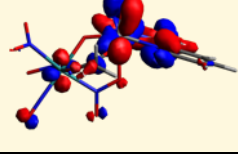
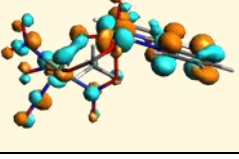
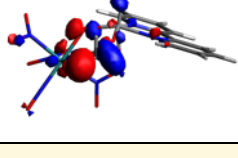
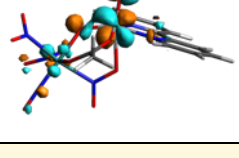
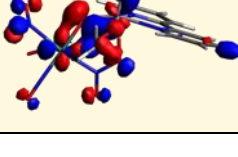
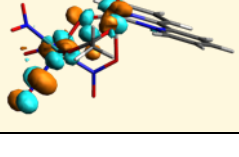
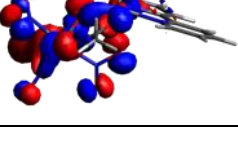
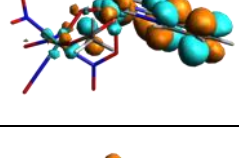
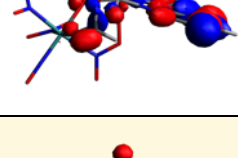
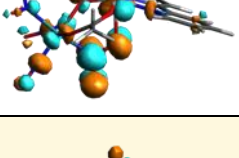
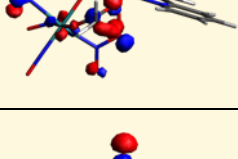
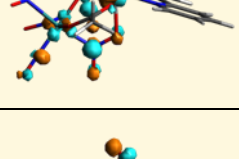
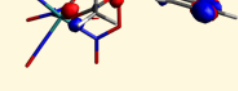
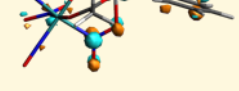
296	6.03375	5.8260		
297	6.03529	0.8796		
298	6.04451	4.1370		
299	6.05418	12.6700		
300	6.05505	10.1400		
301	6.05939	5.9340		
302	6.07918	4.4010		
303	6.0831	0.9282		
304	6.08915	19.6600		
305	6.09745	23.4100		

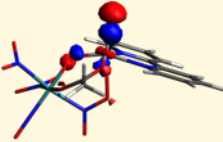
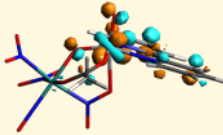
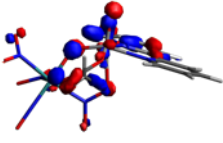
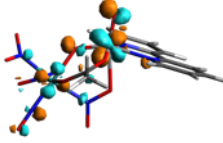
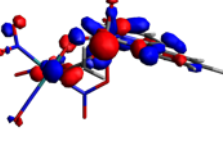
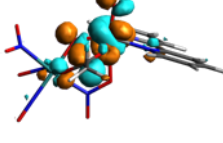
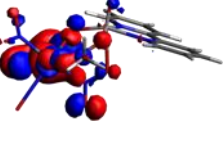
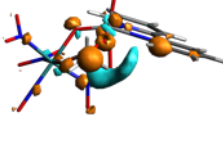
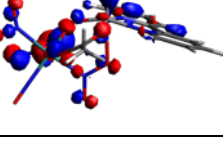
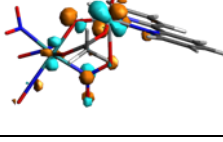
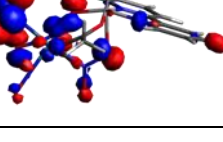
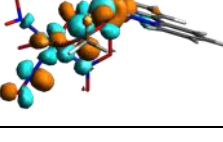
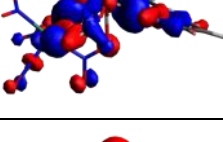
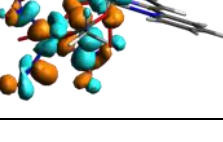
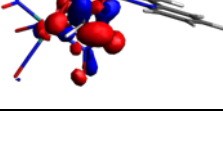
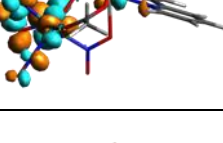
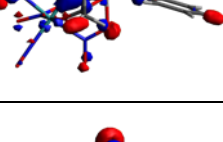
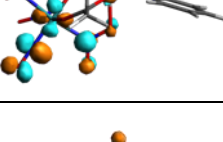
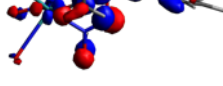
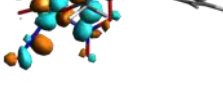
306	6.11169	13.0200		
307	6.12074	18.0200		
308	6.12791	10.4200		
309	6.14636	19.6700		
310	6.15186	7.5200		
311	6.17006	8.4000		
312	6.17454	4.8320		
313	6.17749	13.2300		
314	6.18863	1.4550		
315	6.20205	11.3900		

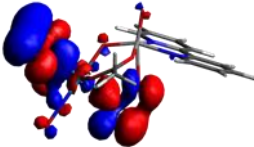
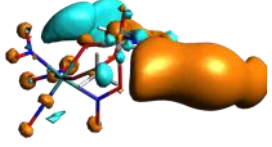
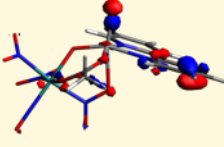
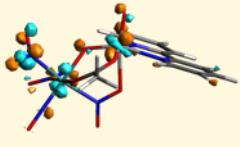
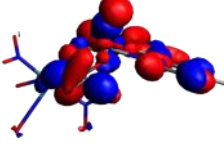
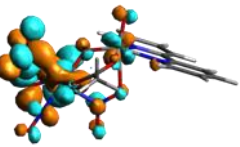
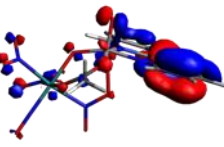
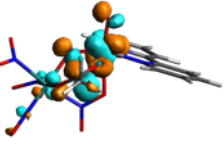
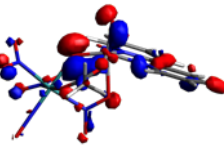
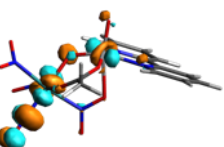
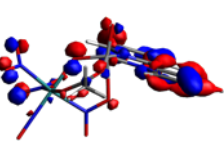
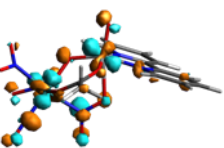
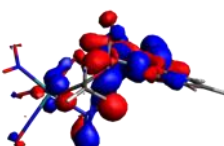
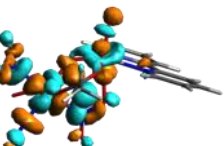
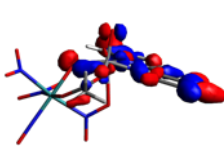
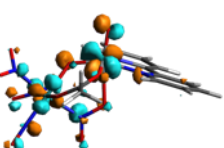
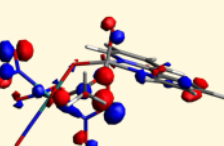
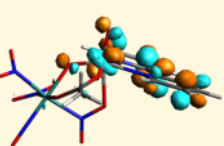
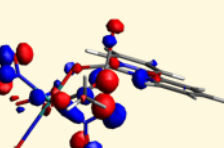
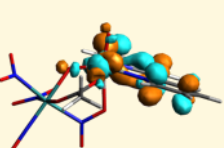
316	6.21021	36.2000		
317	6.21765	12.5000		
318	6.22345	8.6210		
319	6.22892	3.4180		
320	6.23742	8.6750		
321	6.24392	7.4580		
322	6.24966	4.9620		
323	6.25917	2.7220		
324	6.26019	8.3980		
325	6.26734	24.5100		

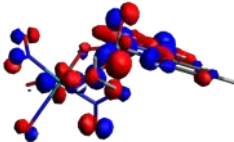
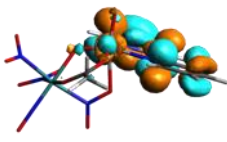
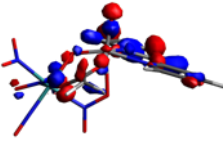
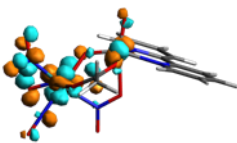
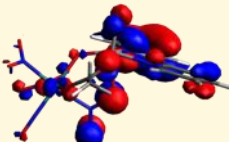
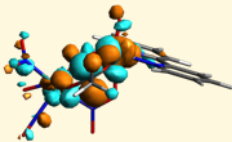
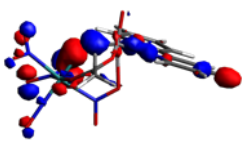
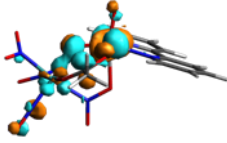
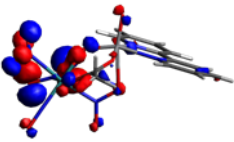
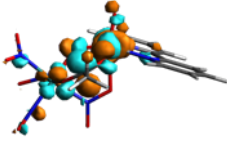
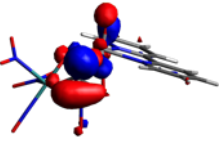
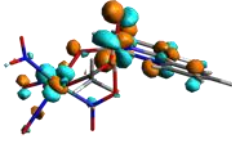
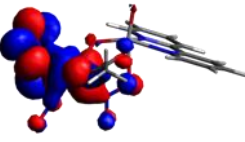
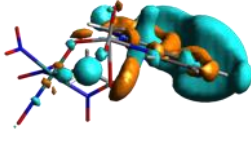
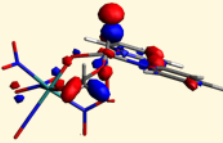
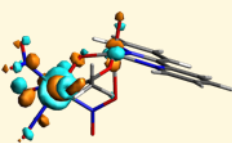
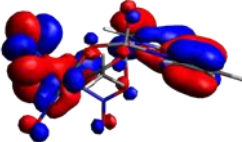
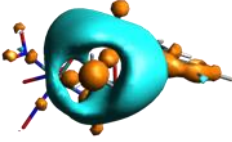
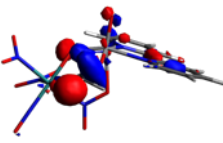
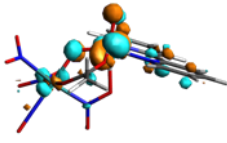
326	6.27584	23.4700		
327	6.28009	3.4350		
328	6.2822	2.3570		
329	6.28843	3.1500		
330	6.29315	4.6090		
331	6.29436	4.0870		
332	6.30448	10.8600		
333	6.30821	3.1730		
334	6.32553	1.8460		
335	6.33402	11.8400		

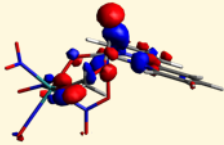
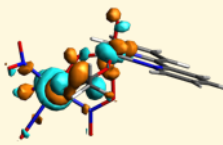
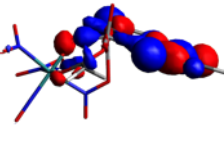
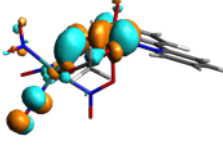
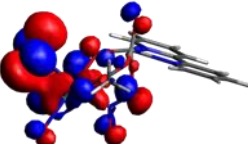
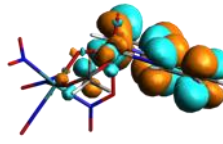
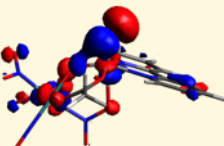
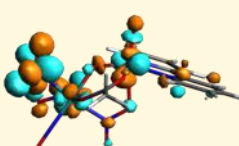
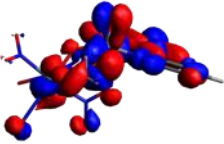
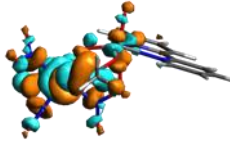
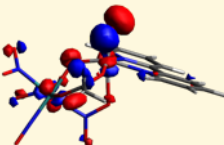
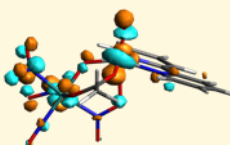
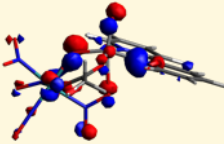
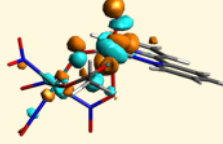
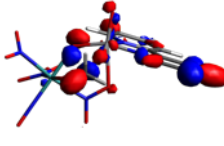
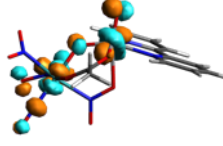
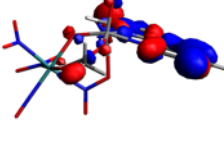
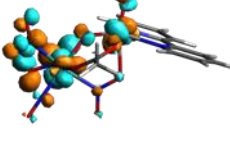
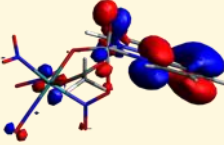
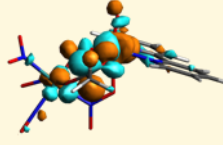
336	6.34182	4.1600		
337	6.34774	1.6060		
338	6.35449	11.2000		
339	6.36538	1.9950		
340	6.37385	18.1300		
341	6.38192	0.3723		
342	6.38329	16.2200		
343	6.40165	2.8990		
344	6.41408	14.2200		
345	6.41795	1.6900		

346	6.42103	3.1870		
347	6.42771	7.3370		
348	6.43377	11.6700		
349	6.43616	21.5800		
350	6.43942	3.8130		
351	6.4455	15.9800		
352	6.45014	5.6410		
353	6.46585	3.6460		
354	6.46982	31.7800		
355	6.47954	13.6600		

356	6.48529	92.3600		
357	6.50133	3.0060		
358	6.51394	5.5270		
359	6.51666	5.0800		
360	6.52054	3.4400		
361	6.53519	5.2070		
362	6.54213	0.5940		
363	6.55147	8.5860		
364	6.55766	2.1540		
365	6.55856	3.9250		

366	6.58108	3.1710		
367	6.58412	36.6100		
368	6.58728	6.5390		
369	6.60244	5.5460		
370	6.6065	6.0630		
371	6.61057	1.6230		
372	6.61326	5.5110		
373	6.62522	8.5920		
374	6.63151	17.0200		
375	6.64141	15.3700		

376	6.64553	4.4650		
377	6.65419	4.0340		
378	6.66458	24.6800		
379	6.66846	3.8150		
380	6.67668	5.0190		
381	6.67936	1.8150		
382	6.69127	0.4689		
383	6.69508	15.2100		
384	6.70598	1.4570		
385	6.71446	1.5830		

386	6.72484	16.8300		
387	6.73566	4.6590		
388	6.74182	0.7458		
389	6.74735	12.4200		
390	6.75416	4.2530		
391	6.76603	12.5400		
392	6.76668	10.3100		
393	6.78276	1.5270		
394	6.78347	9.8890		
395	6.78555	12.8400		

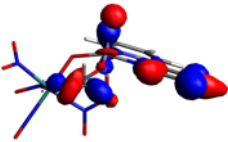
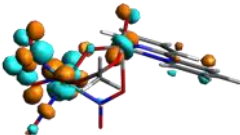
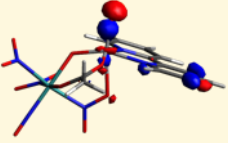
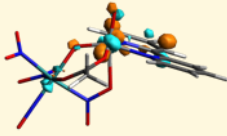
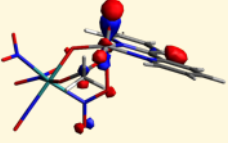
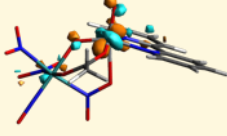
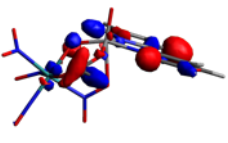
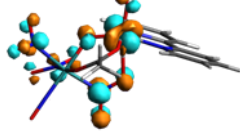
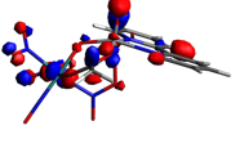
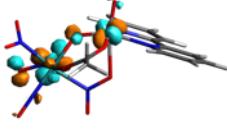
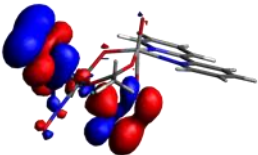
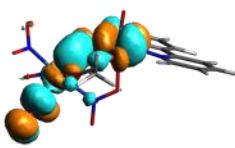
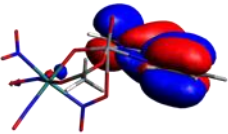
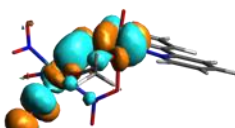
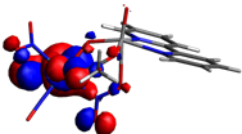
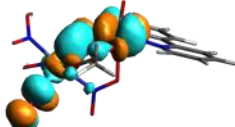
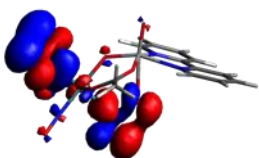
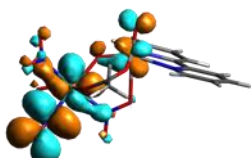
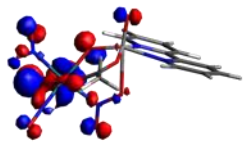
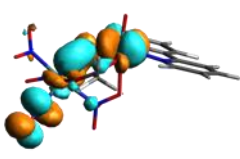
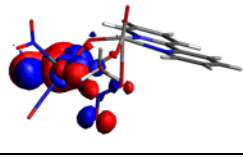
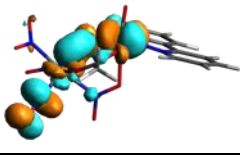
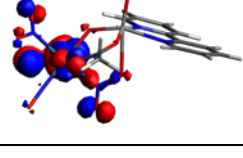
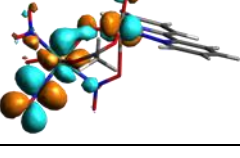
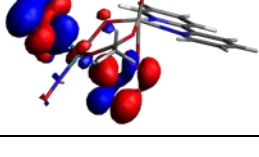
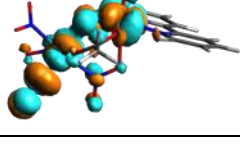
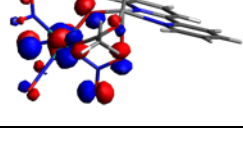
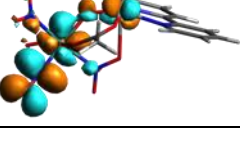
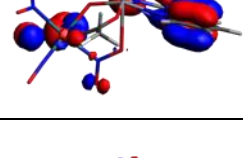
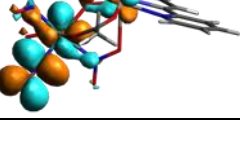
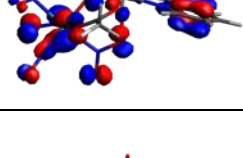
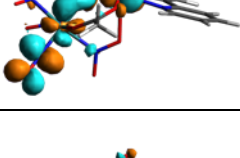
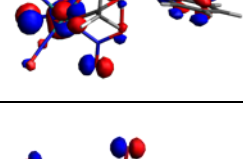
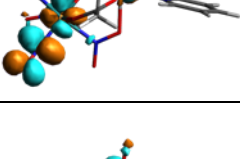
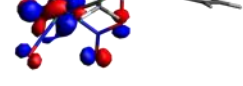
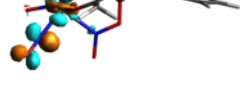
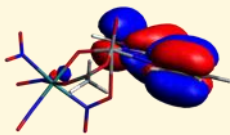
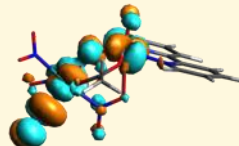
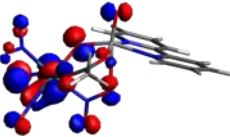
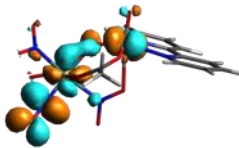
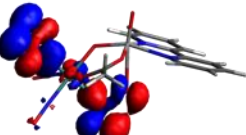
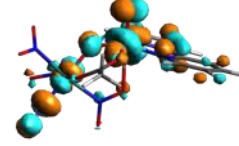
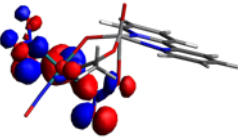
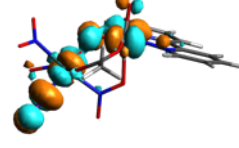
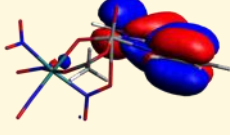
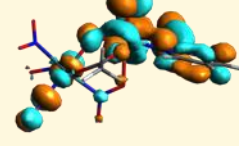
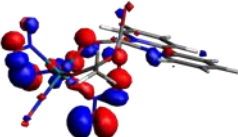
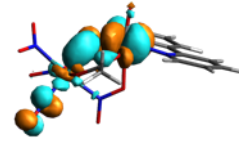
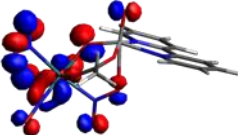
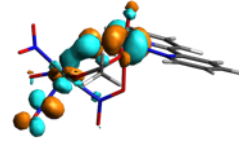
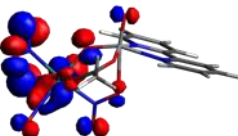
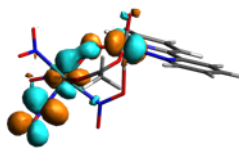
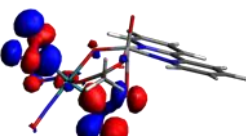
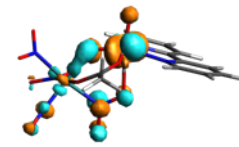
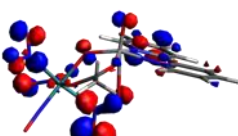
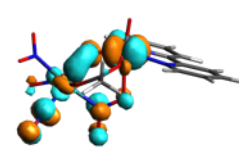
396	6.79552	8.4450		
397	6.80087	47.3400		
398	6.82518	31.7700		
399	6.83265	3.4070		
400	6.84727	4.4730		

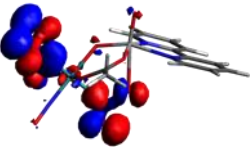
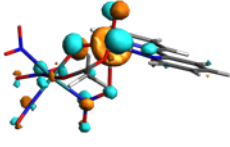
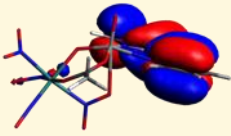
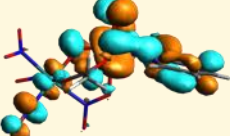
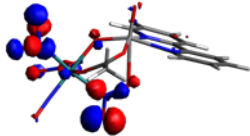
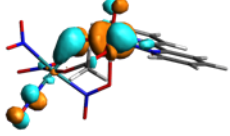
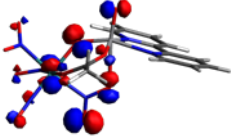
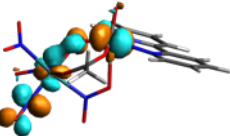
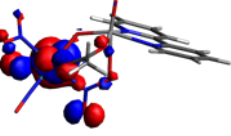
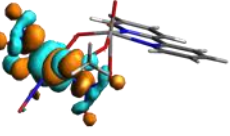
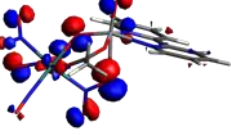
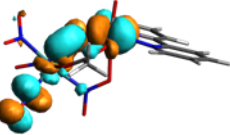
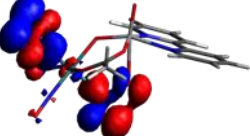
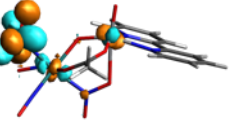
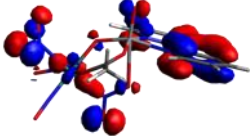
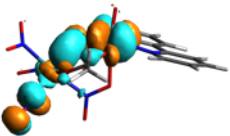
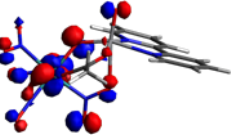
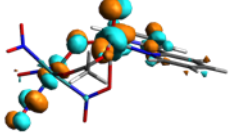
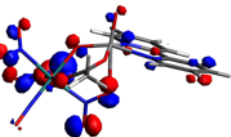
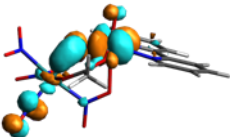
Table S4.

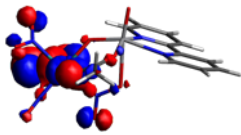
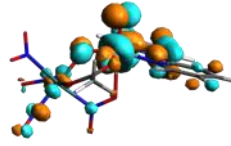
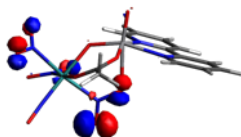
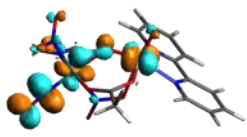
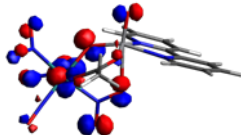
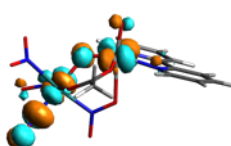
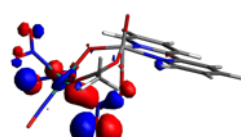
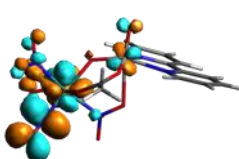
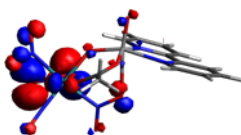
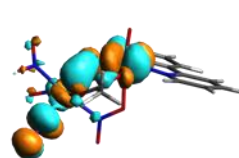
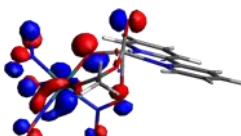
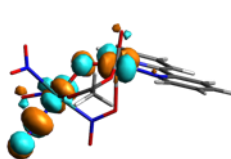
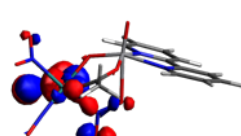
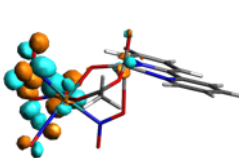
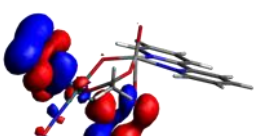
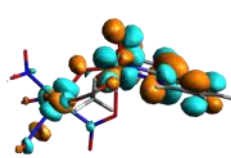
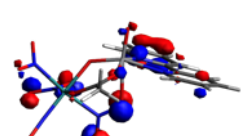
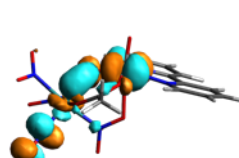
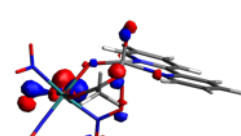
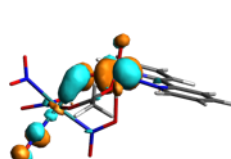
DFT calculations using B3LYP functional

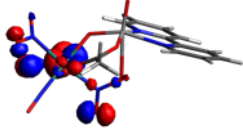
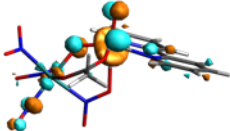
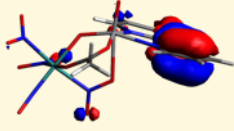
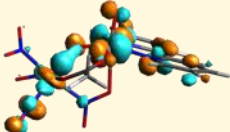
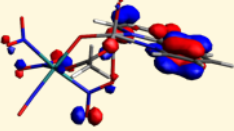
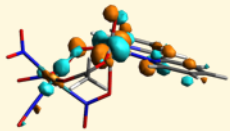
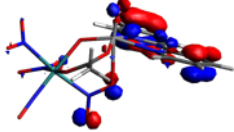
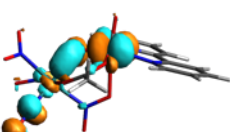
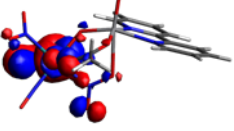
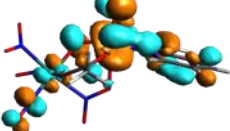
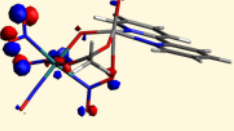
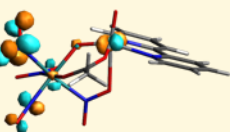
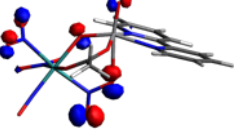
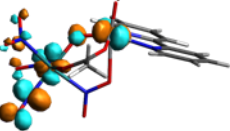
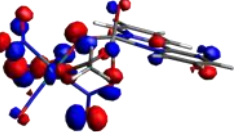
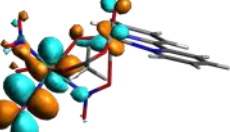
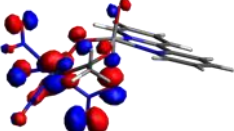
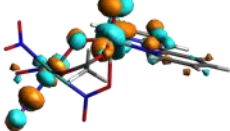
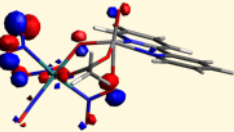
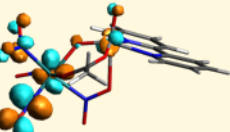
N	Transition Energy, eV	Oscillator strength, 10^3 a.u.	Origin of the transferred electron density, weighted sum of the occupied MO	Destination of the transferred electron density, weighted sum of the occupied MO
1	2.67786	0.4078		
2	2.78304	0.0077		
3	2.95455	0.4771		

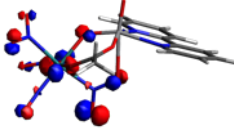
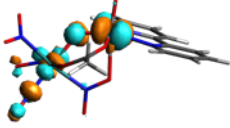
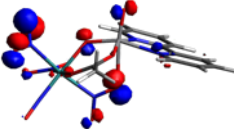
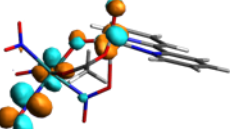
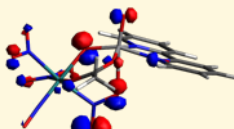
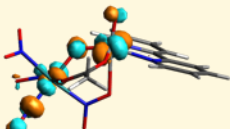
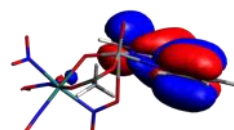
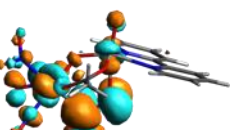
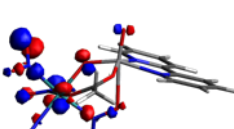
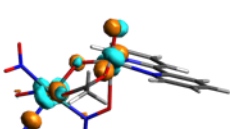
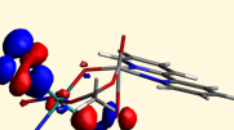
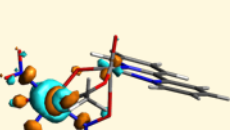
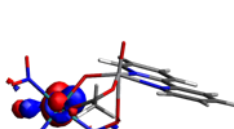
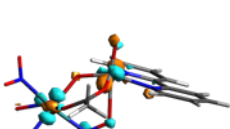
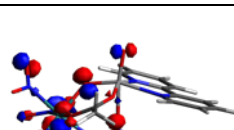
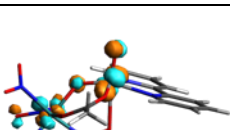
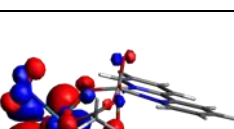
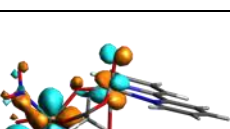
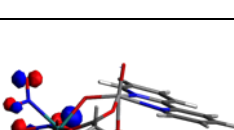
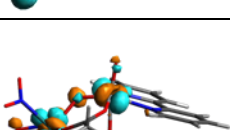
4	3.02389	0.6156		
5	3.12507	0.0837		
6	3.14237	0.9721		
7	3.183	0.2292		
8	3.28456	1.7370		
9	3.41255	1.0750		
10	3.4589	0.5025		
11	3.47688	0.9552		
12	3.48987	1.4830		
13	3.53082	2.5650		

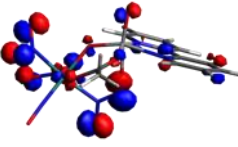
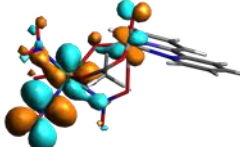
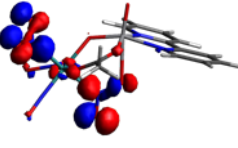
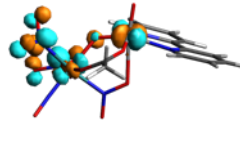
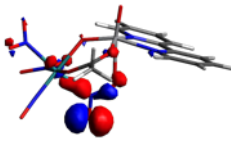
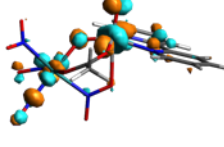
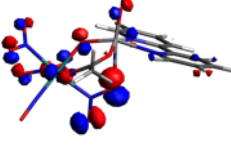
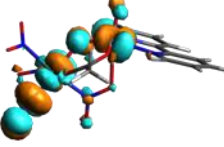
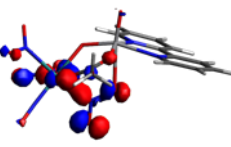
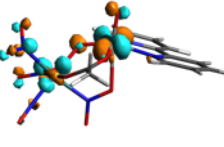
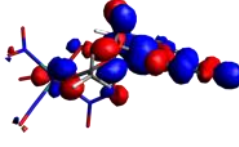
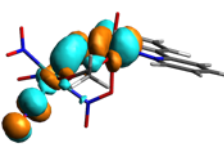
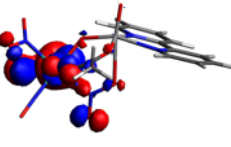
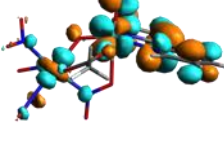
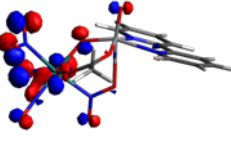
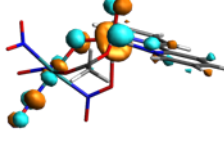
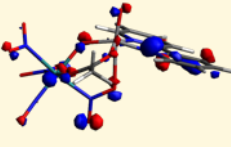
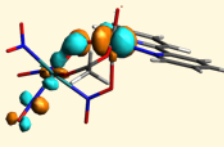
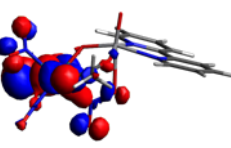
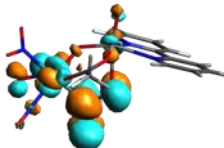
14	3.54217	12.2500		
15	3.58493	1.2090		
16	3.67005	0.4375		
17	3.71037	1.1170		
18	3.71764	28.3100		
19	3.78114	2.9140		
20	3.82163	0.7424		
21	3.88591	6.4600		
22	3.89911	0.3882		
23	3.94155	1.9430		

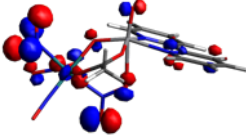
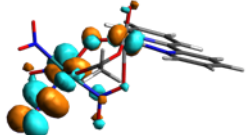
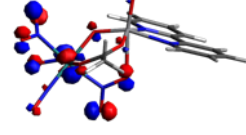
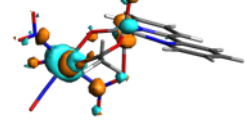
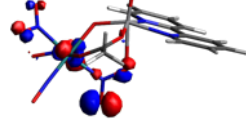
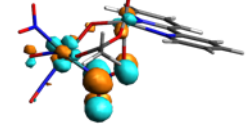
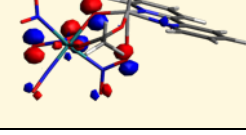
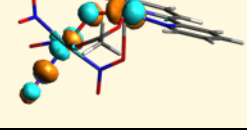
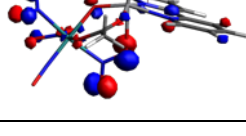
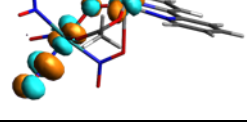
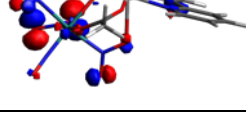
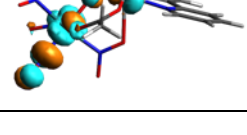
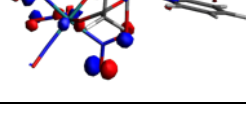
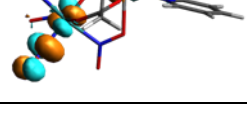
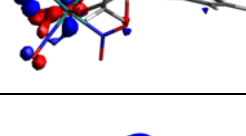
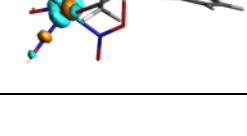
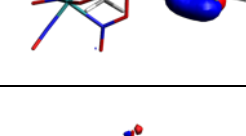
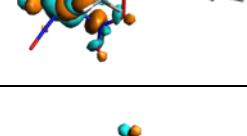
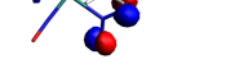
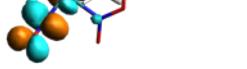
24	3.94675	2.9390		
25	3.966	17.8400		
26	3.97481	1.3550		
27	4.01317	3.8930		
28	4.02192	1.5250		
29	4.04996	0.2411		
30	4.0763	1.0470		
31	4.09549	0.1044		
32	4.11431	0.7174		
33	4.133	0.7139		

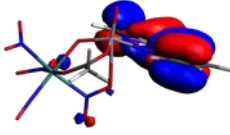
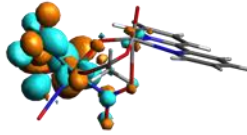
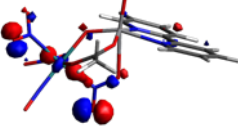
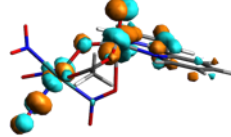
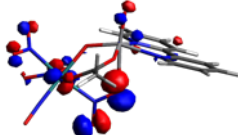
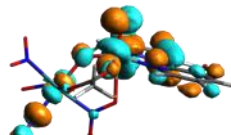
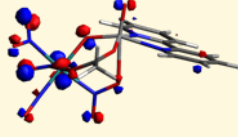
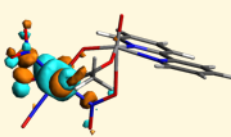
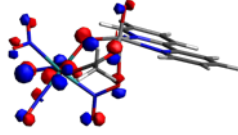
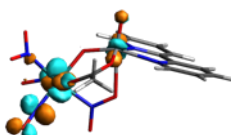
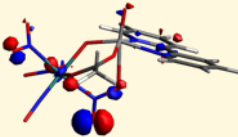
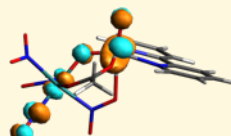
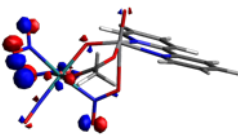
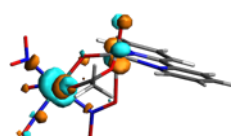
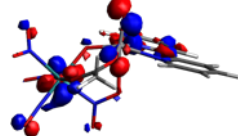
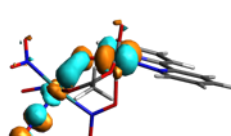
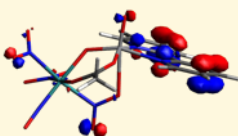
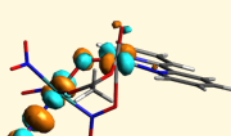
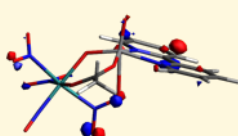
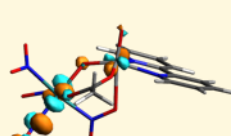
34	4.14714	1.1560		
35	4.17593	2.6570		
36	4.21134	0.6016		
37	4.22324	0.2327		
38	4.24817	1.8300		
39	4.25488	1.0890		
40	4.28313	1.7060		
41	4.29906	0.0807		
42	4.31307	7.5470		
43	4.32301	4.8170		

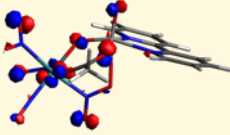
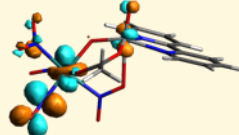
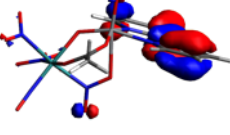
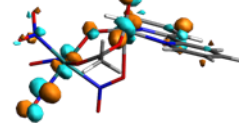
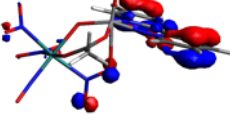
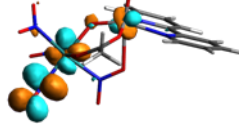
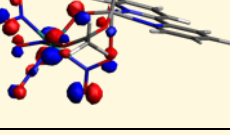
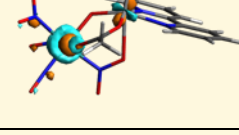
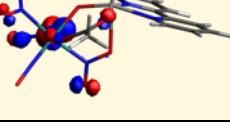
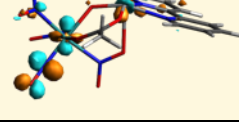
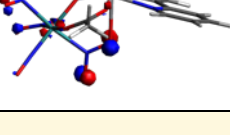
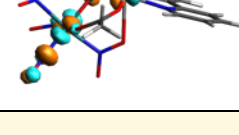
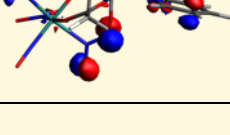
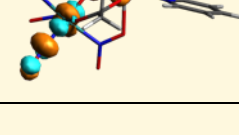
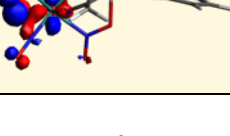
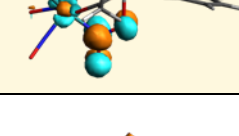
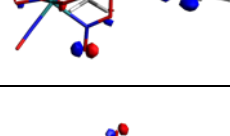
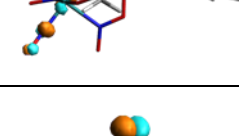
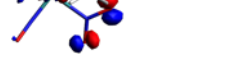
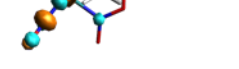
44	4.33617	2.7660		
45	4.36639	69.3900		
46	4.36927	62.4300		
47	4.40386	0.9012		
48	4.41766	0.9628		
49	4.43122	13.3800		
50	4.44146	6.8500		
51	4.47073	2.6980		
52	4.47165	2.9460		
53	4.50012	11.6500		

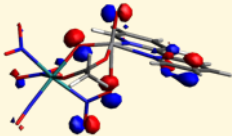
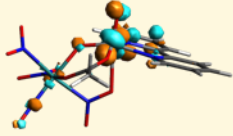
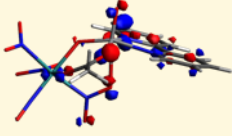
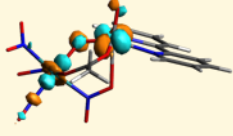
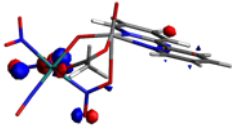
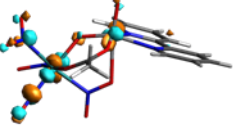
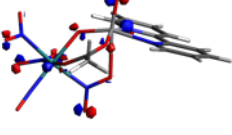
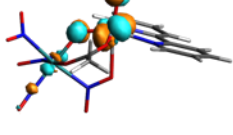
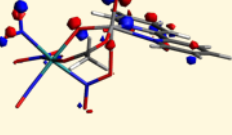
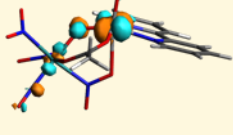
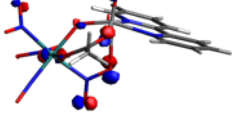
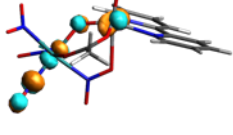
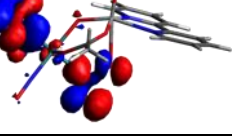
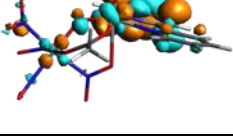
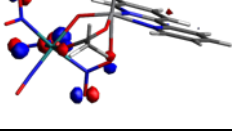
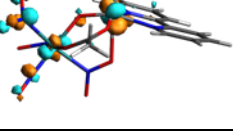
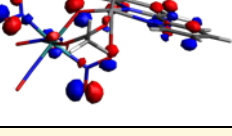
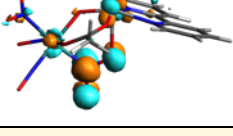
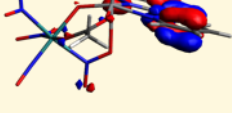
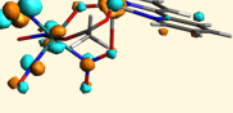
54	4.52963	3.7480		
55	4.55384	0.3494		
56	4.5695	12.6600		
57	4.57812	6.4710		
58	4.59846	3.8160		
59	4.60684	23.5800		
60	4.61164	3.7870		
61	4.63352	0.5288		
62	4.64958	3.1310		
63	4.68803	3.5620		

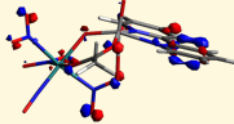
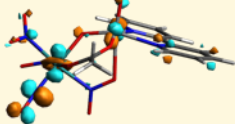
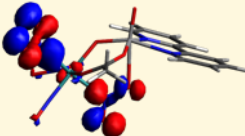
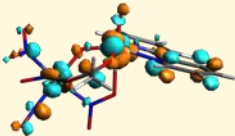
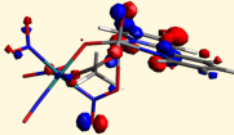
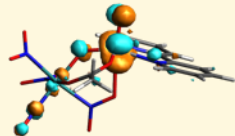
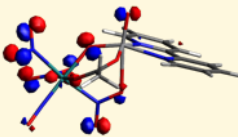
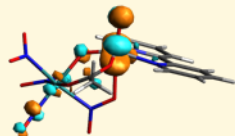
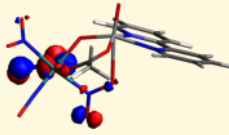

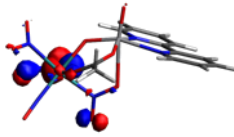
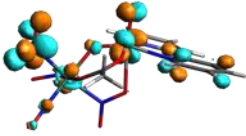
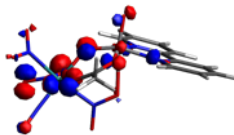
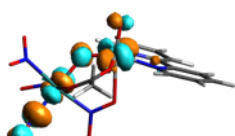
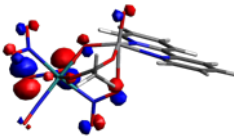
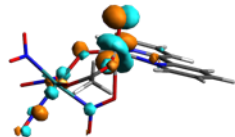
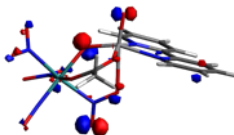
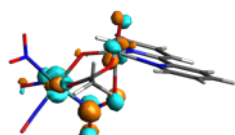
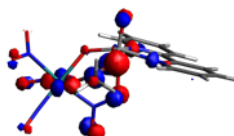
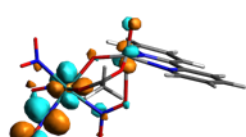
64	4.70424	1.8200		
65	4.72462	4.1290		
66	4.73752	9.0690		
67	4.74696	0.3229		
68	4.75396	0.4954		
69	4.76689	1.4560		
70	4.77301	1.7140		
71	4.78564	1.4390		
72	4.79165	38.6400		
73	4.81665	5.2260		

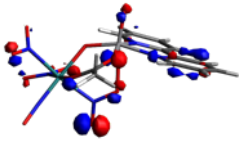
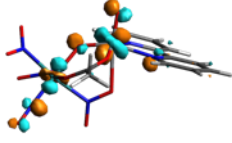
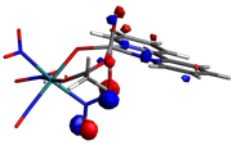
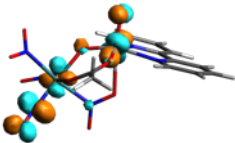
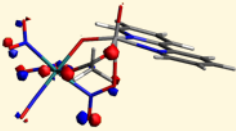
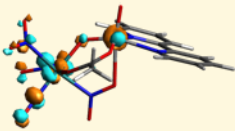
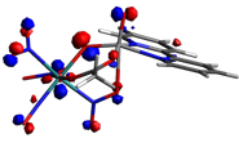
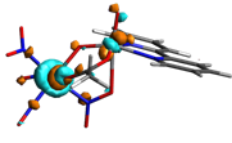
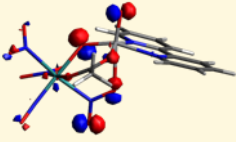
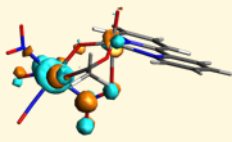
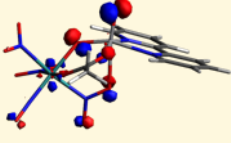
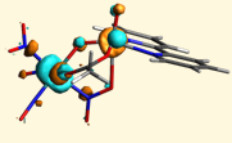
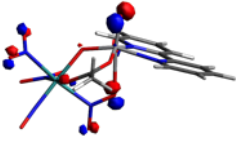
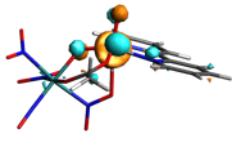
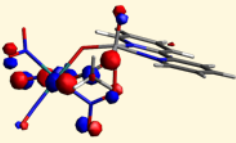
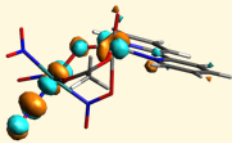
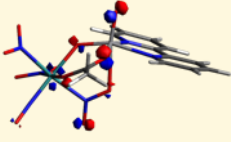
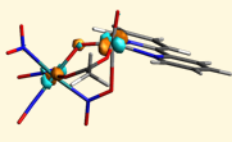
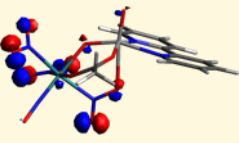
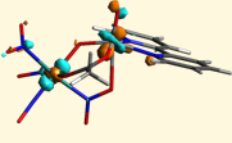
74	4.82913	9.2310		
75	4.85705	1.6590		
76	4.8598	3.2010		
77	4.88653	28.9900		
78	4.89826	2.8740		
79	4.90494	1.6650		
80	4.90904	1.4740		
81	4.93322	4.4960		
82	4.93513	1.9030		
83	4.94869	6.2800		

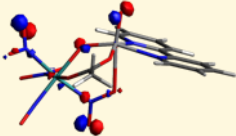
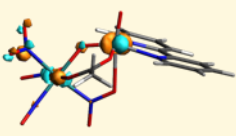
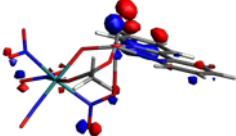
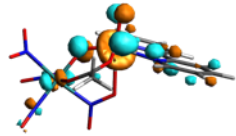
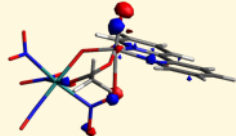
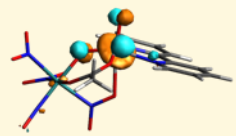
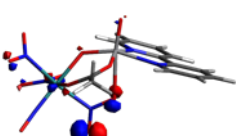
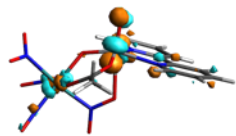
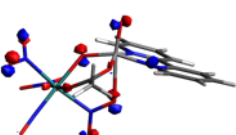
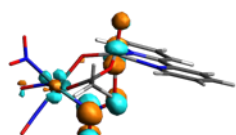
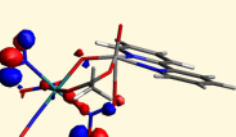
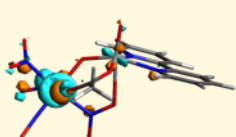
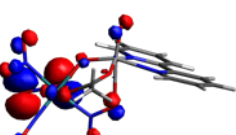
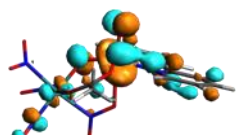
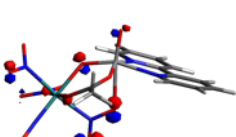
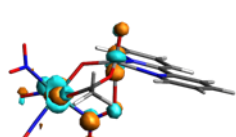
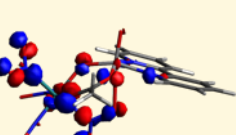
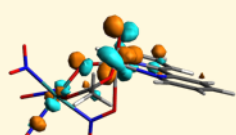
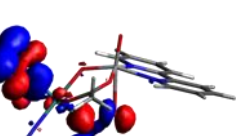
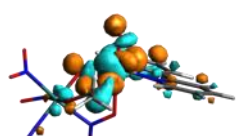
84	4.96281	2.0240		
85	4.97315	9.6890		
86	4.98656	7.7020		
87	5.00118	10.6500		
88	5.00652	4.6130		
89	5.02737	12.3000		
90	5.04122	4.3860		
91	5.05446	7.9660		
92	5.07096	13.3000		
93	5.07333	34.6200		

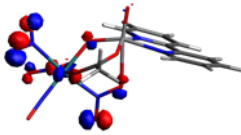
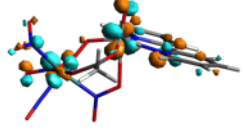
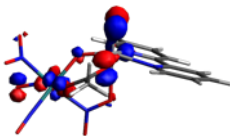
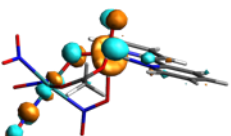
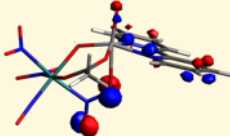
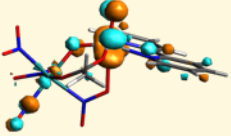
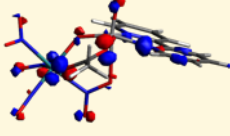
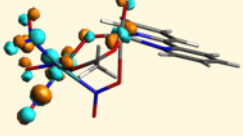
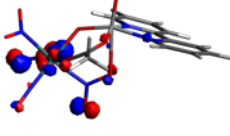
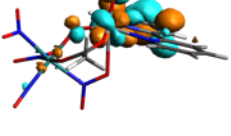
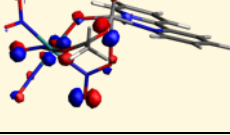
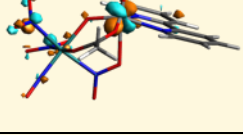
94	5.08021	15.4200		
95	5.08957	7.0190		
96	5.09487	3.5020		
97	5.12066	16.9700		
98	5.12447	14.2300		
99	5.13979	8.5270		
100	5.15666	15.8000		
101	5.16843	16.7500		
102	5.17166	3.3720		
103	5.1826	6.6790		

104	5.19547	17.3300		
105	5.19674	13.1900		
106	5.2169	2.0740		
107	5.22157	5.9450		
108	5.22288	12.2400		
109	5.23839	1.7060		
110	5.24563	1.3890		
111	5.25367	3.9870		
112	5.26299	5.7540		
113	5.27046	14.2000		

114	5.27527	34.8200		
115	5.28167	14.1900		
116	5.29095	15.8400		
117	5.30805	13.7500		
118	5.31751	10.8300		
119	5.32565	4.9080		
120	5.33453	6.5790		
121	5.34322	1.9600		
122	5.35979	4.9250		
123	5.36776	9.4370		

124	5.38008	6.6590		
125	5.38374	8.7960		
126	5.39904	28.9500		
127	5.40434	9.1740		
128	5.40896	10.1400		
129	5.4206	18.3900		
130	5.43337	0.6896		
131	5.45337	17.3800		
132	5.4715	40.2500		
133	5.48062	19.7100		

134	5.50693	56.8800		
135	5.51872	5.9760		
136	5.52385	66.5300		
137	5.54579	5.4780		
138	5.55768	1.8910		
139	5.5637	19.8000		
140	5.57065	0.5322		
141	5.57924	4.7250		
142	5.58247	11.2900		
143	5.59416	9.5750		

144	5.60296	0.1805		
145	5.61553	8.6190		
146	5.62143	23.8000		
147	5.63308	13.0500		
148	5.63794	2.7270		
149	5.65031	15.7900		
150	5.66379	35.6000	